

Contributions of Vimentin to Skeletal Muscle Hypertrophy

By

Joshua Scott Godwin

A dissertation submitted to the Graduate Faculty of
Auburn University
in partial fulfillment of the
requirements for the Degree of
Doctor of Philosophy

Auburn, Alabama
May 4, 2024

Keywords: Intermediate filaments, stromal cells, mechanical loading

Copyright 2024 by Joshua Scott Godwin

Approved by

Michael Roberts, PhD, Chair, Professor of Kinesiology, Auburn University
C. Brooks Mobley, PhD, Assistant Clinical Professor of Kinesiology, Auburn University
Andreas Kavazis, PhD, Professor of Kinesiology, Auburn University
Andrew Frugé, PhD, Associate Professor of Nursing, Auburn University
Christopher Fry, PhD, Associate Professor, College of Health Sciences, University of Kentucky

ABSTRACT

Our laboratory has performed various experiments examining the proteomic alterations that coincide with mechanical overload (MOV)-induced skeletal muscle hypertrophy. With this same intent we first sought to determine how 10 weeks of resistance training in 15 college-aged females affected protein concentrations in different tissue fractions. Training, which promoted significant lower body muscle- and fiber-level hypertrophy, notably increased sarcolemmal/membrane protein content (+10.1%, $p < 0.05$). Sarcolemmal/membrane protein isolates were queried using mass-spectrometry-based proteomics, ~10% (38/387) of proteins were up-regulated (> 1.5 -fold, $p < 0.05$), and one of these targets (the intermediate filament vimentin, VIM) warranted further investigation. VIM expression was first examined in the plantaris muscles of 4-month-old C57BL/6 mice following 10- and 20-days of MOV via synergist ablation. Relative to Sham (control) mice, VIM mRNA and protein content significantly increased in MOV mice. Immunohistochemistry corroborated these findings and showed that VIM was localized to the extracellular matrix (ECM). The 10- and 20-day MOV experiment was replicated in Pax7-DTA mice, and results indicated satellite cell depletion significantly blunted the presence of VIM in the ECM. A series of follow-up cell culture experiments supported that myoblasts, rather than myofibers, likely produce VIM in response to anabolic stimuli. Finally, a third 10- and 20-day MOV experiment was performed in C57BL/6 mice intramuscularly injected with either AAV9-scrambled (control) or AAV9-VIM shRNA. While VIM shRNA injections significantly blunted the presence of VIM (~50%), plantaris masses were similar between injection groups in response to MOV. However, a leftward (smaller) myofiber size shift in response to MOV was observed in VIM shRNA mice, and this

coincided with appreciably more myofibers presenting a regeneration phenotype (MyHC_{emb}-positive fibers with centrally located nuclei). Using a highly integrative approach, we propose that skeletal muscle VIM is a mechanosensitive target predominantly localized to the ECM and produced by satellite cells. Moreover, a disruption in VIM expression during MOV leads to dysfunctional skeletal muscle hypertrophy.

Acknowledgments

The journey of completing this doctoral degree would not have been possible without the support of mentors, friends, and family. First and foremost, I would like to thank Dr. Michael Roberts for the opportunity to complete this doctoral degree in your lab. Your mentorship, counsel, and guidance has been invaluable in my development as a scientist but more importantly has made me a better person. I would be remised without giving a special thanks to Dr. Brooks Mobley for all the help and guidance that you have given me over the past years, your mentorship in and out of lab has truly shaped me into a better researcher and I cannot thank you enough. I would also like thank the rest of my committee, Dr. Kavazis, Dr. Fudge, and Dr. Fry, your guidance throughout my dissertation project was critical in progressing the project to next level and my development as a scientist.

To my friends both in MASL/NAMPL and the kinesiology department, thank you for the incredible friendship and support that you have given that will last a lifetime. You all have made this journey both fulfilling and meaningful. I especially would like to thank Dr. Casey Sexton, Max Michel, and Nick Kontos for being my best friends throughout the process and helping me every step of the way. Without your friendship I would not be the person I am today; I am extremely grateful for you all.

Lastly, I cannot express my thanks and gratitude enough toward my wife Noel for the incredible support that she has given me along way. Without your love and support, I would not have been able to achieve nearly as much. You are the best wife, mother, and friend and without you this would not have been possible.

Table of Contents

Abstract	2
Acknowledgements.....	4
List of Figure.....	6
Chapter 1 (Introduction)	7
Chapter 2 (Literature Review)	10
Chapter 3 (Methods)	34
Chapter 4 (Tentative manuscript).....	49
Chapter References.....	81
Figures.....	98

List of Figures

Figure 1: Basal state (pre-intervention) human sarcolemmal proteome data.....	98
Figure 2: Human sarcolemmal proteome response to resistance training.....	99
Figure 3: Plantaris muscle vimentin expression response to 10- and 20-days of mechanical overload via synergist ablation	100
Figure 4: Vimentin co-localization with stromal cells following mechanical overload.....	101
Figure 5: Vimentin expression in satellite cell depleted muscle following mechanical overload.....	102
Figure 6: General muscle characteristics and vimentin expression in mice treated with AAV9-VIM-shRNA.....	103
Figure 7: AAV-VIM-shRNA mice present a shift toward smaller fibers and more centrally located nuclei.....	104

Chapter I: Introduction

Skeletal muscle is a highly dynamic tissue capable of undergoing marked changes in size and force output in response to increased mechanical tension/load. One of most potent stimuli for skeletal muscle hypertrophy is mechanical overload, either through progressive resistance training in humans or synergist ablation in rodents [1]. Mechano-sensitive/sensing protein pathways are responsible for relaying the mechanical perturbations and tension placed on the skeletal muscle into downstream signals for adaptations to occur [2-4]. A major pathway for mechanotransduction is through transmembrane proteins (integrins) and various accessory proteins that interact with the extracellular matrix, cytoskeletal network, and sarcolemma to propagate signals that enhance muscle protein synthesis [5-7]. Skeletal muscle hypertrophy is governed by several pathways but is ultimately dependent on an increase in muscle protein synthesis and a sustained net positive muscle protein balance [8].

Cytoskeletal and intermediate filaments not only provide structural support to the cell, but also are involved in processes like signal transmission, mechanotransduction and gene regulation [9-11]. With regards to skeletal muscle, intermediate filaments have been shown to be linked to development [12, 13], regeneration [14, 15], and growth [16]. The commonly studied intermediate filament desmin is a muscle specific intermediate filament that been implicated in several processes that govern skeletal muscle homeostasis and is responsive to mechanical loading [17-19]. Furthermore, Joanne et al. [20] showed that mechanical overload induced strength increases were blunted in a desmin knockout mouse model. Contrary to desmin, the intermediate filament vimentin is predominately expressed in immature developing myofibers

and decreases in expression in mature myofibers [21-23]. Interestingly, vimentin expression is linked to active and proliferating satellite cells [21, 24] and appears to be a critical protein involved in myofiber regeneration [25, 26]. Vimentin also plays a key role in several signaling pathways [11]. Most notably, while not in skeletal muscle, a recent study reported that vimentin is linked to governing cell size through interactions with the mTORC1 pathway, and a reduction in mTORC1 signaling and blunted protein synthesis was evident in vimentin-knockout cells [27].

Taken together, skeletal muscle hypertrophy in response to mechanical loading is dependent on several tightly regulated pathways and it appears that various ECM, cytoskeletal and intermediate filament related proteins play an important role in this process. Furthermore, vimentin has been shown to regulate cell size and protein synthesis response in other cell types. However, it is currently unknown if vimentin expression is needed for skeletal muscle hypertrophy during mechanical loading.

Specific Aims of This Proposal

1. Using a viral knockdown of vimentin in a rodent model (e.g., AAV9-mediated gene transfer of shRNA targeting vimentin), determine if skeletal muscle vimentin expression is necessary for mechanical overload induced hypertrophy.
 - a. Determine the approximate time-course for hypertrophy (if any) for vimentin-knockdown-mediated effects to ensue.
2. Examine the muscle protein synthesis response in vimentin depleted tissue in response to mechanical overload.

Hypotheses

1. Viral-mediated knockdown of vimentin will blunt or delay the hypertrophic response during mechanical overload in rodents. Furthermore, hypertrophy may still occur at later time point of overload (20+ days), however at early timepoint (3-14 days) hypertrophy will be blunted.
2. Viral knockout of vimentin will blunt the muscle protein synthesis response to mechanical overload.

Chapter II: Literature Review

General Adaptions to Skeletal Muscle Hypertrophy

Skeletal muscle is an incredibly plastic tissue being able to adapt to a variety of different stressors and stimuli. Skeletal muscle hypertrophy is defined by growth or enlargement of the muscle cell (myofiber). Skeletal muscle hypertrophy is induced by long-term adaptations to tension/load placed on the muscle (i.e., resistance training or mechanical overload via synergist ablation) [1]. The following literature review will describe various topics related to skeletal muscle hypertrophy including: i) the morphological changes that occur during periods of skeletal muscle hypertrophy, ii) alterations in mechanisms that may promote skeletal muscle hypertrophy, and iii) what stromal cells are and how they respond during periods of skeletal muscle hypertrophy.

Morphological Changes with Skeletal Muscle Hypertrophy

During skeletal muscle hypertrophy the myofiber and surrounding structures experience several distinct morphological changes. The key morphological adaptation accompanying skeletal muscle hypertrophy is an increase in myofiber size or fiber cross-sectional area (fCSA). An idea proposed by Millward [28] suggests that the myofiber is akin to an elastic bag containing both myofibrillar and sarcoplasmic proteins. With repeated bouts of tension (mechanical overload), new myofibrillar and sarcoplasmic proteins are added and push against the elastic borders (sarcolemma) of the myofiber (bag). This packing of increased proteins enlarges the myofiber resulting in hypertrophy. Although the “bag theory” is a simple analogy

for skeletal muscle hypertrophy, it emphasizes the importance of several key events that must take place for skeletal muscle hypertrophy to occur, namely accretion of myofibrillar and sarcoplasmic proteins to “fill the bag” and extracellular matrix remodeling to allow for the “expansion of the bag” [29].

Most of the intracellular area in a myofiber is occupied by myofibrils, accounting for ~70-85% of the total area [30-32]. These proteins consist of thick and thin filaments along with various other associated proteins and are largely responsible for active and passive force generation as well as making up sarcomere structure for muscle contractions. Further insight into the ultrastructure of myofibrils and sarcomeres has come from the Glancy laboratory where they utilized 3-D electron microscopy to show that myofibrils can exist in interconnected network and branching can occur [33]. With regards to mechanical loading induces skeletal hypertrophy, several recent human studies have shown that the area within the myofiber that is occupied by myofibrils does not change following various resistance training paradigms [30, 34]. These studies would suggest that myofibrillar content increases in proportion to fCSA increases seen with mechanical loading. While the area occupied by myofibrillar protein remains constant with mechanical loading/resistance training, it is unknown if the cross-sectional area (CSA) of myofibrils is increasing, if there is an increase in the number of myofibrils, or if both are occurring with increase in fCSA. Recently, the Hornberger laboratory has been leading the efforts to answer these questions and unpublished data suggest that both myofibrillar CSA and myofibrillar number are increasing with skeletal muscle hypertrophy in both human and rodent tissue following mechanical loading.

While myofibrils occupy the vast majority of intracellular area in the myofiber, the mitochondria reticulum and sarcoplasmic reticulum occupy ~5-10%, and the cytoplasm

(sarcoplasm) occupies the remainder [35]. Again, the Glancy lab has used 3-D electron microscopy to determine that the mitochondria in skeletal muscle exist in a highly dynamic network [36]. With regards to mechanical loading and hypertrophy in skeletal muscle, several studies have shown that resistance training in humans can alter the mitochondrial dynamics and lead to an increase in mitochondrial protein content [37-40]. Increases in the non-myofibrillar fractions (mitochondria, sarcoplasm, sarcoplasmic reticulum, etc.) during skeletal muscle hypertrophy has been deemed “sarcoplasmic hypertrophy” [41]. Several studies have shown a disproportional response of myofibrillar and non-myofibrillar fractions with skeletal muscle hypertrophy, suggesting that these increases in fCSA are being driven by increases in sarcoplasmic related structures and proteins [31, 42-44]. While these studies suggest a case for sarcoplasmic hypertrophy, the training paradigms, training status, and measurement techniques used make it difficult to determine if true sarcoplasmic hypertrophy was occurring.

Another morphological change that occurs during skeletal muscle hypertrophy is the addition of new myonuclei, deemed myonuclear accretion. This addition of new myonuclei during a period of growth is the basis of the myonuclear domain theory. The myonuclear domain theory is that any one myonuclei can only govern a certain area of myofiber [45-47]. During myofiber hypertrophy, more myonuclei are needed to sustain the myonuclear domain that each individual myonuclei governs [48-50]. The topic of myonuclear domain and myonuclear accretion will be discussed in further detail later in the review.

Finally, it is important to consider that each myofiber is surrounded by a layer of extracellular matrix (ECM). As skeletal muscle hypertrophy occurs it is critical that the surrounding ECM is remodeled to support the increase fCSA [51]. This process and factors

related to ECM remodeling with skeletal muscle hypertrophy will be discussed later in the review.

Increase in Protein Synthesis During Skeletal Muscle Hypertrophy

Skeletal muscle hypertrophy is driven through an increase in skeletal muscle protein synthesis (MPS) above the rate of muscle protein breakdown (MPB) resulting in a net positive protein balance. This increase in (MPS) occurs results in the formation of new myofibrillar and sarcoplasmic proteins and is regulated by a multitude of pathways that are activated during periods of mechanical loading. Moreover, an increase in DNA transcription into RNA and an increase in translation of RNA into protein is required to sustain the growth of the muscle. The processes of increased transcription and translation during skeletal muscle hypertrophy are controlled by several factors that are heavily influenced by mechanical overload and will be discussed in more detail in this section of the review.

Epigenetic Changes That Influence Transcription During Hypertrophy Via Mechanical Loading

Epigenetics are changes in gene expression without the change of the underlying DNA sequence. In skeletal muscle, epigenetic alterations can occur though (but not limited to) three major mechanisms including i) DNA methylation, ii) histone modification via acetylation or methylation, and iii) the regulation of gene expression via microRNAs [52].

DNA Methylation

Skeletal muscle DNA methylation is one of most studies epigenetic alterations that impact gene expression. DNA methylation is the addition of a methyl group on cytosine residues

on a CpG site (cytosine guanine dinucleotide pairing) [1, 52, 53]. DNA methylation occurs through DNA methyltransferase (DNMTs) enzymes and de-methylation occurs through the ten-eleven translocation (TET) enzymes [54-56]. Increased DNA methylation status in a promoter or enhancer region of a gene is generally associated with a downregulation in the RNA transcription of that gene. This transcriptional silencing or repression happens by impairing transcriptional machinery from binding, by compacting DNA, or through chromatin remodeling resulting in transcriptional machinery not being able to access and bind to promoter regions of certain genes [57, 58].

Several studies have sought to determine the role(s) that DNA methylation status have on the adaptive responses to exercise. Human studies, spearheaded by the Sharples laboratory, have shown that DNA methylation status is responsive to resistance training in both acute and chronic conditions, resulting in a state of hypomethylation [56, 59, 60]. Several rodent studies stemming from the McCarthy laboratory have utilized genetic mouse models to label resident and newly acquired myonuclei, and these studies have suggested that DNA methylation is dynamically altered during periods of mechanical overload [61-63]. Furthermore, DNA methylation status is retained during periods of detraining, resulting in the hypothesis of an epigenetic memory or “epi-memory” in skeletal muscle [60, 64]. Another interesting aspect regarding DNA methylation in response to exercise is using methylation status to determine biological age/aging. Two recent studies have shown that DNA methylation status in skeletal muscle takes on a more “youthful or rejuvenated” state following periods of mechanical overload [59, 65].

Histone Modification

Histone modification most often occurs on the N-terminal tails of histones H3 and H4. These N-terminal tails can be prone to several post-translational modifications, namely

acetylation and methylation [52, 66, 67]. Histone modifications are regulated by a group of enzymes that either add acetyl groups (HATs) and methyl groups (HMTs) or remove them (HDACs). Depending on the type of modification and the residue at which the modification occurs, this can either enhance or repress transcription [68]. With regards to skeletal muscle hypertrophy via mechanical loading, histone modification markers have been perceived as indicators of transcriptional activity within the muscle. For instance, a study from Thalacker-Mercer et al. [69] showed the higher responders to resistance training had higher basal levels of acetylated H3K36, leading these authors to hypothesize that higher responders are epigenetically “primed” for increased transcription. Additionally Kirby et al. [70] showed that increased H3K9ac labeling in myonuclei was associated with increased global transcription during mechanical overload in mice. While histone acetylation is generally associated with increases in transcription, histone methylation is associated with transcriptional repression. For example, Seaborne et al. [71] showed global H3K4 trimethylation was lower and an increase in transcription was evident following an acute bout of resistance exercise. What is important to note, however, is that while these data are informative, much in this area has been merely observational. Hence, more mechanistic rodent data are needed to determine if histone modifications are required for the adaptive responses to occur to mechanical overload.

Micro-RNA

Micro-RNAs (miRNAs) are a class of nonprotein-coding RNAs that generally regulate gene expression through the post-transcriptional repression of mRNAs translation [72-74]. Although miRNAs affect almost every tissue type, a group of muscle-specific miRNAs or “myomiRNAs” have been implicated in several key processes involved in skeletal muscle hypertrophy. McCarthy and Esser were the first to use a rodent mechanical overload model to

show a decreased expression of miR-1 and miR-133a during skeletal muscle hypertrophy [75]. Subsequent studies in humans involving varying modalities of resistance training have since confirmed the finding that miR-1 and miR-133a expression is decrease with skeletal muscle hypertrophy [76-78]. Furthermore, miRNAs have been shown to have differential expression in high and low responders to skeletal muscle hypertrophy. Davidsen et al. [79] showed that following 12 weeks of resistance training low responders expressed a downregulation of miR-378, miR-29a, and miR-26a, while expressing an upregulation of miR-451, these results further implicate miRNAs in the regulation of skeletal muscle hypertrophy. While these data have been informative, one study that questions the requirement of miRNAs in promoting the adaptive response to mechanical overload comes from Vechetti et al. [80]. Specifically, these authors generated a skeletal muscle-specific Dicer knockout mouse to show that, despite an 80% knockdown of Dicer expression, only ~50% reduction in muscle miRNAs was observed. More critically, mechanical overload-induced skeletal muscle hypertrophy, atrophy induced by hindlimb unloading, or age-related muscle loss was not affected in this mouse model. Thus, again, more data in this area are needed to confirm the requirement of altered miRNA expression in promoting mechanical overload-induced skeletal muscle hypertrophy.

Ribosome Biogenesis with Mechanical Overload

Ribosomes are the macromolecules responsible for facilitating protein synthesis within the cell [81, 82]. The mature ribosome (80S) is comprised of a small subunit (40S) consisting of 33 ribosomal proteins along with one rRNA (18S) and a large subunit (60S) consisting of 47 ribosomal proteins and 3 rRNAs (28S, 5.8S, 5S) [83-85]. mRNAs interact with ribosomes at several distinct sites. The A-site is where incoming charged tRNAs (bound with an amino acid)

enter the ribosome and bind to the matching codon on the mRNA. This process is also aided by the decoding center that proofreads the codon-anticodon interaction to ensure the correct tRNA is bound. The P-site of the ribosome holds the growing polypeptide chain and, along with the peptidyl transferase center, facilitates the formation of a peptide bond between the amino acid from the A-site tRNA and the growth polypeptide chain in the P-site. The E-site is responsible for the exit of unchanged tRNAs that have donated their amino acids to the elongating polypeptide chain [86, 87].

The beginning of protein synthesis, or translation initiation, is a process involving multiple eukaryotic initiation factors, tRNA charged with methionine (Met), both the 40S and 60S subunits, and the 5' cap of mRNA. The first step of translation initiation is the formation of the 43S pre-initiation complex, which consists of the 40S subunit, Met-tRNA, and several initiation factors. This 43S pre-initiation complex then binds to the 5' cap of mRNA, the pre-initiation complex scans for the AUG start codon on the mRNA, and the translation initiation factors disassociate from the complex. Finally, the 60S subunit is assembled to the 40S subunit and Met-tRNA and translation ensues [88, 89]. Translation elongation is the repeated process of decoding mRNA, peptidyl transfer, and tRNA translocation and exiting [90]. Translation elongation continues until a stop codon is reached. Once this stop codon is reached, release factors bind, and the completed protein is released followed by the dissociation of the ribosomal subunits. Once the protein is released, it is subjected to further processing and folding to create the functional protein [91, 92].

Ribosome biogenesis is the process through which new ribosomes are synthesized. This highly complex and well-orchestrated process starts in the nucleolus with the transcription of rDNA and requires the coordinated actions of ribosomal proteins, numerous processing, export,

and assembly factors [93, 94]. Ribosome biogenesis requires all three RNA polymerases. RNA Pol-I is responsible for transcription of the 45S rDNA genes resulting in 47/45S pre-rRNA, pre-rRNA is then processed into 28S, 18S, and 5.8S rRNA [95]. RNA Pol-II transcribes mRNAs that encode ribosomal proteins along with other processing and assembly related proteins. RNA Pol-III is responsible for generating 5S rRNA and tRNAs [96-98]. Transcription of the 45S rDNA gene by Pol-I is considered the rate limiting step for ribosome biogenesis [4, 99, 100]. The Pol-I machinery is accompanied by several transcription factors (e.g., UBF, c-Myc), the selectivity factor-1 (SL-1) that is composed of multiple TATA binding protein associated factors (TAFs) and transcription initiation factor-1 (TIF-1a), and the 14 subunit Pol-I holoenzyme [101]. These factors collectively make up the Pol-I regulon, and the binding of these factors to the upstream promoter controls the transcription initiation rate of rDNA and ensures the availability of the core Pol-1 machinery for efficient transcription of rDNA genes [84, 102, 103]. Once 47/45S pre-rRNA is processed into 28S, 18S, and 5.8S rRNAs and 5S rRNA is transcribed, ribosomal proteins are imported back into the nucleolus where they assemble with rRNAs to form the large and small subunits. The 40S and 60S subunits are then exported out of nucleolus but do not form the mature 80s ribosome until translation initiation occurs [85, 96].

Given that ~80% of total RNA content of cells is rRNA, total RNA is used as a surrogate marker for measuring ribosome content or capacity [104]. In 1973, Millward published a report showing skeletal muscle protein synthesis scaled linearly with changes in rRNA [105]. Subsequent studies have shown that mechanical loading of skeletal muscle increases rRNA and total RNA concentrations following both acute and chronic loading, suggesting mechanical overload increases ribosomal content/capacity in skeletal muscle [106-113]. In the initial stages of mechanical overload, rRNA transcription peaks at 3 days and precedes rRNA accumulation

and hypertrophy [114]. With mechanical overload, ribosome biogenesis occurs in a pulsatile fashion that is different than basal ribosomal production [93]. Human studies have shown that rDNA transcription occurs after a single bout of resistance exercise, being detected within 4-hours post-exercise and persisting 48-72 hours following resistance exercise bouts [93, 115-117]. Furthermore, in humans, skeletal muscle hypertrophy is often detected after 15-20 resistance training session [118-120] and given the pulsative nature of ribosome biogenesis in response to mechanical overload, it seems that ribosome biogenesis precedes hypertrophy [85, 94]. This concept is reinforced by several studies in both humans and rodents, showing that the degree skeletal muscle hypertrophy associated with different loading paradigms is linked to the magnitude of ribosome biogenesis [112, 113, 121, 122].

During skeletal muscle hypertrophy, ribosome biogenesis is controlled/regulated by several different factors and pathways. Probably the most influential pathways involved in the regulation of ribosome biogenesis during skeletal muscle hypertrophy is mTORC1 signaling. Studies conducted by the Nader laboratory [102, 123] showed that increases in rRNA concentration in serum treated myotubes is abrogated by rapamycin (inhibitor of mTORC1), concluding that ribosome biogenesis in myotubes is in part stimulated by mTORC1 signaling. Furthermore, the Nader laboratory showed that mTORC1 can localize in the nucleus and bind to the rDNA promoter, again reiterating that mTORC1 signaling regulates ribosome biogenesis. Another potential regulator of ribosome biogenesis is rDNA copy number. rDNA copies can vary by hundreds of copies between individuals, and some evidence indicates that rDNA copy number is associated with ribosome biogenesis markers following an acute bout of resistance training [61]. In addition to rDNA copy number having a potential role in ribosome biogenesis, the epigenetic state, especially methylation status, of rDNA promotor regions has been shown to

regulate transcription of rRNA genes and is responsive to mechanical loading [61] (<https://www.biorxiv.org/content/10.1101/2023.08.03.551775v1>). Hence, this collective evidence supports that ribosome biogenesis is important for the skeletal muscle hypertrophic response to mechanical overload.

mTORC1 and Mechanical Overload

One of the most studied pathways involved in increasing MPS during skeletal muscle hypertrophy is the mammalian or mechanistic target of rapamycin complex 1 (mTORC1) signaling pathway. mTOR is a protein kinase in the PI3K family of protein kinases, and mTORC1 contains six accessory proteins [124, 125]. Activation of mTORC1 leads to several phosphorylation events that ultimately lead to enhanced translation and protein synthesis [126].

In skeletal muscle, mTORC1 can be activated by several distinct mechanisms. Growth factors, like IGF-1, can bind to cell surface receptors to activate PI3K/Akt signaling, which in turn, inhibits TSC1/2 allowing Rheb to activate mTORC1 [127]. Another mechanism of mTORC1 activation is amino acid sensing. Briefly, amino acids promote the Ragulator-Rag-GTPase mediated translocation of mTOR to the lysosome [128]. This translocation of mTOR to the lysosome results in mTOR associating with Rheb, which in turn, activates mTORC1 [129-132]. Probably the most applicable mechanism for mTORC1 activation with the context of mechanical overload is the mechanical stretch induced increases in diacylglycerol kinase zeta (DGK ζ) and/or phospholipase D (PLD) leading to increased intracellular phosphatidic acid (PA) content and the subsequent increase in mTORC1 activation [3, 133]. This pathway, along with other mechanical stretch/tension induced activators of mTORC1, will be discussed later in the review.

In the context of skeletal muscle hypertrophy, the primary function of the mTORC1 complex is to enhance protein synthesis by phosphorylating downstream targets involved in cell growth. Such downstream targets include kinases (e.g., p70S6K), proteins involved in translation initiation (e.g., 4E-BP1), and proteins involved in translation elongation (e.g., eEF2K) [134, 135]. The mTORC1-mediated phosphorylation of p70S6K activates this latter kinase, and its increased activity enables it to phosphorylate ribosomal protein S6 (rpS6). Although the complete consequences of rpS6 phosphorylation are still being elucidated, it has been shown that this event leads to conformational changes in the ribosome that are hypothesized to facilitate the recruitment and assembly of the translation pre-initiation complex [136]. On the other hand, the mTORC1-mediated phosphorylation of 4E-BP1 and eEF2K inhibits these proteins allowing for activation of eIF4E and eEF2, respectively, resulting the enhanced translation initiation and elongation [137]. While the main function of mTORC1 is to phosphorylate targets related to protein synthesis, mTORC1 plays a key role in facilitating ribosome biogenesis, inhibiting myostatin, limiting autophagy related breakdown of proteins, and aiding in cell cycle progression [102, 138-141].

mTORC1 signaling and function during skeletal muscle hypertrophy via mechanical overload has been well characterized. Several key studies at the turn of the century and early 2000's sparked a wide range of additional studies to understand the response and mechanisms of mTORC1 signaling during skeletal muscle hypertrophy. First, Baar and Esser (1999) [142] showed phosphorylation of p70s6k after acute bout associated with the degree of hypertrophy in rodents. These findings were later confirmed by showing prolonged increases in p70s6k occurred in response to hypertrophy stimulus [143]. Bodine (2001) [144] used the mTOR inhibitor rapamycin and showed blunted hypertrophy following 14 days of mechanical overload. This

resulted in a decrease in phosphorylation of p70s6k, showing that p70s6k is a downstream target of mTOR [130]. This seminal work on mTOR signaling in skeletal muscle led to a multitude of additional rodent studies, further cementing mTORC1 signaling as a key regulator of increased muscle protein synthesis following mechanical overload [145-149]. In addition to the numerous rodent studies, the response of mTORC1 signaling and its related downstream targets have also been heavily researched and characterized in humans following various bouts of resistance training and nutritional states [150-163].

Upstream activators of mTORC1 with mechanical overload have not been as well studied as the downstream targets. Both AKT and IGF1 are upstream activators of mTORC1 and have been shown to be responsive to mechanical loading [164-169]. This increase in both IGF1 and AKT signaling post mechanical loading led to the hypothesis that increased mTORC1 activation/signaling post mechanical loading was due to increased IGF1 and AKT signaling [170-172]. While IGF1 and AKT activation of mTORC1 probably happens during mechanical overload of skeletal muscle, several recent studies have shown that mTORC1 activation and increased protein synthesis still occurs despite IGF1 receptor or AKT inhibition [173-176]. Other upstream activators of mTOR are also responsive to mechanical loading, such as amino acid sensing/transport, along with factors that inhibit mTORC1 signaling. For instance, following mechanical loading or resistance exercise the amino acid-sensing protein Vps34 and the amino acid transport protein LAT1 are upregulated potentially leading to increased mTORC1 activation [177-179]. Another upstream regulator of mTORC1, TSC2 inhibits mTORC1 signaling by converting GTP-Rheb into inactive GDP-Rheb at the lysosome [180]. With mechanical loading and resistance training, localization of TSC2 to the lysosome is reduced leading to increased GTP-Rheb and mTORC1 activation [154, 181, 182]. While several upstream activators of

mTORC1 are responsive to mechanical loading, the activation of mTORC1 through mechanical tension and mechano-sensing is potentially the most important and driving factor of mTORC1 signaling with mechanical loading/resistance exercise, and this is further discussed in the next section of this review.

Mechano-sensing Pathways in Skeletal Muscle

The idea of mechanotransduction or mechano-sensing during mechanical loading induced skeletal muscle hypertrophy was originally established by Goldberg et al. [107] in 1975 and since been further refined and investigated [2, 3, 183-186]. Mechanotransduction occurs when mechanical or physical perturbations in the basal lamina, sarcolemma, or cytoskeletal structure leads to downstream signaling events, most commonly activating mTORC1 and resulting in increased protein synthesis [1].

One of the main mechanotransduction pathways involving the downstream activation of mTORC1 is phosphatidic acid (PA) diacylglycerol (DAG) kinase pathway. The Hornberger laboratory has been at the forefront of investigation into the role of this pathway during mechanical loading, showing that stimulating DAG kinase results in an increase in PA concentrations and mTORC1 signaling [187, 188]. This group also showed that PA can directly bind to mTORC1, and to further strengthen the importance this pathway, they used a murine DGK ζ knockout mouse to show these mice exhibit impaired fCSA, protein accretion, and plantaris masses [133, 189, 190]. Human data from Thalacker-Mercer et al. [69] showed that higher levels of DGK ζ mRNA expression corresponded to higher hypertrophic responders following resistance training. Together these studies show that the mechanical induced activation

of DAG kinases results in increased PA concentrations leading to mTORC1 signaling and increased protein synthesis.

Another potential pathway for mechanotransduction induce skeletal muscle hypertrophy involves activation of transmembrane integrins and other accessory proteins that ultimately lead to mTORC1 signaling and increased protein synthesis [5]. Focal adhesion kinase (FAK) is a key protein in this pathway and has been shown to be increased in abundance and activity following acute and chronic overload in rodent muscle [191]. It has been further shown that FAK autophosphorylation precedes p70S6K activity in overloaded mice and shRNA-mediated FAK knockdown *in-vitro* leads to reduced protein synthesis and hypertrophy in myotubes [184, 192]. FAK co-localizes with integrins on the interior portion of the sarcolemma, and numerous lines of evidence support that FAK autophosphorylation associates with increased mTORC1 signaling [193-196]. Additional evidence of integrin and FAK pathway upregulation with mechanical loading comes from Chaillou et al. [7] showing increased mRNA expression of several integrin-linked kinase related genes in the early phase of synergist ablation. The aforementioned studies provide numerous lines of evidence for integrin and FAK mediated mechanotransduction, however several studies have challenged this hypothesis. Using a mouse model overexpressing the $\alpha_{7\text{BX}2}$ -integrin subunit ($\alpha_7\text{Tg}$ mouse), Boppart et al. [197] showed mTORC1 signaling was reduced following one bout of eccentric exercise, however the same $\alpha_7\text{Tg}$ mouse model performing multiple bouts of the same eccentric exercise experienced rapid increases in muscle hypertrophy [6]. In human skeletal muscle, studies have showed that FAK phosphorylation is not altered during a bout of resistance training despite an upregulation in p70S6K. and following chronic resistance training with eccentric contractions only elicits an increase in FAK phosphorylation even though concentric contractions (which produce less FAK phosphorylation)

result in the same level of hypertrophy [198, 199]. Taken together it is difficult to determine if integrin and FAK activation via mechanotransduction is involved in loading induced skeletal muscle hypertrophy.

Extracellular Matrix Remodeling and Adaptations to Mechanical Loading

The extracellular matrix (ECM) of skeletal muscle consists of a complex network of collagens, glycoproteins, proteoglycans, elastin, and various other proteins [200, 201]. ECM organization is defined by the layers including the epimysium that surrounds and supports the entire muscle, the perimysium that surrounds muscle fascicles, and the endomysium that surrounds each individual muscle fiber [202]. The ECM plays several key functions in mechanical load induced hypertrophy including providing structure, stiffness, force transmission, mechano-transduction, cell-to-cell communication, being a growth factor reservoir, and being involved with various other molecular aspects of skeletal muscle [28, 203-206].

ECM remodeling with mechanical loading and resistance training

ECM remodeling is starting to become recognized as a critical component of skeletal muscle hypertrophy from mechanical loading. As discussed earlier in this review, the Millward “bag theory” suggests that the “bag” (i.e., the ECM and its proteins) must remodel and expand for sustained increases in myofiber growth. In support of this concept of ECM remodeling during mechanical loading, multiple studies have sought to investigate the extent and necessity of ECM remodeling in both rodent and human models of skeletal muscle hypertrophy. Using synergist ablation in rats, Mendias et al. [205] showed that 3, 7, and 28 days of mechanical overload led to an increase in muscle concentrations of a collagen cross-link marker (pyridinoline) and a decrease in collagen structural stability marker (hydroxyproline). The authors also show that

mRNAs of several collagen proteins and MMPs were upregulated at one or multiple time points following overload. Additional studies in rodent models have provided further evidence that ECM remodeling and adaptations occur following mechanical loading [206-209].

Akin to the rodent data, multiple human studies have also demonstrated ECM remodeling and adaptations occur following various bouts of resistance training. For instance, collagen synthesis rates and gene/protein expression of several remodeling genes are increased following both acute and chronic bouts of resistance training [210-213]. Another concept regarding ECM remodeling and adaptations with skeletal muscle hypertrophy may involve higher and lower hypertrophic responders to resistance training. The premise behind this concept is that high responders may have enhanced ECM remodeling allowing for the enhanced expansion of myofibers, whereas low responders would have diminished ECM remodeling thereby constraining myofiber growth. With regards to higher and lower responders and ECM content, MacDougall et al. [214] showed that connective tissue content (as a percentage of imaged tissue) did not differ between body builders and non-exercised controls, despite the former cohort exhibiting larger fCSA values. To further explore the differences in ECM content and remodeling in higher and lower responders, Godwin et al. [215] showed that ECM content and remodeling markers were largely equal between responder cohorts following 10 weeks of resistance training. However, these data lacked time course resolution, and it remains possible that differences between cohorts may have been evident earlier in the training intervention.

Given the collective evidence in both rodent models and humans, it is clear that ECM remodeling and adaptations occur in response to mechanical loading induced skeletal muscle hypertrophy. However, this research is largely spurious and disjointed, and further research is needed to examine the time course of ECM remodeling, if ECM remodeling occurs prior to

hypertrophy or alongside it, and if ECM remodeling is required for optimal myofiber hypertrophy.

ECM as a growth factor reservoir

One of the key roles the ECM plays in skeletal muscle is being a reservoir for various growth factors [51, 216]. The ECM provides a latent pool of IGF-1, a positive regulator of skeletal muscle hypertrophy, through binding with ECM components like proteoglycans like decorin [217, 218]. In addition to binding and sequestering IGF-1, decorin also plays a role in IGF-1 signal transduction and the breakdown of decorin via MMP-2 can facilitate the release of IGF-1 further highlighting the role of ECM remodeling in skeletal muscle hypertrophy [219, 220]. Another growth factor that is sequestered in the ECM is the TGF- β superfamily of cytokines. Unlike IGF-1, TGF- β signaling is a negative regulator of skeletal muscle hypertrophy, inhibiting protein synthesis and satellite cell proliferation [221, 222]. Like IGF-1, TGF- β binds to decorin and other glycan proteins in the ECM, and the ECM-mediated regulation of TGF- β signaling results in healthy growth and development whereas dysregulation of TGF- β signaling leads to various maladaptive muscle traits [223, 224]. The ECM also stores and regulates the concentration of fibroblast growth factor (FGF). FGF signaling in skeletal muscle stimulates satellite cell proliferation and inhibits differentiation [225]. Like IGF-1 and TGF- β , FGF is regulated in part by proteoglycans which are required for FGF signal transduction to upregulate satellite cell proliferation and can temporally act to sequester FGF to permit differentiation [226-228]. The ECM's role as a growth factor reservoir further highlights the importance and impact the ECM has on regulating proper skeletal muscle growth and development.

Cell-To-Cell Communication in ECM Remodeling

ECM remodeling and adaptations are facilitated through the coordinated interactions of fibro-adipogenic progenitors (FAPs), fibroblasts, immune cells, and satellite cells [51, 229]. Details of each cell types' characteristics and function will be discussed later in the review, however it is important to note that these cells play a critical role in the homeostasis of ECM regulation during mechanical loading. For instance, FAPs and fibroblasts are the primary cells responsible for collagen deposition in skeletal muscle and are heavily influenced by their interaction with satellite cells [230-233]. Both resident and infiltrating macrophages are a significant source of TGF- β , which is a major regulating factor of ECM, as discussed above. Furthermore, the interaction between FAPs and macrophages can modulate the fibrotic status of the muscle environment [234]. Apart from communication with FAPs, satellite cells regulate ECM through communication with endothelial cells and the muscle fiber itself [235]. Genetic depletion of satellite cells or fusion incompetent satellite cells lead to excessive ECM deposition and a lack of ECM remodeling [230, 233, 236-238].

Introduction to Stromal Cells

Myofibers spatially occupy ~85-90% of muscle tissue, however a variety of other cells type reside within the ECM and basal lamina of muscle cells. The stromal cells that reside in muscle tissue include resident macrophages, FAPs, fibroblasts, adipocytes, and satellite cells [214, 239-242]. The number of each stromal cell within muscle tissue constantly changes with factors such as muscle fiber type composition, aging, and training status affecting these cell counts [243, 244]. Nonetheless, single cell/nuclei sequencing data in rodents have estimated that within the muscle tissue, the total nuclear pool consist of ~50-70% myonuclei, 20% FAPs, 17% endothelial cells, 4% pericytes, 4% resident immune cells (macrophages/neutrophils), 3%

neuronal, and 2% satellite cells [239, 245]. These stromal cells play an important role in the regulation and communication of multiple key aspects that facilitate skeletal muscle adaptations to mechanical loading.

Satellite Cells and Mechanical Loading

Satellite cells are the *bona fide* stem cell in adult skeletal muscle. Residing close to the myofiber outside the plasma membrane but within the basal lamina, satellite cells typically remain in a quiescent state until activated by a stressor (injury or growth) [246-248]. Satellite cells are primarily identified by expression of the transcription factor Pax7, and a lack of Pax7 positive cells during early development or preventing satellite cell fusion during development leads to diminished skeletal muscle growth [49, 248-251]. Satellite cells serve multiple functions in skeletal muscle tissue. Satellite cells, once activated, can fuse to existing myofibers and either be involved in repairing damaged areas of the myofiber or can contribute to the accumulation of new myonuclei [252-255]. Another function of satellite cells that is starting to gain more appreciation are the fusion-independent roles satellite cells have in regulating homeostatic conditions in skeletal muscle [233, 235, 256-260].

Early rodent work by Schiaffino and colleagues showed that following mechanical overload, satellite cells exhibit increased proliferation and some of these satellite cells become incorporated (or fuse) into the overloaded fibers [254, 255]. These early findings have since been supported by a multitude of human studies, showing an increase in myonuclear number and satellite cells following various resistance training paradigms [118, 241, 247, 261-267]. Furthermore, myonuclear number has been shown to scale with myofiber size in both mice and humans [49, 50]. While myonuclear content scales with cell size, myonuclear domain (area in

which each myonuclei govern) size is flexible during earlier stages of hypertrophy, especially in type 2 myofibers in humans [268-271].

To answer more intricate questions regarding satellite cell necessity and function, several genetic mouse models have been employed. Most notably, the Pax7-DTA mouse utilizes the Cre-loxP system to drive the expression of diphtheria toxin A in a cell-specific manner to effectively deplete satellite cells [272]. The first to use the Pax7-DTA mouse was McCarthy et al. [273] in 2011 where the authors reported that the removal of ~90% of satellite cells followed by 14 days of mechanical overload did not impair muscle growth. In contrast to the McCarthy group, Egner et al. [274] replicated the approach of McCarthy but showed that satellite cells are necessary for load-induced hypertrophy. The key difference between the two studies was that McCarthy and colleagues used adult mice (aged 4 months), whereas Egner and colleagues used juvenile mice (aged 2-3 months). This difference was later confirmed by Murach et al. [275] who reported an impairment in hypertrophy after overload in juvenile (aged 2 months) Pax7-DTA mice. Further evidence supporting the necessity of satellite cell fusion during development comes from Millay et al. [276], whereby the authors used a genetic myomaker knockout mouse model (a protein needed for myoblast fusion) to show that myoblast (satellite cell) fusion is necessary for proper muscle development. This group also utilized the myomaker knockout mouse to prevent myonuclear accretion during 14-days of overload, and these findings agreed with Egner colleagues in that satellite cell fusion is required for increased muscle hypertrophy after 14-days of mechanical overload [237]. While the synergist ablation model is useful in inducing a large amount of hypertrophy, it is often a supra-physiological model in that the degree of overload stimulus is rarely achieved in humans. To examine if satellite cell fusion and myonuclear accretion are required for skeletal muscle hypertrophy with a more physiological

stimulus, Goh et al. [238] utilized the myomaker knockout mouse with 8 weeks of HIIT on an inclined treadmill, showing blunted hypertrophy and intolerance to exercise without muscle progenitor fusion. Like the aforementioned study, Englund et al. [277] also showed blunted hypertrophy following 8-weeks of progressive weighted wheel running using the Pax7-DTA model.

Satellite cells also play a significant non-fusion role in skeletal muscle adaptations to mechanical loading [278]. One of the more prominent non-fusion roles of satellite cells is the cell-to-cell communication in the regulation of extracellular matrix content and remodeling with mechanical loading and repair. Studies have shown communication between satellite cells and fibroblasts during regeneration [256, 279]. In the absence of substantial muscle damage, but with unaccustomed resistance exercise, satellite cell proliferation is associated with an upregulation of ECM remodeling genes [280]. More compelling evidence of satellite cell involvement in ECM remodeling comes a series of studies from Fry and colleagues [230, 233]. Using the Pax7-DTA model, these authors reported that skeletal muscle hypertrophy was blunted after 8-weeks of overload, and this coincided with a significant increase in fibrosis. Further *in vitro* experiments from these studies showed that muscle progenitor cells communicate with fibroblasts via miRNA containing exosomes to regulate various collagen related genes. Satellite cells also communicate with other stromal cells (e.g., FAPs, macrophages, endothelial cells, and mesenchymal progenitors) during early stages of skeletal muscle hypertrophy [231, 235, 260, 281].

These studies mentioned above provide a strong case for the necessity of satellite cells during skeletal muscle hypertrophy. Outside of the common role of satellite fusion and myonuclear accretion, satellite cells also demonstrate an appreciable role in non-fusion related signaling and communication with other cell types to regulate the skeletal muscle micro-

environment. Furthermore, these studies show that even with a more physiologically relevant stimulus, satellite cells are needed to support long-term skeletal muscle adaptations.

Fibroblasts and Mechanical Loading

Skeletal muscle fibroblasts are mononuclear cells residing in the interstitial space between muscle fibers and are identified by expression of the Tcf4 transcription factor [256, 282, 283]. In skeletal muscle, fibroblasts produce ECM components like collagen and other scaffolding proteins and have been heavily implicated in the regeneration and development of skeletal muscle [282, 283]. In regenerating muscle, fibroblast Tcf4 expression is associated with increases in ECM accumulation, showing further support for fibroblast's role in ECM component synthesis [284]. Murphy et al. [256] utilized a combination of Pax7^{CreER} and Tcf4^{CreER} mouse models to show that communication between satellite cells and fibroblasts is critical for both development and regeneration in skeletal muscle. Further evidence of satellite cell and fibroblast communication comes from Fry et al. [230, 233], briefly discussed above. In these studies, Fry et al. show that in satellite depleted mice following chronic mechanical overload, skeletal muscle hypertrophy is impaired. The authors also reported that satellite cell-derived exosomes containing miR-206 regulate fibroblast production of collagen synthesis by modulating the activity of Rrbp1. They also reported that in the absence of satellite cells, and thus miR-206 containing exosomes, Rrbp1 expression is increased in fibroblasts leading to excessive collagen synthesis and ECM accumulation. Collectively, these studies show that fibroblasts and their role in communication with other stromal cell types are critical for proper regeneration and regulation of skeletal muscle tissue.

Fibro-adipogenic Progenitor Cells and Mechanical Loading

Fibro-adipogenic progenitor cells (FAPs) are interstitial mesenchymal progenitors that are generally characterized by PDGFR α expression and exist within skeletal muscle in a dynamic state, meaning they can adopt multiple lineages [285, 286]. FAPs are essential for proper regeneration and maintenance of skeletal muscle due to their ability to adopt multiple lineages and through their interaction with other cell types [231, 287-290]. Evidence of the necessity of FAPs comes from the Rando laboratory using a PDGFR α ^{CreER} mouse model to genetically deplete FAPs prior to injury, showing that muscle regeneration is greatly impaired in FAP depleted muscle [290]. With regards to mechanical loading, Kaneshige et al. [231] used a PDGFR α -GFP genetic mouse model to show FAPs are responsive to mechanical loading and undergo modest proliferation 2-4 days following tenotomy. These authors also used the PDGFR α ^{CreER} mouse to determine if FAPs are essential for proper adaptations to mechanical loading, showing that in the absence of FAPs adaptations are impaired. These along with findings suggest that FAP communication with satellite cells during various stimuli are essential for proper adaptations [291, 292]. In human skeletal muscle, FAPs are responsive to damaged and regenerating tissue and are associated with expansion of ECM [284]. Furthermore, following resistance training in human skeletal muscle the percentage of proliferating FAPs has been shown to increase [293] and a subset of FAPs co-expressing Twist-2 is also responsive to resistance training [294]. Collectively these studies suggest that, like satellite cells, FAPs are essential in the homeostatic maintenance of skeletal muscle in response to a variety of stimuli.

Macrophages and Mechanical Loading

In skeletal muscle, macrophages play a variety of roles in supporting proper homeostasis of the muscle tissue [295, 296]. With regards to mechanical loading and resistance training, several studies show that both pro-inflammatory (M1) and anti-inflammatory (M2) sub-

populations increase in young adults and older adults [297-299]. In addition to increased macrophage number, macrophage recruitment has been shown to be necessary for skeletal muscle hypertrophy following mechanical overload [300]. It has also been shown that macrophages produce factors that promote growth (IGF-1) and ECM remodeling (TGF- β) [301, 302]. A recent study by Peck et al. [303] sought to investigate the effects of resistance training on ECM remodeling mechanisms. These authors performed several *in vitro* experiments showing electrically stimulated myotubes secrete leukemia inhibitory factor (LIF), which in turn, increases production of MMP-14 from macrophages. These data, along with others showing diminished hypertrophic outcomes in older participants with high abundance of pro-inflammatory macrophages [304], highlight the importance of macrophage involvement in skeletal muscle hypertrophy.

Conclusion

The topics and studies discussed above highlight the intricate nature of skeletal muscle hypertrophy induced via mechanical loading. Multiple pathways are tightly regulated and are involved to meet the end goal of increased protein synthesis and protein accumulation. It is also important to highlight the complex coordination and communication between various stromal cells within the skeletal muscle tissue and their role in remodeling the muscle micro-environment to enable proper hypertrophic growth. While these studies show the advancements that have been made in understanding these processes, mechanisms involved in the regulation of skeletal muscle hypertrophy via mechanical loading are frequently being researched and will continue to be expanded upon.

Chapter III: Methods

Human Participants

The human data portion of this investigation is a secondary analysis of a study that was approved by the Auburn University Institutional Review Board (IRB) (Protocol # 19-249 MDR 1907), conformed the standards set by the latest revisions of the Declaration of Helsinki, and was registered as a clinical trial (NCT04707963). The intent of the originally approved trial was to determine if daily peanut protein supplementation (SUP) versus no supplementation (control group [CON]), affected RT-related adaptations [305]. In the present study we utilized a subset of muscle samples still available from the previously mentioned study (i.e., 9 women from the SUP group and 6 women from the CON group). Our sub-sample presented no differences between SUP and CON groups for fCSA ($P = 0.264$), vastus lateralis cross-sectional area (by ultrasonography) ($P = 0.421$), thigh cross-sectional area (by peripheral computed tomography) ($P = 0.855$), as previously demonstrated (34836236). Therefore, we collapsed data from SUP and CON groups to perform the analyses presented herein. Samples were from 15 young women (age: 21 ± 2 yr, body mass index: 24.6 ± 3.7 kg/m²) who had not participated in RT programs, were free of obvious cardiovascular or metabolic disease or other conditions contraindicating participation in exercise programs or donating muscle biopsies, and who were not pregnant or trying to become pregnant.

Experimental Design for Human Training Study

Initially, after muscle imaging assessments (results previously published and not presented here), muscle samples were collected through biopsies obtained from vastus lateralis. Afterwards, participants engaged in familiarization sessions with the RT protocol and test procedures. After familiarization sessions, participants started an RT program with 2 sessions per week for 10 weeks. Seventy-two hours after the last RT session all assessments (including the procurement of a muscle biopsy) were repeated. For more details related to the study design and resistance training program, readers are referred to Sexton et al. [305].

Vastus Lateralis Muscle Biopsies

The pre- and post-intervention vastus lateralis muscle biopsies were performed from the right leg. Initially the participants laid down on an athletic table where the upper thigh was shaved and cleaned with 70% isopropanol. A subcutaneous injection of 1% lidocaine (0.8 mL) was administered. After 5 minutes, the area was cleaned with chlorhexidine solution. Thereafter, a 7 mm-width pilot incision was made through the dermis with a sterile No. 11 surgical blade (AD Surgical; Sunnyvale, CA, USA). The 5-gauge biopsy needle was inserted into the pilot incision, through the muscle fascia, and ~2 cm into the muscle (for a total depth of ~4-7 cm) where a 40-80 mg sample was collected while applying suction. Following biopsies, tissue was rapidly teased of blood and connective tissue. A portion of the tissue (~10–20mg) was preserved in optimal cutting temperature (OCT) media for histology (Tissue-Tek®, Sakura Finetek Inc.; Torrance, CA, USA), slow frozen in liquid nitrogen-cooled isopentane, and subsequently stored at –80°C. Another portion of the tissue (~30–50mg) was placed in pre-labeled foils, flash frozen in liquid nitrogen, and subsequently stored at –80°C for other molecular analyses described below.

Resistance Training Program

The resistance training program was described in detail previously [305]. Briefly, resistance training bouts consistent of participants performing a 45° leg press, leg extension, hex-bar deadlifts, flat barbell bench press, and wide-grip cable pulldown exercises. The same exercise order was followed for all training sessions, and two day per week training sessions consisted of performing 4 sets of 10 repetitions for each exercise one day per week, and 5 sets of 6 repetitions for each exercise one day per week. Two-minute rest intervals between sets and exercises were allotted throughout the training intervention. The training load was progressively increased on a session-by-session basis using the rating of perceived exertion (RPE) scale of 1-10 (“really easy” to “really hard”) so that each set was performed close to concentric muscle failure.

Sarcoplasmic and sarcolemmal protein isolations

Isolation of sarcoplasmic and sarcolemmal protein from muscle tissue was performed initially using a high-fidelity membrane protein extraction kit according to manufacturer’s recommendations (Mem-PRE Plus Membrane Protein Extraction Kit; Thermo Fisher Scientific; Waltham, MA, USA). This process yielded solubilized sarcoplasmic and sarcolemmal protein isolates.

Protein concentrations for both fractions were determined in duplicate the same day as protein isolations to minimize freeze-thaw effects using a commercially available assay (BCA Protein Assay Kit; Thermo Fisher Scientific). Thereafter, fractions were stored at -80°C until

analysis occurred. Duplicate coefficient of variation (CV) values for the sarcoplasmic and sarcolemmal proteins readings were 2.3% and 2.4%, respectively.

Proteomics on sarcolemmal protein isolates

Sarcolemmal protein isolates were shipped to a commercial vendor for proteomics using a nanoLC-MS/MS platform (Creative Proteomics; Shirley, NY, USA). Briefly, samples were treated with 50 mM ammonium bicarbonate, and resultant solutions were transferred to Microcon devices YM-10 (Millipore; Burlington, MA, USA). Samples were then centrifuged at 12,000g at 4°C for 10 minutes. Protein concentrates were again treated with 50 mM ammonium bicarbonate and centrifuged again. Concentrates were then reduced using 10 mM DTT at 56°C for 1 hour and alkylated by 20 mM IAA at room temperature in dark for 1 hour. Following reduction reactions, and one wash with 50 mM ammonium bicarbonate and centrifugation (12,000g at 4°C for 10 minutes), concentrates were incubated with 100 µL of 50 mM ammonium bicarbonate and free trypsin (ratio of 1:50) at 37°C overnight. Samples were then centrifuged at 12,000g at 4°C for 10 minutes, and 100 µL of 50 mM ammonium bicarbonate was added to Microcon devices and centrifuged (total of two washes). Peptides were then isolated, lyophilized to near dryness, and resuspend in 20 µL of 0.1% formic acid for LC-MS/MS analysis.

Nanoflow UPLC was performed using the Ultimate 3000 nano UHPLC system (Thermo Fisher Scientific). Associated hardware included a trapping column (PepMap C18, 100Å, 100 µm×2 cm, 5µm) and analytical column (PepMap C18, 100Å, 75 µm × 50 cm, 2 µm). Mobile phase A consisted of 0.1% formic acid in water, and mobile phase B consisted of 0.1% formic acid in 80% acetonitrile. UPLC runs consisted of 1 µL injections, a linear gradient from 2-8% buffer B for 3 minutes, from 8-20% buffer B for 56 minutes, 20-40% buffer B in 37 minutes,

then from 4-90% buffer B for 4 minutes. Back-end mass spectrometry (MS) scans were performed between 300-1,650 m/z at a resolution of 60,000 at 200 m/z. The automatic gain control target for the full scan was set to 3e6. MS/MS scans were operated in Top20 mode using the following settings: resolution 15,000 at 200 m/z; automatic gain control target 1e5; maximum injection time 19 milliseconds; normalized collision energy at 28%; isolation window of 1.4 Th; charge state exclusion: unassigned, 1, > 6; dynamic exclusion 30 seconds.

MS files were analyzed against a HUMAN protein database using Maxquant (v1.6.1.14). Search parameters were set as follows: i) the protein modifications were carbamidomethylation (C) (fixed), oxidation (M) (variable), ii) the enzyme specificity was set to trypsin, iii) the maximum missed cleavages were set to 2, iv) the precursor ion mass tolerance was set to 10 ppm, and v) MS/MS tolerance was 0.6 Da. 1866 total peptides were identified, and these proteins were further queried using the PANTHER Classification system (pantherdb.org) to delineate sarcolemmal membrane-associated proteins, which yielded 386 total peptides. These peptides were then subjected to statistical analyses where up-regulated and down-regulated proteins from pre-to-post training were considered to exceed a ± 1.5 -fold threshold ($p < 0.05$) as recommended by Levin [306]. Notably, all proteomic data are presented as relative spectra values.

Mice Experiments

Mouse experiments not involving AAV9 injections (female wild-type C57BL/6 and Pax7-DTA sham and overload mice) were conducted in accordance with the institutional guidelines for the care and use of laboratory animals as approved by the Animal Care and Use Committee of the University of Kentucky. All mice were housed in a climate-controlled room and maintained on a 14:10 hour light-dark cycle, food and water were allowed ad libitum. For

satellite cell depleted mice the *Pax7^{CreER/+}; Rosa26^{DTA/+}* strain, called Pax7-DTA throughout, was generated as previously described [273]. Mouse experiments involving AAV9 injections were approved by the Animal Care and Use Committee of the University of Nebraska. Again, mice were housed in a climate-controlled room and maintained on a 14:10 hour light-dark cycle, food and water were allowed ad libitum. For AAV9 experiments, female wild-type C57BL/6 mice were anesthetized under isoflurane, and plantaris muscles were injected with 30 uL (5x10⁹ particles) of either AAV9 VIM shRNA (catalog #: AA09-MSE096513-AVE001-A00) or AAV9 scr. shRNA (catalog #: SHD05); both of which were commercially developed (GeneCopoeia; Rockville, MD, USA) and contained a CMV promoter and GFP reporter. Following 30-days of viral incubation, mice were subjected to unilateral synergist ablation or sham surgeries as described below.

Conditional Ablation of Satellite Cells

Adult (≥ 4 months of age) Pax7-DTA mice described elsewhere (21828094) were administered an intraperitoneal injection of either a vehicle (15% ethanol in sunflower seed oil) or tamoxifen (2 mg/day) for 5 consecutive days. Following a 2-week washout period, vehicle and tamoxifen-treated mice were divided into sham or synergist ablation (10-day or 20-day) groups.

Synergist Ablation Surgeries in Mice

Surgical removal of synergist muscles (part of gastrocnemius and soleus) to subject the plantaris muscle to mechanical overload was performed as previously described (21828094). Briefly, mice were anesthetized with an intraperitoneal injection of ketamine (100 mg/kg) and xylazine (10 mg/kg), a longitudinal incision was made on the dorsal aspect of the lower

hindlimb, and the tendon of the gastrocnemius muscle was isolated and used as a guide to excise the soleus and part of the gastrocnemius. The incision was then sutured, and the animals were allowed to recover. Sham surgeries involved similar incision and suture procedures without the excision of muscle. Ten or 20-days following surgeries, mice were anesthetized, euthanized via cervical dislocation, and the plantaris muscle was excised. Immediately following removal, plantaris muscles were weighed and either flash-frozen in liquid nitrogen or prepared for immunohistochemical analysis via preservation in OCT media.

Human Muscle Immunohistochemistry

Human fCSA Determination. Human skeletal muscle samples were examined for mean fiber cross-sectional area (fCSA) using immunohistochemistry (IHC) as previously described by our laboratory [305]. Briefly, slides with sections were dried 10 minutes at room temperature. Triton-X (0.5%) in phosphate buffer solution (PBS) was used to permeabilize the sections for 5 minutes. Thereafter, slides were washed in PBS for 5 minutes and subsequently incubated in blocking solution for 15 minutes (Pierce Super Blocker; Thermo Fisher Scientific). Slides were incubated in primary antibody solution (1x PBS, 5% of Pierce Super Blocker Solution, and 2% [or a 1:50 dilution] of rabbit anti-dystrophin IgG1 [catalog #: GTX15277; Genetex Inc.; Irvine, CA, USA] and mouse anti-myosin I IgG1 (catalog #: A4.951 Developmental Studies Hybridoma Bank; Iowa City, IA, USA) for 1 hour. Slides were then washed for 5 minutes in PBS and incubated in a secondary antibody solution (1x base of PBS, and 1% [or 1:100 dilution] Texas Red-conjugated anti-rabbit IgG [catalog #: TI-1000; Vector Laboratories, Burlingame, CA, USA] and Alexa Fluor 488-conjugated anti-mouse IgG1 (catalog #: A-11001; Thermo Fisher Scientific) for 1 hour in the dark at room temperature. Slides were then mounted in fluorescent

media and imaged using a fluorescent microscope (Nikon Instruments, Melville, NY, USA) with a 10x objective lens. Open-sourced software (MyoVision) was used to analyze all images for mean fCSA [307].

Phalloidin staining. For determination of myofibril area per fiber, F-actin labelling using phalloidin-conjugated to Alexa Fluor 594 (AF594) was performed. Briefly, serial sections were allowed to air dry for ~1.5 – 2 hours at room temperature followed by fixation in chilled acetone for 5 minutes. Sections were then incubated with 3% H₂O₂ for 15 minutes and true black (catalog #: 23007 Biotium; Fremont, CA, USA) for 1 minute to reduce auto-fluorescence. Sections were then blocked with 2.5% BSA/5% goat serum for 1 hour. Sections were incubated overnight in 4°C with mouse anti-dystrophin MANDY S8 (1:20) (catalog #: 8H11; Developmental Studies Hybridoma Bank). The following morning, sections were incubated for 1 hour with phalloidin conjugated to AF594 (1:100) (catalog #: A12381; Thermo Fisher Scientific) and Alex Fluor 488-conjugated anti-mouse IgG1 (1:250) (catalog #: A11001; Thermo Fisher Scientific). Sections were incubated with DAPI (1:10,000) (catalog #: D3571; Thermo Fisher Scientific) for 15 minutes. Slides were then mounted with glass cover slips using 50/50 PBS+glycerol. Digital images were captured using a fluorescent microscope (Nikon Instruments) using a 20x objective. Quantification of myofibril area per fiber was performed using ImageJ software (National Institutes of Health; Bethesda, MD, USA) according to previous reports [34, 308]. Briefly, images were split into RGB channels, and the red channel image was converted to gray scale. The threshold function was then used to generate a binary black/white image of stained versus portions of fibers. Fibers were then traced, and myofibril area were provided as a percentage per fiber area. Representative images of analysis are provided in results. The coefficient of variation (CV) between two measurements performed 72 hours apart was 0.26% [308].

Mouse Plantaris Immunohistochemistry

Vimentin area and fCSA determinations. Mouse plantaris muscles preserved for IHC were sectioned at 7- μ m thickness using a cryotome (Leica Biosystems; Buffalo Grove, IL, USA) and adhered to multiple positively charged slides for the interrogation of various targets as explained in this and subsequent paragraphs. Following slide adhesion, sections were allowed to air dry prior to being stored at -80°C until further analysis.

Sections from sham mice and mice subjected to mechanical overload were stained for vimentin, dystrophin, and nuclei to assess myofiber characteristics and vimentin expression. Briefly, samples were fixed in ice cold acetone for 5 minutes followed by 3% hydrogen peroxide (H₂O₂) for 10 minutes and true black incubation for 1 minutes to reduce autofluorescence. Sections were then blocked with 5% goat serum/2.5% BSA for at least 1 hour before overnight incubation at 4°C of an antibody cocktail consisting of rabbit anti-vimentin (1:100) (catalog #: 5741; Cell Signaling Technologies; Danvers, MA, USA), mouse anti-dystrophin IgG2b (1:50) (catalog ID: Mandy S8; Developmental Studies Hybridoma Bank), and 2.5% BSA. After primary antibody incubations, sections were incubated for 1 hour with a secondary antibody cocktail consisting of anti-rabbit AF488 (Vector Laboratories), anti-mouse IgG2b AF594 (catalog #: A-21145; Thermo Fisher Scientific), and PBS. Following secondary antibodies, sections were incubated with DAPI (1:10,000) (catalog #: D3571; Thermo Fisher Scientific) for 10 minutes. Coverslips were then added using PBS + glycerol as mounting media. Digital images of entire sections were captured using a fluorescent microscope (20x objective; Zeiss Axio imager.M2) and motorized scanning stage.

Satellite Cells and Vimentin Co-expression. Sections stained for satellite cells and vimentin to determine co-expression were first fixed in ice cold acetone for 5 minutes followed by 3% H₂O₂ incubation for 10 minutes. Sections were then subjected to an epitope retrieval protocol. This protocol first involved incubating sections with sodium citrate for 2 minutes at room temperature followed by incubation in pre-warmed (65°C) sodium citrate. Sections were then placed in a water bath incubator until they reached 92°C. Sections were then incubated for 11 minutes at 92°C and allowed to cool in water bath until 50°C then cooled to room temperature. Following epitope retrieval, sections were incubated with true black for 1 minute to reduce autofluorescence. Sections were then blocked using 5% goat serum/2.5% BSA for at least 1 hour followed by biotin and streptavidin blocking solutions for 15 minutes each. Sections were incubated with an antibody cocktail containing: i) mouse anti-Pax7 IgG1 (1:100), ii) mouse anti-dystrophin IgG2b (1:50), rabbit anti-vimentin (1:100), and 2.5% BSA overnight at 4°C. Following primary antibody incubations, sections were incubated with biotin-SP-conjugated goat anti-mouse IgG1 (1:1,000) (catalog #: 111-065-003; Jackson ImmunoResearch; West Grove, PA, USA) in 2.5% BSA for 90 minutes. Sections were then incubated with a secondary antibody cocktail consisting of SA-HRP (1:500) (catalog #: S-911; Thermo Fisher Scientific), goat anti-rabbit AF488 (1:250) (Vector Laboratories), and goat anti-mouse IgG2b AF647 (1:250) (catalog #: A21242; Thermo Fisher Scientific) for one hour. TSA AF555 (1:200) (catalog #: B-40955; Thermo Fisher Scientific) was added for 20 minutes, followed by DAPI for 10 minutes. Coverslips were added using PBS + glycerol as mounting medium. Digital images of entire sections were captured using a fluorescent microscope (20x objective; Zeiss Axio imager.M2) and motorized scanning stage. Co-expression of vimentin and satellite cells was determined by area of vimentin per Pax7+/DAPI+ cells.

Fibroblast and Vimentin Co-expression. Sections stained for fibroblasts and vimentin to determine co-expression were first fixed with ice cold acetone for 5 minutes, followed by incubation with 3% H₂O₂ for 10 minutes. Sections then underwent epitope retrieval as described above, followed by incubation with true black for one minute to reduce autofluorescence. Sections were then blocked with 5% goat serum/2.5% BSA for at least one hour followed by biotin and streptavidin solution blocking for 15 minutes each. Following the blocking step, sections were incubated overnight at 4°C with rabbit anti-TCF4 (1:100) (catalog #: 2569; Cell Signaling Technologies) in 2.5% BSA. Sections were then incubated with goat biotin-conjugated anti-rabbit IgG (1:1000) (catalog #: 111-065-046; Jackson ImmunoResearch) in 2.5% BSA for 90 minutes, followed by incubation with SA-HRP (1:500) for one hour. Sections were then incubated with TSA-488 (1:400) (catalog #: B-40953; Thermo Fisher Scientific) for 20 minutes followed by incubation with DAPI for 10 minutes. Sections were briefly checked under microscope to ensure proper staining for TCF4 before being re-fixed in 4% PFA for 10 minutes followed by blocking with 5% goat serum/2.5% BSA and biotin/streptavidin solutions for at least one hour. Sections were then incubated overnight at 4°C with antibody cocktail consisting of mouse anti-dystrophin IgG2b (1:50), rabbit anti-vimentin (1:100), and 2.5% BSA. Sections were then incubated with a secondary antibody cocktail consisting of goat anti-rabbit AF555 (1:250), and goat anti-mouse IgG2b AF647 (1:250) for one-hour, followed by incubation with DAPI for 10 minutes. Coverslips were added using PBS + glycerol as mounting medium. Digital images of entire sections were captured using a fluorescent microscope (20x objective; Zeiss Axio imager.M2) and motorized scanning stage. Co-expression of vimentin and fibroblasts was determined by area of vimentin per TCF4+/DAPI+ cells.

Fibro-adipogenic Progenitors and Vimentin Co-expression. Only wild type mouse plantaris sections were stained for fibro-adipogenic progenitors (FAPs) and vimentin to determine the co-expression of the two using IHC. Briefly, sections were fixed with 4% PFA for 10 minutes, then incubated with 3% H₂O₂ for 15 minutes, and true black for one minute to reduce autofluorescence. Sections were then blocked with 2.5% BSA/0.1% Triton-X for at least one hour. Following the blocking step, sections were incubated overnight at 4°C with an antibody cocktail consisting of goat anti-mouse PDGFR α (1:100) (catalog #: AF1062; R&D Systems; Minneapolis, MN, USA), rabbit anti-vimentin (1:100), and 2.5% BSA. Sections were then incubated with secondary antibody cocktail for two hours consisting of donkey anti-goat AF555 (1:250) (catalog #: A-21432; Thermo Fisher Scientific), donkey anti-rabbit AF488 (1:250) (catalog #: A-21206; Thermo Fisher Scientific), and Wheat germ agglutinin (WGA) (1:50) (catalog #: W-32466; Thermo Fisher Scientific). Sections were then incubated with DAPI for 10 minutes and coverslips were added using PBS + glycerol as mounting medium. Digital images of entire sections were captured using a fluorescent microscope (20x objective; Zeiss Axio imager.M2) and motorized scanning stage. Co-expression of vimentin and fibroblasts was determined by area of vimentin per PDGFR α ⁺/DAPI⁺ cells.

Macrophage and Vimentin Co-expression. Again, only wild type mouse muscle was stained for macrophages and vimentin to determine the co-expression of the two using IHC. Briefly, sections were fixed with ice cold acetone for 10 minutes followed by incubated with 3% H₂O₂ for 10 minutes. Sections were then blocked with 5% goat serum/2.5% BSA for at least one hour. Sections were then incubated overnight at 4°C with antibody cocktail consisting of rat anti-F4/80 (1:100) (catalog #: MCA497; Bio-Rad Laboratories; Hercules, CA, USA), rabbit anti-vimentin (1:100), and mouse anti-dystrophin IgG2b (1:50). Following overnight incubation with

primary antibodies, sections were incubated with goat anti-rat biotin (1:500) (catalog #: 31830; Thermo Fisher Scientific) in 2.5% BSA for 90 minutes. Sections were then incubated with secondary antibody cocktail for one hour consisting of SA-HRP (1:500), goat anti-rabbit AF488 (1:250), and goat anti-mouse IgG2b AF647 (1:250). TSA AF555 (1:200) was added for 20 min, followed by DAPI for 10 minutes. Coverslips were added using PBS + glycerol as mounting medium. Digital images of entire sections were captured using a fluorescent microscope (20x objective; Zeiss Axio imager.M2) and motorized scanning stage. Co-expression of vimentin and fibroblast was determined by area of vimentin per F4/80+/DAPI+ cells.

Cell Culture Experiments

Low passage (passage 3-5) immortalized C2C12 myoblasts (ATCC; Manassas, VA, USA) were used to determine vimentin protein expression throughout various stages of proliferation and differentiation as well as in response to an anabolic stimulus (insulin-like growth factor, IGF-1), and experiments occurred in a humidified CO₂ incubator at 37°C using 5% CO₂-95% room air. Myoblasts (100,000 cells per mL) were seeded onto six-well plates in growth medium (GM) containing Dulbecco's modified Eagle's Medium (DMEM; Corning, Corning, NY) supplemented with 10% fetal bovine serum and 1% penicillin/streptomycin. Once cells reached confluency (~85-90%), differentiation was induced by switching to differentiation medium (DM), consisting of DMEM supplemented with 2% horse serum. Once complete differentiation into myotubes was reached, cells in one experiment were treated with 10 µM arabinosylcytosine (AraC; Sigma, St. Louis, MO, USA) for 24 hours to kill unfused myoblasts [309]. Myotubes were then treated with either PBS (CTL) or various doses (100 ng/mL, 200 ng/mL, 400 ng/mL) of recombinant mouse IGF-1 (catalog #: 791-MG-050; R&D Systems) for

24 hours. A separate set plates that did not receive AraC treatments were used to determine how unfused myoblasts affected vimentin expression. Finally, a third set of plates were examined at 0 days, 1 day, 3 days, 5 days, and 7 days after the initiation of differentiation to determine how differentiation affected vimentin expression. At the end of experimental time lines, cells were washed with PBS and 500 μ L of 1x cell lysis buffer (catalog #: 9803S; Cell Signaling Technologies) was used to collect lysates. Lysates were then centrifuged at 500 g for 5 minutes (4°C), supernatants were transferred to 1.7 mL microtubes, and lysates were stored at -80°C until western blotting.

Western Blotting and qPCR

For myotube lysate western blotting, protein concentrations were determined using a commercially available bicinchoninic acid (BCA) kit (Thermo Fisher Scientific). Cell lysates were prepared at a concentration of 1 μ g/ μ L and 15 μ L of sample were loaded onto gradient SDS-polyacrylamide gels. Western blotting procedures throughout were performed as previously described from our laboratory [215] using the rabbit anti-vimentin antibody described above (1:1,000). Membranes were developed using chemiluminescent substrate (EMD Millipore) and imaged using a gel documentation system (ChemiDoc Touch; Bio-Rad Laboratories). Vimentin protein band densities were obtained using associated software (Image Lab v6.0.1; Bio-Rad Laboratories) and normalized to Ponceau lane densities. Target/Ponceau density ratios were normalized to either vehicle-control treatments (IGF-1 experiments) or day 0 differentiation (differentiation phase experiments).

Plantaris muscle RNA and protein from one mouse experiment (Fig. 2 in Results) were isolated using the modified Trizol-bromochloropropane protocol described by Wen et al.

(32777951). Following RNA isolation, the RNA pellet was resuspended in 20 μ L of RNase-free water and RNA concentrations were determined in duplicate at an absorbance of 260 nm by using a NanoDrop Lite (Thermo Scientific). Thereafter, cDNA (1 μ g) was synthesized using a commercial qScript cDNA SuperMix (Quanta Biosciences, Gaithersburg, MD, USA) per the manufacturer's recommendations. qPCR was performed with gene-specific primers and SYBR-green-based methods (Quanta Biosciences) with gene-specific primers designed with primer design software (Primer3Plus, Cambridge, MA, USA) using a real-time PCR thermal cycler (Bio-Rad Laboratories). Protein was isolated from the organic phase as described by Wen et al. [310], and vimentin was interrogated using the rabbit anti-vimentin antibody described above (1:1,000). Vimentin protein band densities were obtained as described in the prior paragraph and normalized to Ponceau lane densities. Target/Ponceau density ratios were normalized to the Sham group.

Statistical Analyses

Statistical analyses were performed using GraphPad Prizm (Version 9.3.1; San Diego, CA). Human dependent variables (including proteomics data) were analyzed using dependent samples t-tests. All mouse experiments variables were analyzed using one-way ANOVAs and Tukey's post-hoc corrections were applied for multiple comparisons analysis. Pax7-DTA and AAV9 mouse experiment variables were analyzed using two-way ANOVAs with Tukey's post-hoc corrections for multiple comparisons analysis. Select associations between dependent variables were also analyzed using Pearson correlations. All data are presented as mean \pm standard deviation (SD) values, and statistical significance was set at $p < 0.05$.

Chapter IV: Tentative manuscript (to be submitted to eLife)

Vimentin is a cytoskeletal protein mechanistically associated with mechanical overload-induced skeletal muscle hypertrophy

Joshua S. Godwin¹, J. Max Michel¹, Cleiton A. Libardi², Andreas N. Kavazis¹, Christopher S. Fry³, Andrew D. Frugé^{1,4}, Mariah McCashland⁵, Ivan Vechetti⁵, C. Brooks Mobley^{1,*}, Michael D. Roberts^{1,*}

¹Nutrabort Applied and Molecular Physiology Laboratory, School of Kinesiology, Auburn University, Auburn, AL, USA; ²MUSCULAB–Laboratory of Neuromuscular Adaptations to Resistance Training, Department of Physical Education, Federal University of Sao Carlos, Sao Carlos, Brazil; ³Department of Athletic Training & Clinical Nutrition, University of Kentucky, KY, USA; ⁴College of Nursing, Auburn University, Auburn, AL, USA; ⁵Department of Nutrition and Health Sciences, University of Nebraska, NE, USA

Running title: Vimentin and skeletal muscle hypertrophy

Keywords: cytoskeletal protein, mechanical overload, muscle protein synthesis, extracellular matrix, skeletal muscle hypertrophy

Co-correspondence:

Michael D. Roberts, PhD
Auburn University Alumni Professor
Nutrabort Applied and Molecular Physiology Laboratory
School of Kinesiology, Auburn University
Email: mdr0024@auburn.edu

C. Brooks Mobley, PhD
Assistant Clinical Professor
Nutrabort Applied and Molecular Physiology Laboratory
School of Kinesiology, Auburn University
Email: moblecb@auburn.edu

ABSTRACT

Our laboratory has performed various experiments examining the proteomic alterations that coincide with mechanical overload (MOV)-induced skeletal muscle hypertrophy. With this same intent we first sought to determine how 10 weeks of resistance training in 15 college-aged females affected protein concentrations in different tissue fractions. Training, which promoted significant lower body muscle- and fiber-level hypertrophy, notably increased sarcolemmal/membrane protein content (+10.1%, $p < 0.05$). Sarcolemmal/membrane protein isolates were queried using mass-spectrometry-based proteomics, ~10% (38/387) of proteins were up-regulated (>1.5 -fold, $p < 0.05$), and one of these targets (the intermediate filament vimentin, VIM) warranted further investigation. VIM expression was first examined in the plantaris muscles of 4-month-old C57BL/6 mice following 10- and 20-days of MOV via synergist ablation. Relative to Sham (control) mice, VIM mRNA and protein content significantly increased in MOV mice. Immunohistochemistry corroborated these findings and showed that VIM was localized to the extracellular matrix (ECM). The 10- and 20-day MOV experiment was replicated in Pax7-DTA mice, and results indicated satellite cell depletion significantly blunted the presence of VIM in the ECM. A series of follow-up cell culture experiments supported that myoblasts, rather than myofibers, likely produce VIM in response to anabolic stimuli. Finally, a third 10- and 20-day MOV experiment was performed in C57BL/6 mice intramuscularly injected with either AAV9-scrambled (control) or AAV9-VIM shRNA. While VIM shRNA injections significantly blunted the presence of VIM (~50%), plantaris masses were similar between injection groups in response to MOV. However, a leftward (smaller) myofiber size shift in response to MOV was observed in VIM shRNA mice, and this coincided with appreciably more myofibers presenting a regeneration phenotype (MyHC_{emb}-

positive fibers with centrally located nuclei). Using a highly integrative approach, we propose that skeletal muscle VIM is a mechanosensitive target predominantly localized to the ECM and produced by satellite cells. Moreover, a disruption in VIM expression during MOV leads to dysfunctional skeletal muscle hypertrophy.

INTRODUCTION

Skeletal muscle is a highly dynamic tissue capable of undergoing marked changes in size and force output in response to increased mechanical tension/load. The most potent stimulus for skeletal muscle hypertrophy is mechanical overload, either through progressive resistance training in humans or synergist ablation in rodents [1]. Mechano-sensitive protein signaling pathways are responsible for relaying the mechanical perturbations and tension placed on skeletal muscle into downstream signals for adaptations to occur [2-4]. A major pathway for mechanotransduction is through transmembrane proteins (integrins) and various accessory proteins that interact with the extracellular matrix (ECM), cytoskeletal network, and sarcolemma to propagate signals that enhance muscle protein synthesis [5-7].

Cytoskeletal and intermediate filaments not only provide structural support to the cell, but also are involved in processes like signal transmission, mechanotransduction, and gene regulation [9-11]. Intermediate filaments in muscle cells have also been shown to be linked to development [12, 13], regeneration [14, 15], and growth [16]. The commonly studied intermediate filament is desmin, which is a muscle-specific target that has been implicated in several processes that govern skeletal muscle homeostasis and is responsive to mechanical loading [17-19]. For instance, Joanne et al. [20] reported that mechanical overload induced strength increases were blunted in a desmin knockout mouse model. Contrary to desmin, the intermediate filament vimentin (VIM) is predominately expressed in immature developing myofibers and decreases in expression in mature myofibers [21-23]. Interestingly, VIM expression is linked to active and proliferating satellite cells [21, 24] and appears to be critical for myofiber regeneration [25, 26]. VIM also plays a key role in several signaling pathways [11]. Most notably, while not in skeletal muscle, a recent study reported that VIM is linked to

governing cell size through interactions with the mTORC1 pathway, and a reduction in mTORC1 signaling and blunted protein synthesis was evident in VIM-knockout cells [27].

Taken together, skeletal muscle hypertrophy in response to mechanical loading is dependent on several tightly regulated pathways and it appears that various ECM, cytoskeletal and intermediate filament related proteins play an important role in this process. Furthermore, VIM has been shown to regulate cell size and protein synthesis response in other cell types. Herein, we performed shotgun proteomics on the sarcolemmal/ECM fraction of human skeletal muscle and show that: i) 10 weeks of resistance training increases sarcolemmal/ECM VIM protein expression, and ii) a significant positive correlation exists between the training-induced sarcolemmal VIM protein levels and changes in mean muscle fiber cross-sectional area. Through a series of experiments in mice subjected to mechanical overload, we show that VIM expression in the ECM is upregulated in a satellite-cell-dependent manner during synergist ablation-induced skeletal muscle hypertrophy. Finally, viral-mediated knockdown experiments in mice subjected to synergist ablation show that a blunting of VIM expression does not affect gross measures of hypertrophy in skeletal muscle but may delay/impair the regeneration and remodeling processes. Collectively, these data support the upregulation of VIM being responsive to mechanical overload-induced skeletal muscle hypertrophy, and sufficient upregulation of VIM expression is needed for proper skeletal muscle hypertrophy to occur.

METHODS

Human Participants

The human data portion of this investigation is a secondary analysis of a study that was approved by the Auburn University Institutional Review Board (IRB) (Protocol # 19-249 MDR

1907), conformed the standards set by the latest revisions of the Declaration of Helsinki, and was registered as a clinical trial (NCT04707963). The intent of the originally approved trial was to determine if daily peanut protein supplementation (SUP) versus no supplementation (control group [CON]), affected RT-related adaptations [305]. In the present study we utilized a subset of muscle samples still available from the previously mentioned study (i.e., 9 women from the SUP group and 6 women from the CON group). Our sub-sample presented no differences between SUP and CON groups for fCSA ($P = 0.264$), vastus lateralis cross-sectional area (by ultrasonography) ($P = 0.421$), thigh cross-sectional area (by peripheral computed tomography) ($P = 0.855$), as previously demonstrated [305]. Therefore, we collapsed data from SUP and CON groups to perform the analyses presented herein. Samples were from 15 young women (age: 21 ± 2 yr, body mass index: 24.6 ± 3.7 kg/m²) who had not participated in RT programs, were free of obvious cardiovascular or metabolic disease or other conditions contraindicating participation in exercise programs or donating muscle biopsies, and who were not pregnant or trying to become pregnant.

Experimental Design for Human Training Study

Baseline assessments included muscle imaging assessments and vastus lateralis biopsies being obtained in the overnight fasted state. Immediately afterwards, participants engaged in familiarization sessions with the RT protocol and test procedures. Approximately 3-5 days following familiarization sessions, participants initiated an RT program with 2 sessions per week for 10 weeks. Seventy-two hours after the last RT session all assessments (including the procurement of a muscle biopsy) were repeated. For more details related to the study design and resistance training program, readers are referred to Sexton et al. [305].

Vastus Lateralis Muscle Biopsies

Pre- and post-intervention vastus lateralis muscle biopsies were performed from the right leg. Initially the participants laid down on an athletic table where the upper thigh was shaved and cleaned with 70% isopropanol. A subcutaneous injection of 1% lidocaine (0.8 mL) was administered. After 5 minutes, the area was cleaned with chlorhexidine solution. Thereafter, a 7 mm-width pilot incision was made through the dermis with a sterile No. 11 surgical blade (AD Surgical; Sunnyvale, CA, USA). A sterile 5-gauge biopsy needle was then inserted into the pilot incision, through the muscle fascia, and ~2 cm into the muscle (for a total depth of ~4-7 cm) where a 40-80 mg sample was collected while applying suction. Following biopsies, tissue was rapidly teased of blood and connective tissue. A portion of the tissue (~10–20mg) was preserved in optimal cutting temperature (OCT) media for histology (Tissue-Tek®, Sakura Finetek Inc.; Torrance, CA, USA), slow frozen in liquid nitrogen-cooled isopentane, and subsequently stored at –80°C. Another portion of the tissue (~30–50mg) was placed in pre-labeled foils, flash frozen in liquid nitrogen, and subsequently stored at –80°C for other molecular analyses described below. Tissue triage procedures occurred over a 3-minute period.

Resistance Training Program

The resistance training program was described in detail previously [305]. Briefly, resistance training bouts consistent of participants performing a 45° leg press, leg extension, hex-bar deadlifts, flat barbell bench press, and wide-grip cable pulldown exercises. The same exercise order was followed for all training sessions, and two day per week training sessions consisted of performing 4 sets of 10 repetitions for each exercise one day per week, and 5 sets of

6 repetitions for each exercise one day per week. Two-minute rest intervals between sets and exercises were allotted throughout the training intervention. The training load was progressively increased on a session-by-session basis using the rating of perceived exertion (RPE) scale of 1-10 (“really easy” to “really hard”) so that each set was performed close to concentric muscle failure.

Sarcoplasmic and Sarcolemmal Protein Isolations

Isolation of sarcoplasmic and sarcolemmal protein from muscle tissue was performed initially using a high-fidelity membrane protein extraction kit according to manufacturer’s recommendations (Mem-PRE Plus Membrane Protein Extraction Kit; Thermo Fisher Scientific; Waltham, MA, USA). This process yielded solubilized sarcoplasmic and sarcolemmal protein isolates.

Protein concentrations for both fractions were determined in duplicate the same day as protein isolations to minimize freeze-thaw effects using a commercially available assay (BCA Protein Assay Kit; Thermo Fisher Scientific). Thereafter, fractions were stored at -80°C until downstream analyses occurred. Duplicate coefficient of variation (CV) values for the sarcoplasmic and sarcolemmal proteins readings were 2.3% and 2.4%, respectively.

Proteomics on Sarcolemmal Protein Isolates

Sarcolemmal protein isolates were shipped to a commercial vendor for proteomics using a nanoLC-MS/MS platform (Creative Proteomics; Shirley, NY, USA). Briefly, samples were treated with 50 mM ammonium bicarbonate and resultant solutions were transferred to Microcon devices YM-10 (Millipore; Burlington, MA, USA). Samples were then centrifuged at 12,000 g at

4°C for 10 minutes. Protein concentrates were again treated with 50 mM ammonium bicarbonate and centrifuged again. Concentrates were then reduced using 10 mM DTT at 56°C for 1 hour and alkylated by 20 mM IAA at room temperature in dark for 1 hour. Following reduction reactions, and one wash with 50 mM ammonium bicarbonate and centrifugation (12,000g at 4°C for 10 minutes), concentrates were incubated with 100 µL of 50 mM ammonium bicarbonate and free trypsin (ratio of 1:50) at 37°C overnight. Samples were then centrifuged at 12,000 g at 4°C for 10 minutes, and 100 µL of 50 mM ammonium bicarbonate was added to Microcon devices and centrifuged (total of two washes). Peptides were then isolated, lyophilized to near dryness, and resuspend in 20 µL of 0.1% formic acid for LC-MS/MS analysis.

Nanoflow UPLC was performed using the Ultimate 3000 nano UHPLC system (Thermo Fisher Scientific). Associated hardware included a trapping column (PepMap C18, 100Å, 100 µm×2 cm, 5 µm) and analytical column (PepMap C18, 100Å, 75 µm × 50 cm, 2 µm). Mobile phase A consisted of 0.1% formic acid in water, and mobile phase B consisted of 0.1% formic acid in 80% acetonitrile. UPLC runs consisted of 1 µL injections, a linear gradient from 2-8% buffer B for 3 minutes, from 8-20% buffer B for 56 minutes, 20-40% buffer B in 37 minutes, then from 4-90% buffer B for 4 minutes. Back-end mass spectrometry (MS) scans were performed between 300-1,650 m/z at a resolution of 60,000 at 200 m/z. The automatic gain control target for the full scan was set to $3e^6$. MS/MS scans were operated in Top20 mode using the following settings: resolution 15,000 at 200 m/z; automatic gain control target $1e^5$; maximum injection time 19 milliseconds; normalized collision energy at 28%; isolation window of 1.4 Th; charge state exclusion: unassigned, 1, >6; dynamic exclusion 30 seconds.

MS files were analyzed against a HUMAN protein database using Maxquant (v1.6.1.14). Search parameters were set as follows: i) the protein modifications were carbamidomethylation

(C) (fixed), oxidation (M) (variable), ii) the enzyme specificity was set to trypsin, iii) the maximum missed cleavages were set to 2, iv) the precursor ion mass tolerance was set to 10 ppm, and v) MS/MS tolerance was 0.6 Da. 1866 total peptides were identified, and these proteins were further queried using the PANTHER Classification system (pantherdb.org) to delineate plausible cellular functions of the identified sarcolemmal membrane-associated proteins. These peptides were then subjected to statistical analyses where up-regulated and down-regulated proteins from pre-to-post training were considered to exceed a ± 1.5 -fold threshold ($p < 0.05$) as recommended by Levin [306]. Notably, all proteomic data are presented as relative spectra values normalized to total spectra per sample.

Mice Experiments

Mouse experiments not involving AAV9 injections (female wild-type C57BL/6 and Pax7-DTA sham and overload mice) were conducted in accordance with the institutional guidelines for the care and use of laboratory animals as approved by the Animal Care and Use Committee of the University of Kentucky (protocol #'s: 2008-0291). All mice were housed in a climate-controlled room and maintained on a 14:10 hour light-dark cycle, food and water consumption were allowed *ad libitum*. For satellite cell depleted mice the *Pax7^{CreER/+}*; *Rosa26^{DTA/+}* strain, called Pax7-DTA throughout, was generated as previously described [273]. Both sets of mice were subjected to dual-leg synergist ablation or sham surgeries.

Mouse experiments involving AAV9 injections were approved by the Animal Care and Use Committee of the University of Nebraska (protocol #: 2091). Again, mice were housed in a climate-controlled room and maintained on a 14:10 hour light-dark cycle, food and water consumption were allowed *ad libitum*. For AAV9 experiments, female wild-type C57BL/6 mice

were anesthetized under isoflurane, and plantaris muscles were injected with 30 uL (5×10^9 particles) of either AAV9 VIM shRNA (catalog #: AA09-MSE096513-AVE001-A00) or AAV9 scrambled-shRNA (catalog #: SHD05); both of which were commercially developed (GeneCopoeia; Rockville, MD, USA) and contained a CMV promoter and GFP reporter. Following 30-days of viral incubation, mice were subjected to unilateral synergist ablation or sham surgeries.

Conditional Ablation of Satellite Cells

Adult (≥ 4 months of age) Pax7-DTA mice were administered an intraperitoneal injection of either a vehicle (15% ethanol in sunflower seed oil) or tamoxifen (2 mg/day) for 5 consecutive days. Following a 2-week washout period, vehicle and tamoxifen-treated mice were divided into sham or synergist ablation (10-day or 20-day) groups.

Synergist Ablation Surgeries in Mice

Surgical removal of synergist muscles (part of gastrocnemius and soleus) to subject the plantaris muscle to mechanical overload was performed as previously described [273]. Briefly, mice were anesthetized with an intraperitoneal injection of ketamine (100 mg/kg) and xylazine (10 mg/kg), a longitudinal incision was made on the dorsal aspect of the lower hindlimb, and the tendon of the gastrocnemius muscle was isolated and used as a guide to excise the soleus and part of the gastrocnemius. The incision was then sutured, and the animals were allowed to recover in home cages. Sham surgeries involved similar incision and suture procedures without the excision of muscle. Ten or 20-days following surgeries, mice were anesthetized, euthanized via cervical dislocation, and the plantaris muscle was excised. Immediately following removal,

plantaris muscles were weighed and either flash-frozen in liquid nitrogen or prepared for immunohistochemical analysis via preservation in OCT media.

Human Muscle Immunohistochemistry

Human fCSA Determination. Human skeletal muscle samples were examined for mean fiber cross-sectional area (fCSA) using immunohistochemistry (IHC) as previously described by our laboratory [305]. Briefly, slides with sections were dried for 10 minutes at room temperature. Triton-X (0.5%) in phosphate buffer solution (PBS) was used to permeabilize the sections for 5 minutes. Thereafter, slides were washed in PBS for 5 minutes and subsequently incubated in blocking solution for 15 minutes (Pierce Super Blocker; Thermo Fisher Scientific). Slides were incubated in primary antibody solution (1x PBS, 5% of Pierce Super Blocker Solution, and 2% [or a 1:50 dilution] of rabbit anti-dystrophin IgG1 [catalog #: GTX15277; Genetex Inc.; Irvine, CA, USA] and mouse anti-myosin I IgG1 (catalog #: A4.951 Developmental Studies Hybridoma Bank; Iowa City, IA, USA) for 1 hour. Slides were then washed for 5 minutes in PBS and incubated in a secondary antibody solution (1x base of PBS, and 1% [or 1:100 dilution] Texas Red-conjugated anti-rabbit IgG [catalog #: TI-1000; Vector Laboratories, Burlingame, CA, USA] and Alexa Fluor 488-conjugated anti-mouse IgG1 (catalog #: A-11001; Thermo Fisher Scientific) for 1 hour in the dark at room temperature. Slides were then mounted in fluorescent media and imaged using a fluorescent microscope (Nikon Instruments, Melville, NY, USA) with a 10x objective lens. Open-sourced software (MyoVision) was used to analyze all images for mean fCSA [307].

Phalloidin staining. For determination of myofibril area per fiber, F-actin labelling using phalloidin-conjugated to Alexa Fluor 594 (AF594) was performed. Briefly, serial sections were

allowed to air dry for ~1.5–2 hours at room temperature followed by fixation in chilled acetone for 5 minutes. Sections were then incubated with 3% H₂O₂ for 15 minutes and true black (catalog #: 23007 Biotium; Fremont, CA, USA) for 1 minute to reduce auto-fluorescence. Sections were then blocked with 2.5% BSA/5% goat serum for 1 hour. Sections were incubated overnight in 4°C with mouse anti-dystrophin MANDY S8 (1:20) (catalog #: 8H11; Developmental Studies Hybridoma Bank). The following morning, sections were incubated for 1 hour with phalloidin conjugated to AF594 (1:100) (catalog #: A12381; Thermo Fisher Scientific) and Alex Fluor 488-conjugated anti-mouse IgG1 (1:250) (catalog #: A11001; Thermo Fisher Scientific). Sections were incubated with DAPI (1:10,000) (catalog #: D3571; Thermo Fisher Scientific) for 15 minutes. Slides were then mounted with glass cover slips using 50/50 PBS+glycerol. Digital images were captured using a fluorescent microscope (Nikon Instruments) using a 20x objective. Quantification of myofibril area per fiber was performed using ImageJ software (National Institutes of Health; Bethesda, MD, USA) according to previous reports [34, 308]. Briefly, images were split into RGB channels, and the red channel image was converted to gray scale. The threshold function was then used to generate a binary black/white image of stained versus portions of fibers. Fibers were then traced, and myofibril area were provided as a percentage per fiber area. The coefficient of variation (CV) between two measurements performed 72 hours apart was 0.26% [308].

Mouse Plantaris Immunohistochemistry

VIM area and fCSA determinations. Mouse plantaris muscles preserved for IHC were sectioned at 7 µm thicknesses using a cryotome (Leica Biosystems; Buffalo Grove, IL, USA) and adhered to multiple positively charged slides for the interrogation of various targets as

explained in this and subsequent paragraphs. Following slide adhesion, sections were allowed to air dry prior to being stored at -80°C until further analysis.

Sections from sham mice and mice subjected to mechanical overload were first stained for VIM, dystrophin, and nuclei. Briefly, samples were fixed in ice cold acetone for 5 minutes followed by 3% hydrogen peroxide (H₂O₂) for 10 minutes and true black incubation for 1 minute to reduce autofluorescence. Sections were then blocked with 5% goat serum/2.5% BSA for at least 1 hour before overnight incubation at 4°C of an antibody cocktail consisting of rabbit anti-vimentin (1:100) (catalog #: 5741; Cell Signaling Technologies; Danvers, MA, USA), mouse anti-dystrophin IgG2b (1:50) (catalog ID: Mandy S8; Developmental Studies Hybridoma Bank), and 2.5% BSA. After primary antibody incubations, sections were incubated for 1 hour with a secondary antibody cocktail consisting of anti-rabbit AF488 (Vector Laboratories), anti-mouse IgG2b AF594 (catalog #: A-21145; Thermo Fisher Scientific), and PBS. Following secondary antibody incubations, sections were incubated with DAPI (1:10,000) (catalog #: D3571; Thermo Fisher Scientific) for 10 minutes. Coverslips were then added using PBS + glycerol as mounting media. Digital images of entire sections were captured using a fluorescent microscope (20x objective; Zeiss Axio imager.M2) and motorized scanning stage.

Satellite Cell and VIM Co-expression. Sections stained for satellite cells and VIM to determine co-expression were first fixed in ice cold acetone for 5 minutes followed by 3% H₂O₂ incubation for 10 minutes. Sections were then subjected to an epitope retrieval protocol. This protocol first involved incubating sections with sodium citrate for 2 minutes at room temperature followed by incubation in pre-warmed (65°C) sodium citrate. Sections were then placed in a water bath incubator until they reached 92°C. Sections were then incubated for 11 minutes at 92°C and allowed to cool in water bath until 50°C then cooled to room temperature. Following

epitope retrieval, sections were incubated with true black for 1 minute to reduce autofluorescence. Sections were then blocked using 5% goat serum/2.5% BSA for at least 1 hour followed by biotin and streptavidin blocking solutions for 15 minutes each. Sections were incubated with an antibody cocktail containing: i) mouse anti-Pax7 IgG1 (1:100), ii) mouse anti-dystrophin IgG2b (1:50), rabbit anti-vimentin (1:100), and 2.5% BSA overnight at 4°C. Following primary antibody incubations, sections were incubated with biotin-SP-conjugated goat anti-mouse IgG1 (1:1,000) (catalog #: 111-065-003; Jackson ImmunoResearch; West Grove, PA, USA) in 2.5% BSA for 90 minutes. Sections were then incubated with a secondary antibody cocktail consisting of SA-HRP (1:500) (catalog #: S-911; Thermo Fisher Scientific), goat anti-rabbit AF488 (1:250) (Vector Laboratories), and goat anti-mouse IgG2b AF647 (1:250) (catalog #: A21242; Thermo Fisher Scientific) for one hour. TSA AF555 (1:200) (catalog #: B-40955; Thermo Fisher Scientific) was added for 20 minutes, followed by DAPI for 10 minutes. Coverslips were added using PBS + glycerol as mounting medium. Digital images of entire sections were captured using a fluorescent microscope (20x objective; Zeiss Axio imager.M2) and motorized scanning stage. Co-expression of VIM and satellite cells was determined by area of VIM per Pax7+/DAPI+ cells.

Fibroblast and VIM Co-expression. Sections stained for fibroblasts and vimentin to determine co-expression were first fixed with ice cold acetone for 5 minutes, followed by incubation with 3% H₂O₂ for 10 minutes. Sections then underwent epitope retrieval as described above, followed by incubation with true black for 1 minute to reduce autofluorescence. Sections were then blocked with 5% goat serum/2.5% BSA for at least one hour followed by biotin and streptavidin solution blocking for 15 minutes each. Following the blocking step, sections were incubated overnight at 4°C with rabbit anti-TCF4 (1:100) (catalog #: 2569; Cell Signaling

Technologies) in 2.5% BSA. Sections were then incubated with goat biotin-conjugated anti-rabbit IgG (1:1000) (catalog #: 111-065-046; Jackson ImmunoResearch) in 2.5% BSA for 90 minutes, followed by incubation with SA-HRP (1:500) for 1 hour. Sections were then incubated with TSA-488 (1:400) (catalog #: B-40953; Thermo Fisher Scientific) for 20 minutes followed by incubation with DAPI for 10 minutes. Sections were briefly checked under microscope to ensure proper staining for TCF4 before being re-fixed in 4% PFA for 10 minutes followed by blocking with 5% goat serum/2.5% BSA and biotin/streptavidin solutions for at least 1 hour. Sections were then incubated overnight at 4°C with antibody cocktail consisting of mouse anti-dystrophin IgG2b (1:50), rabbit anti-vimentin (1:100), and 2.5% BSA. Sections were then incubated with a secondary antibody cocktail consisting of goat anti-rabbit AF555 (1:250), and goat anti-mouse IgG2b AF647 (1:250) for 1 hour, followed by incubation with DAPI for 10 minutes. Coverslips were added using PBS + glycerol as mounting medium. Digital images of entire sections were captured using a fluorescent microscope (20x objective; Zeiss Axio imager.M2) and motorized scanning stage. Co-expression of VIM and fibroblasts was determined by area of vimentin per TCF4+/DAPI+ cells.

Fibro-adipogenic Progenitor and VIM Co-expression. Only wild type mouse plantaris sections were stained for fibro-adipogenic progenitors (FAPs) and vimentin to determine the co-expression of the two using IHC. Briefly, sections were fixed with 4% PFA for 10 minutes, then incubated with 3% H₂O₂ for 15 minutes, and true black for 1 minute to reduce autofluorescence. Sections were then blocked with 2.5% BSA/0.1% Triton-X for at least 1 hour. Following the blocking step, sections were incubated overnight at 4°C with an antibody cocktail consisting of goat anti-mouse PDGFR α (1:100) (catalog #: AF1062; R&D Systems; Minneapolis, MN, USA), rabbit anti-vimentin (1:100), and 2.5% BSA. Sections were then incubated with secondary

antibody cocktail for two hours consisting of donkey anti-goat AF555 (1:250) (catalog #: A-21432; Thermo Fisher Scientific), donkey anti-rabbit AF488 (1:250) (catalog #: A-21206; Thermo Fisher Scientific), and Wheat germ agglutinin (WGA) (1:50) (catalog #: W-32466; Thermo Fisher Scientific). Sections were then incubated with DAPI for 10 minutes and coverslips were added using PBS + glycerol as mounting medium. Digital images of entire sections were captured using a fluorescent microscope (20x objective; Zeiss Axio imager.M2) and motorized scanning stage. Co-expression of vimentin and fibroblasts was determined by area of VIM per PDGFR α + / DAPI+ cells.

Macrophage and VIM Co-expression. Again, only wild type mouse muscle was stained for macrophages and VIM to determine the co-expression of the two using IHC. Briefly, sections were fixed with ice cold acetone for 10 minutes followed by incubated with 3% H₂O₂ for 10 minutes. Sections were then blocked with 5% goat serum/2.5% BSA for at least one hour. Sections were then incubated overnight at 4°C with antibody cocktail consisting of rat anti-F4/80 (1:100) (catalog #: MCA497; Bio-Rad Laboratories; Hercules, CA, USA), rabbit anti-vimentin (1:100), and mouse anti-dystrophin IgG2b (1:50). Following overnight incubation with primary antibodies, sections were incubated with goat anti-rat biotin (1:500) (catalog #: 31830; Thermo Fisher Scientific) in 2.5% BSA for 90 minutes. Sections were then incubated with secondary antibody cocktail for one hour consisting of SA-HRP (1:500), goat anti-rabbit AF488 (1:250), and goat anti-mouse IgG2b AF647 (1:250). TSA AF555 (1:200) was added for 20 minutes, followed by DAPI for 10 minutes. Coverslips were added using PBS + glycerol as mounting medium. Digital images of entire sections were captured using a fluorescent microscope (20x objective; Zeiss Axio imager.M2) and motorized scanning stage. Co-expression of vimentin and fibroblast was determined by area of VIM per F4/80+ / DAPI+ cells.

Embryonic Myosin. AAV9-shRNA mouse plantaris muscles were stained for the presence of embryonic myosin heavy chain (MyHC_{emb}). Briefly, sections were fixed with ice cold acetone for 5 minutes followed by incubated with 3% H₂O₂ for 10 minutes. Sections were then blocked with 5% goat serum/2.5% BSA for at least one hour. Sections were then incubated overnight at 4°C with antibody cocktail consisting of mouse anti-dystrophin IgG2b (1:50) and mouse anti-eMHC IgG1 (1:50) (catalog ID: F1.652; Developmental Studies Hybridoma Bank). Sections were then incubated with secondary antibody cocktail for one hour consisting of goat anti-mouse IgG2b AF647 (1:250) and goat anti-mouse IgG1 AF488 (1:250). Sections were then incubated with DAPI for 10 minutes and coverslips were added using PBS + glycerol as mounting medium. Digital images of entire sections were captured using a fluorescent microscope (20x objective; Zeiss Axio imager.M2) and motorized scanning stage.

Cell Culture Experiments

Low passage (passage 3-5) immortalized C2C12 myoblasts (ATCC; Manassas, VA, USA) were used to determine vimentin protein expression throughout various stages of proliferation and differentiation as well as in response to an anabolic stimulus (insulin-like growth factor, IGF-1), and experiments occurred in a humidified CO₂ incubator at 37°C using 5% CO₂-95% room air. Myoblasts (100,000 cells per mL) were seeded onto six-well plates in growth medium (GM) containing Dulbecco's modified Eagle's Medium (DMEM; Corning, Corning, NY) supplemented with 10% fetal bovine serum and 1% penicillin/streptomycin. Once cells reached confluency (~85-90%), differentiation was induced by switching to differentiation medium (DM), consisting of DMEM supplemented with 2% horse serum. Once complete differentiation into myotubes was achieved, cells in one experiment were treated with 10 μM

arabinosylcytosine (AraC; Sigma, St. Louis, MO, USA) for 24 hours to reduce the number of unfused myoblasts [309]. Myotubes were then treated with either PBS (CTL) or various doses (100 ng/mL, 200 ng/mL, 400 ng/mL) of recombinant mouse IGF-1 (catalog #: 791-MG-050; R&D Systems) for 24 hours. A separate set plates that did not receive AraC treatments were used to determine how the enrichment of unfused myoblasts affected VIM expression. Finally, a third set of plates were examined at 0 days, 1 day, 3 days, 5 days, and 7 days after the initiation of differentiation to determine how differentiation affected VIM expression. At the end of experimental time lines, cells were washed with PBS and 500 μ L of 1x cell lysis buffer (catalog #: 9803S; Cell Signaling Technologies) was used to scrape wells and collect lysates. Lysates were then centrifuged at 500 g for 5 minutes (4°C), supernatants were transferred to 1.7 mL microtubes, and lysates were stored at -80°C until western blotting.

Western Blotting and qPCR

Western blotting procedures throughout were performed as previously described from our laboratory [215] using the rabbit anti-vimentin antibody described above (1:1,000). For myotube lysate western blotting, protein concentrations were determined using a commercially available bicinchoninic acid (BCA) kit (Thermo Fisher Scientific). Cell lysates were prepared at a concentration of 1 μ g/ μ L and 15 μ L of sample were loaded onto 4-15% gradient SDS-polyacrylamide gels (Bio-Rad Laboratories). Membranes were developed using chemiluminescent substrate (EMD Millipore) and imaged using a gel documentation system (ChemiDoc Touch; Bio-Rad Laboratories). Vimentin protein band densities were obtained using associated software (Image Lab v6.0.1; Bio-Rad Laboratories) and normalized to Ponceau lane

densities. Target/Ponceau density ratios were normalized to either vehicle-control treatments (IGF-1 experiments) or day 0 differentiation (differentiation phase experiments).

Plantaris muscle RNA and protein from one mouse experiment (Fig. 2 in Results) were isolated using the modified Trizol-bromochloropropane protocol described by Wen et al. [310]. Following RNA isolation, the RNA pellet was resuspended in 30 μ L of RNase-free water and RNA concentrations were determined in duplicate at an absorbance of 260 nm by using a NanoDrop Lite (Thermo Scientific). Thereafter, cDNA (1 μ g) was synthesized using a commercial qScript cDNA SuperMix (Quanta Biosciences, Gaithersburg, MD, USA) per the manufacturer's recommendations. qPCR was performed with gene-specific primers and SYBR-green-based methods (Quanta Biosciences) with gene-specific primers designed with primer design software (Primer3Plus, Cambridge, MA, USA) using a real-time PCR thermal cycler (Bio-Rad Laboratories). Protein was isolated from the organic phase as described by Wen et al. [310], and VIM was interrogated using the rabbit anti-vimentin antibody described above (1:1,000). VIM protein band densities were obtained as described in the prior paragraph and normalized to Ponceau lane densities. Target/Ponceau density ratios were normalized to the Sham group.

Statistical Analyses

Statistical analyses were performed using GraphPad Prism (Version 10.2; San Diego, CA, USA). Human dependent variables (including proteomic data) were analyzed using dependent samples t-tests. All mouse experiments variables were analyzed using one-way ANOVAs and Tukey's post-hoc tests were applied when significant model effects were observed. Pax7-DTA and AAV9 mouse experiment variables were analyzed using two-way

ANOVAs with Tukey's post-hoc tests being performed when significant main effects or interactions were observed. Select associations between dependent variables were also analyzed using Pearson correlations. All data are presented as mean \pm standard deviation (SD) values, and a two-tailed statistical significance of $p < 0.05$ was used throughout.

RESULTS

Pre-intervention Sarcolemmal Proteome Characteristics and Adaptions to this Protein Pools following 10 Weeks of Resistance Training

Given that the sarcolemmal proteome of human skeletal muscle has not been investigated to our knowledge, Figure 1 provides highlights of these data from pre-intervention biopsies. Notably, 387 proteins were detected, and PANTHER protein classification analysis revealed the enrichment of 4 ECM proteins, 7 transmembrane signal receptor proteins, 21 cell adhesion proteins, 61 scaffold/adaptor proteins, 75 membrane traffic proteins, 97 transporter proteins, and 122 cytoskeletal proteins (Figure 1a). The top enriched proteins from each protein class are also presented in Figure 1, and all raw data are available in Supplemental File 2.

INSERT FIGURE 1 HERE

Resistance training significantly increased whole-body lean mass (2.1%), vastus lateralis muscle cross-sectional area (14.2%), mean fiber cross-sectional area (17.8%), and deadlift strength (32%) (Supplemental Fig. 1). Sarcolemmal protein concentrations also significantly increased with 10 weeks of training (10.1%; Supplemental Fig. 1). Resistance training upregulated 9.6% (38/387) of the detected proteins (>1.5 -fold increase, $p < 0.05$; Figure 2a), and PANTHER protein

classes shown to be upregulated above this 9.6% threshold included scaffold/adaptor proteins (9.8%, 6/61), transporter proteins (13.4%, 13/97), and transmembrane signal receptor proteins (14.3%, 1/7). Training downregulated 4.1% (16/387) of the detected proteins (>1.5-fold decrease, $p < 0.05$; Figure 2b), and PANTHER protein classes shown to be downregulated at or above this 4.1% threshold included transporter proteins (4.1%, 4/97), membrane traffic proteins (5.3%, 4/75), and cytoskeletal proteins (5.7%, 7/122; Figure 2b).

The pre-to-post intervention change scores of 3 enriched proteins upregulated with training were significantly correlated to changes in fiber cross sectional area (fCSA) including the cytoskeletal protein vimentin (VIM; $r = 0.652$, $p = 0.009$), the transporter protein prosaposin (PSAP; $r = 0.714$, $p = 0.003$), and transporter protein growth hormone-inducible transmembrane protein (GHITM; $r = 0.626$, $p = 0.013$) (Figure 2c). Given the compelling literature on VIM cited earlier in the paper, and the relatively high enrichment of this protein compared to the other two targets (see Figure 2a), we decided to further pursue the role and function of VIM in the context of skeletal muscle hypertrophy.

INSERT FIGURE 2 HERE

Vimentin Expression Following 10- and 20-days Synergist Ablation in Mice

Following 10- and 20-days of mechanical overload (MOV) via synergist ablation, VIM expression was measured at the mRNA level via qPCR, protein level via western blotting, and visually using immunohistochemistry. *Vim* mRNA was significantly upregulated with mechanical overload (ANOVA $p < 0.001$), and post hoc testing revealed that 10-day MOV values were greater than Sham and 20-day MOV mice ($p < 0.001$, and $p = 0.007$, respectively),

whereas values in 20-day MOV mice were not statistically different from Sham mice ($p = 0.181$; Figure 3a). Protein expression of VIM was also significantly upregulated with MOV ($p < 0.001$). Like mRNA expression patterns, VIM protein was upregulated in 10-day MOV compared Sham and 20-day MOV mice ($p < 0.001$ for both comparisons) and levels were not statistically different between Sham and 20-day MOV mice ($p = 0.059$; Figure 3b). Immunohistochemistry indicated that VIM was exclusively localized to the ECM (Figure 3f), and the percent area occupied by VIM on 20x objective fields of view were significantly higher in MOV versus Sham mice (ANOVA $p < 0.001$, 10-day versus Sham $p < 0.001$, 20-day versus Sham $p = 0.006$; Figure 3c). When Fig. 3c data were normalized to fiber number, VIM content was still shown to be significantly higher in MOV versus Sham mice (ANOVA $p < 0.001$, 10-day versus Sham $p < 0.001$, 20-day versus Sham $p = 0.006$; Figure 3d). Other muscle characteristics in response to 10-20-day MOV are presented in Supplemental Figure 2.

INSERT FIGURE 3 HERE

Vimentin Co-localization with Resident Skeletal Muscle Stromal Cells

Given visual confirmation that VIM is localized to the ECM, we decided to measure the co-localization of this target with different stromal cells residing in the ECM. We first queried the Tabula Muris single cell sequencing database [311] (method: FACS; tissue: limb muscle), and results indicated highest enrichments in macrophages and satellite cells. We then decided to investigate the co-localization of VIM with satellite cells, fibroblasts, fibro-adipocyte progenitor cells (FAPs), and macrophages in Sham as well as 10-day and 20-day MOV mice using immunohistochemistry. Satellite cells (Pax7+/DAPI+ cells per fiber) were significantly higher in

MOV versus Sham mice (ANOVA $p < 0.001$, 10-day versus Sham $p < 0.001$, 20-day versus Sham $p = 0.002$; Figure 4a). VIM area (normalized to satellite cell number) was also significantly higher in MOV versus Sham mice (ANOVA $p = 0.001$, 10-day versus Sham $p = 0.003$, 20-day versus Sham $p = 0.003$; Figure 4a). Although fibroblasts (TCF4+/DAPI+ cells per fiber) were significantly higher in MOV versus Sham mice (ANOVA $p < 0.001$, 10-day versus Sham $p < 0.001$, 20-day versus Sham $p = 0.003$), VIM area (normalized to fibroblast number) was not affected with MOV (ANOVA $p = 0.581$; Figure 4b). While FAP counts (PDGFR α +/DAPI+ cells per fiber) were not affected with MOV ($p = 0.280$), VIM area (normalized to FAP number) was significantly higher in MOV versus Sham mice (ANOVA $p < 0.001$, 10-day versus Sham $p < 0.001$, 20-day versus Sham $p < 0.001$; Figure 4c). Macrophages (F4/80+/DAPI+ cells per fiber) were significantly higher in 10-day MOV versus Sham mice (ANOVA $p < 0.001$, 10-day versus Sham $p < 0.001$). However, values in 20-day versus 10-day MOV mice were lower ($p = 0.016$), and 20-day MOV versus Sham mice values were similar ($p = 0.366$; Figure 4d). VIM area (normalized to macrophage number) was significantly higher in MOV versus Sham mice (ANOVA $p < 0.001$, 10-day versus Sham $p < 0.001$, 20-day versus Sham $p < 0.001$; Figure 4d), albeit this marker was lower in 20-day versus 10-day mice ($p = 0.024$). Taken together, the Tabula Muris data along with these co-localization experiments warranted further examination between satellite cells, fibroblasts, and VIM expression.

INSERT FIGURE 4 HERE

Vimentin Expression in Response to MOV following the Depletion of Satellite Cells

To further explore the interaction of satellite cells and VIM expression following MOV, we used the Pax7-DTA mouse (Pax7^{CreER/+}; Rosa26^{DTA/+}) to effectively deplete satellite cell number prior to 10- and 20-days of MOV; note, general muscle characteristics are presented in Supplemental Figure 3. Satellite cell number was significantly depleted in tamoxifen (TAM)-treated mice at all time points ($p < 0.001$; Figure 5c). VIM expression based on percent area occupied by VIM (Figure 5a) and percent area of VIM per fiber (Figure 5b) revealed a significant treatment (TAM vs. vehicle), time, and interaction effects (all $p < 0.001$). Further analysis showed that VIM (% area and %area per fiber) was again responsive to 10- and 20-day MOV in vehicle-treated mice (Figure 5a/b). However, this response was significantly attenuated in TAM-treated mice that lacked satellite cells.

Given the modest (but significant) elevation in VIM expression following 20-days MOV in TAM-treated mice that lacked satellite cells, we next measured fibroblast numbers to determine if an increase in this outcome was a potential cause for the increase in VIM expression. Notably, the fibroblast response with MOV was similar in vehicle- and TAM-treated mice (Figure 5d). Hence, we interpret these data as fibroblasts not being predominantly responsible for the MOV-induced increases in VIM expression.

INSERT FIGURE 5 HERE

To further elucidate the role satellite cells may have in VIM expression, a series of cell culture experiments were performed whereby C₂C₁₂ myotubes with (AraC-) and without (AraC+) residual myoblasts were treated with incremental doses of rIGF-1 (as described in the Methods section). While both sets of myotubes experienced dose-dependent increases in cell diameters

(Supplemental Figure 4a), VIM protein expression only increased in myotubes containing residual myoblasts (Supplemental Figure 4b). Moreover, in a separate experiment examining VIM expression during the time course of differentiation, a steady and consistent loss of VIM was observed across the 0-7-day post-differentiation timepoints (Supplemental Figure 4c). Hence, these experiments provide added confidence that myoblasts, rather than other cell types, are the likely source of VIM. Further, these *in vitro* data support that VIM expression is responsive to an anabolic stimulus.

AAV VIM shRNA Against Vimentin Does Not Affect Measures of Gross Muscle Hypertrophy but May Lead to Delayed Long-Term Adaptations

To determine if VIM is needed for rapid skeletal muscle hypertrophy, we used an AAV9 VIM shRNA (versus scrambled) construct to knock down VIM expression prior to 10- and 20-days of MOV. Immunohistochemistry of GFP indicated that ~50% of myofibers were infected with AAV9 in both injection groups (Supplemental Figure 5). Plantaris weights normalized to body weights revealed a significant effect of time ($p = 0.001$), while no effect of treatment or interaction was detected ($p = 0.887$ and $p = 0.334$, respectively; Figure 6a). Similar outcomes were also observed for fiber number (Figure 6b), whole-muscle cross-sectional area (Figure 5c), and mean fiber cross-sectional area (fCSA; Figure 6d) whereby each of these variables demonstrated significant time effects ($p = 0.007$, $p = 0.013$, and $p = 0.018$, respectively) but no treatment or interaction effects ($p > 0.05$ for all measures). Myonuclei per fiber revealed significant time and treatment effects ($p = 0.012$ and $p = 0.019$) but no interaction ($p = 0.279$; Figure 6e).

VIM expression as measured by percent of total area occupied and percent area per fiber revealed significant time ($p < 0.001$ for both), treatment ($p < 0.001$ for both), and interaction effects ($p < 0.001$ and $p = 0.007$, respectively). Further analysis revealed that VIM expression measured as both percent area of VIM and percent area of VIM per fiber was significantly blunted in the VIM shRNA mice following both 10- and 20-day MOV compared to scrambled mice (10-day $p = 0.004$ and $p = 0.003$; 20-day $p = 0.001$ and $p = 0.003$; Figure 6f/g).

INSERT FIGURE 6 HERE

While a blunting of VIM expression did not affect measures of gross skeletal muscle hypertrophy following 10- and 20-day MOV, a noted shift toward smaller fibers was evident in VIM shRNA versus scrambled mice based on fCSA histogram distributions (Figure 7a/b). Evidence of morphologically impaired myofiber hypertrophy was observed in VIM shRNA mice who presented more centrally located myonuclei (interaction $p < 0.001$; Figure 7c) and myofibers that stained positive for embryonic myosin (interaction $p < 0.001$; Figure 7e).

INSERT FIGURE 7 HERE

DISCUSSION

Skeletal muscle VIM expression is responsive to mechanical loading as evidenced by increases in this protein in the sarcolemmal fraction following chronic resistance training in humans and an increased presence in the ECM following 10- and 20-days of synergist ablation in mice. The VIM-stromal cell co-localization experiments in mice indicate that, apart from fibroblasts,

increases in this protein outpace the expansion stromal cell counts during MOV. However, given the strong visual co-localization with satellite cells as well as the queried Tabula Muris data, we used the Pax7-DTA mouse model to determine the relationship between satellite cell abundance and VIM expression. This model showed that VIM expression is reduced in satellite cell-depleted mice following MOV compared to satellite cell-intact mice, and our *in vitro* data lend further evidence to satellite cells being a prominent source of VIM. Lastly, targeted viral knockdown with an AAV9 VIM shRNA resulted in a blunting of VIM expression following 10- and 20-days of MOV in mice compared to scrambled mice. This blunting of VIM expression did not affect gross measures of skeletal muscle growth (i.e., plantaris weight, fiber number, mean fCSA). However, a notable increase in the number of smaller fibers was evident in VIM shRNA mice and this was accompanied by a marked increase in MyHC_{emb}-positive fibers with centrally located nuclei following 10- and 20-days of MOV.

As no other study has sought to directly examine how VIM may facilitate skeletal muscle hypertrophy, our discussion is somewhat limited to hypotheses based on our observations. However, there are data that resonate with some of our findings. Using a time course of MOV in mice, Chaillou et al. 2013 [7] reported that Vim mRNA expression is elevated in skeletal muscle and further links VIM as a potential competent of a pro-hypertrophic mechano-sensing pathway. Moreover, the knockdown or knockout of VIM expression has been linked to decreases in cell size and protein synthesis pathways [27, 312-314], albeit these studies have examined other cell types and our fCSA and whole section CSA data are conceptually discordant with these reports. Perhaps what is most concordant with our findings, however, are select studies indicating VIM is involved with the regeneration process in several tissue types including skeletal muscle [25, 315]. In this regard, VIM expression during regeneration in skeletal muscle has been shown to be

elevated 7-days post injury, and others have reported that VIM expression is linked to key aspects of satellite cell involvement in the regeneration process [21, 24, 316]. Also notable are data linking VIM to the family of immediate-early genes that are rapidly upregulated in cells that are stimulated from quiescence [12]. Extending this notion to our data implies that increased VIM expression is needed to activate satellite cells. However, our findings indicating that shRNA-mediated VIM knockdown did not interfere with the MOV-induced increase in satellite cell number contrasts this hypothesis. Notwithstanding, these prior reports along with our observations of VIM knockdown promoting a regenerative phenotype following MOV warrant continued research in this area of muscle biology.

Aside from the current observations, several outstanding issues remain. First, while we posit that VIM is a mechanosensitive target, our *in vitro* data indicate that this target is also responsive to IGF-1. Indeed, both stimuli elicit similar cell signaling events (e.g., mammalian target of rapamycin complex-1 activation), and there are distinct differences between growth factor signaling and mechanotransduction in skeletal muscle [1]. Also notable are studies that have mapped the VIM promoter and suggested that various transcription factors driven by pro-inflammatory ligands (e.g., heterodimers binding to AP-1 sites, NF- κ B) drive gene expression [317, 318]. Hence, investigations parsing out the upstream signals that upregulate VIM gene/protein expression in skeletal muscle during rapid growth are needed.

Limitations

This study possesses various limitations. First, the bulk of our investigation hinged on rodent findings, and this was due to human tissue limitations. Hence, future time course resistance training investigations should aim to implement IHC to replicate our rodent findings.

Additionally, the AAV9 experiments utilized unilateral synergist ablation and the growth response compared to the dual leg synergist ablation model utilized for the other mouse experiments in this study resulted in differential hypertrophy responses (see fCSA profiles of Fig. 3a versus 7b). We also did not examine whether shRNA-mediated VIM knockdown impaired muscle function and this requires further inquiry. Finally, while we posit that our shRNA experiments provided valuable preliminary evidence in this area of muscle biology, elegant genetic mouse models knocking out VIM in a cell-specific fashion (e.g., satellite cell VIM-KO mice) could continue to confirm or refute our hypotheses put forth herein.

Conclusions

Using an integrative approach with cell culture, rodent, and human experiments, we posit that VIM is a mechanosensitive target in skeletal muscle that is predominantly localized to the ECM and is produced by satellite cells in response to mechanical overload. Moreover, the disruption in VIM expression during periods of mechanical overload leads to a dysregulated regenerative response that is suggestive of impaired skeletal muscle hypertrophy.

AUTHOR CONTRIBUTIONS

This study fulfilled dissertation requirements for J.S.G., and J.S.G., C.B.M., and M.D.R. conceived the idea for this study. C.S.F., A.D.F and A.N.K. were committee members who provided continued support throughout the project. C.A.L., I.V., A.D.F., and M.D.R. provided significant resources to complete various project aims. J.M.M. and M.M. performed multiple experiments throughout, which warranted co-authorship. J.S.G. and M.D.R. primarily drafted the manuscript, and all co-authors provided feedback as well as intellectual contributions. All

authors have read and approved the final version of this manuscript and agree to be accountable for all aspects of the work in ensuring that questions related to the accuracy or integrity of any part of the work are appropriately investigated and resolved. All persons designated as authors qualify for authorship.

ACKNOWLEDGMENTS

Reagent costs (e.g., reagents, antibodies, mice) were purchased through discretionary laboratory funds of M.D.R. (gift donation by Renaissance Periodization), I.V., and C.A.L. C.A.L. was also supported by the The São Paulo Research Foundation (#2020/13613-4) and National Council for Scientific and Technological Development (#311387/2021-7).

CONFLICTS OF INTEREST

None of the authors have financial or other conflicts of interest to report regarding these data.

DATA AVAILABILITY STATEMENT

The data that support the findings of this study are available from the corresponding author (mdr0024@auburn.edu) upon reasonable request.

REFERENCES

1. Roberts, M.D., et al., *Mechanisms of mechanical overload-induced skeletal muscle hypertrophy: current understanding and future directions*. *Physiol Rev*, 2023. **103**(4): p. 2679-2757.
2. Hornberger, T.A. and K.A. Esser, *Mechanotransduction and the regulation of protein synthesis in skeletal muscle*. *Proc Nutr Soc*, 2004. **63**(2): p. 331-5.
3. Hornberger, T.A., *Mechanotransduction and the regulation of mTORC1 signaling in skeletal muscle*. *Int J Biochem Cell Biol*, 2011. **43**(9): p. 1267-76.
4. Kirby, T.J., *Mechanosensitive pathways controlling translation regulatory processes in skeletal muscle and implications for adaptation*. *J Appl Physiol (1985)*, 2019. **127**(2): p. 608-618.
5. Boppart, M.D. and Z.S. Mahmassani, *Integrin signaling: linking mechanical stimulation to skeletal muscle hypertrophy*. *Am J Physiol Cell Physiol*, 2019. **317**(4): p. C629-C641.
6. Zou, K., et al., *The alpha(7)beta(1)-integrin increases muscle hypertrophy following multiple bouts of eccentric exercise*. *J Appl Physiol (1985)*, 2011. **111**(4): p. 1134-41.
7. Chaillou, T., et al., *Time course of gene expression during mouse skeletal muscle hypertrophy*. *J Appl Physiol (1985)*, 2013. **115**(7): p. 1065-74.
8. Schiaffino, S., et al., *Molecular Mechanisms of Skeletal Muscle Hypertrophy*. *J Neuromuscul Dis*, 2021. **8**(2): p. 169-183.
9. Palmisano, M.G., et al., *Skeletal muscle intermediate filaments form a stress-transmitting and stress-signaling network*. *J Cell Sci*, 2015. **128**(2): p. 219-24.
10. Danielsson, F., et al., *Vimentin Diversity in Health and Disease*. *Cells*, 2018. **7**(10).
11. Ivaska, J., et al., *Novel functions of vimentin in cell adhesion, migration, and signaling*. *Exp Cell Res*, 2007. **313**(10): p. 2050-62.
12. Paulin, D., et al., *Vimentin: Regulation and pathogenesis*. *Biochimie*, 2022. **197**: p. 96-112.
13. Oshima, R.G., *Intermediate filaments: a historical perspective*. *Exp Cell Res*, 2007. **313**(10): p. 1981-94.
14. Lindqvist, J., et al., *Nestin contributes to skeletal muscle homeostasis and regeneration*. *J Cell Sci*, 2017. **130**(17): p. 2833-2842.
15. DePianto, D. and P.A. Coulombe, *Intermediate filaments and tissue repair*. *Exp Cell Res*, 2004. **301**(1): p. 68-76.
16. Goldmann, W.H., *Intermediate filaments and cellular mechanics*. *Cell Biol Int*, 2018. **42**(2): p. 132-138.
17. Woolstenhulme, M.T., et al., *Desmin increases with high-intensity concentric contractions in humans*. *Muscle Nerve*, 2005. **31**(1): p. 20-4.
18. Woolstenhulme, M.T., et al., *Temporal response of desmin and dystrophin proteins to progressive resistance exercise in human skeletal muscle*. *J Appl Physiol (1985)*, 2006. **100**(6): p. 1876-82.
19. Shah, S.B., et al., *Structural and functional roles of desmin in mouse skeletal muscle during passive deformation*. *Biophys J*, 2004. **86**(5): p. 2993-3008.
20. Joanne, P., et al., *Absence of Desmin Results in Impaired Adaptive Response to Mechanical Overloading of Skeletal Muscle*. *Front Cell Dev Biol*, 2021. **9**: p. 662133.

21. Vaittinen, S., et al., *The expression of intermediate filament protein nestin as related to vimentin and desmin in regenerating skeletal muscle*. J Neuropathol Exp Neurol, 2001. **60**(6): p. 588-97.
22. Abe, T., et al., *Myocyte differentiation generates nuclear invaginations traversed by myofibrils associating with sarcomeric protein mRNAs*. J Cell Sci, 2004. **117**(Pt 26): p. 6523-34.
23. Stauber, W.T. and C.A. Smith, *Cellular responses in exertion-induced skeletal muscle injury*. Mol Cell Biochem, 1998. **179**(1-2): p. 189-96.
24. Vater, R., M.J. Cullen, and J.B. Harris, *The expression of vimentin in satellite cells of regenerating skeletal muscle in vivo*. Histochem J, 1994. **26**(12): p. 916-28.
25. Cizkova, D., T. Soukup, and J. Mokry, *Expression of nestin, desmin and vimentin in intact and regenerating muscle spindles of rat hind limb skeletal muscles*. Histochem Cell Biol, 2009. **131**(2): p. 197-206.
26. Akkila, W.M., et al., *Molecular cloning of up-regulated cytoskeletal genes from regenerating skeletal muscle: potential role of myocyte enhancer factor 2 proteins in the activation of muscle-regeneration-associated genes*. Biochem J, 1997. **325** (Pt 1)(Pt 1): p. 87-93.
27. Mohanasundaram, P., et al., *Cytoskeletal vimentin regulates cell size and autophagy through mTORC1 signaling*. PLoS Biol, 2022. **20**(9): p. e3001737.
28. Millward, D.J., *A protein-stat mechanism for regulation of growth and maintenance of the lean body mass*. Nutr Res Rev, 1995. **8**(1): p. 93-120.
29. Millward, D.J. and K. Smith, *The application of stable-isotope tracers to study human musculoskeletal protein turnover: a tale of bag filling and bag enlargement*. J Physiol, 2019. **597**(5): p. 1235-1249.
30. Ruple, B.A., et al., *Myofibril and Mitochondrial Area Changes in Type I and II Fibers Following 10 Weeks of Resistance Training in Previously Untrained Men*. Front Physiol, 2021. **12**: p. 728683.
31. MacDougall, J.D., et al., *Muscle ultrastructural characteristics of elite powerlifters and bodybuilders*. Eur J Appl Physiol Occup Physiol, 1982. **48**(1): p. 117-26.
32. Alway, S.E., et al., *Functional and structural adaptations in skeletal muscle of trained athletes*. J Appl Physiol (1985), 1988. **64**(3): p. 1114-20.
33. Willingham, T.B., et al., *The unified myofibrillar matrix for force generation in muscle*. Nat Commun, 2020. **11**(1): p. 3722.
34. Michel, J.M., et al., *Proteolytic markers associated with a gain and loss of leg muscle mass with resistance training followed by high-intensity interval training*. Exp Physiol, 2023. **108**(10): p. 1268-1281.
35. Glancy, B. and R.S. Balaban, *Energy metabolism design of the striated muscle cell*. Physiol Rev, 2021. **101**(4): p. 1561-1607.
36. Glancy, B., et al., *Mitochondrial reticulum for cellular energy distribution in muscle*. Nature, 2015. **523**(7562): p. 617-20.
37. Porter, C., et al., *Resistance Exercise Training Alters Mitochondrial Function in Human Skeletal Muscle*. Med Sci Sports Exerc, 2015. **47**(9): p. 1922-31.
38. Parry, H.A., M.D. Roberts, and A.N. Kavazis, *Human Skeletal Muscle Mitochondrial Adaptations Following Resistance Exercise Training*. Int J Sports Med, 2020. **41**(6): p. 349-359.

39. Lim, C., et al., *Resistance Exercise-induced Changes in Muscle Phenotype Are Load Dependent*. *Med Sci Sports Exerc*, 2019. **51**(12): p. 2578-2585.
40. Mesquita, P.H.C., et al., *Acute and chronic effects of resistance training on skeletal muscle markers of mitochondrial remodeling in older adults*. *Physiol Rep*, 2020. **8**(15): p. e14526.
41. Roberts, M.D., et al., *Sarcoplasmic Hypertrophy in Skeletal Muscle: A Scientific "Unicorn" or Resistance Training Adaptation?* *Front Physiol*, 2020. **11**: p. 816.
42. Haun, C.T., et al., *Muscle fiber hypertrophy in response to 6 weeks of high-volume resistance training in trained young men is largely attributed to sarcoplasmic hypertrophy*. *PLoS One*, 2019. **14**(6): p. e0215267.
43. Penman, K.A., *Ultrastructural changes in human striated muscle using three methods of training*. *Res Q*, 1969. **40**(4): p. 764-72.
44. Vann, C.G., et al., *Effects of High-Volume Versus High-Load Resistance Training on Skeletal Muscle Growth and Molecular Adaptations*. *Front Physiol*, 2022. **13**: p. 857555.
45. Roman, W. and E.R. Gomes, *Nuclear positioning in skeletal muscle*. *Semin Cell Dev Biol*, 2018. **82**: p. 51-56.
46. Allen, D.L., R.R. Roy, and V.R. Edgerton, *Myonuclear domains in muscle adaptation and disease*. *Muscle Nerve*, 1999. **22**(10): p. 1350-60.
47. Bagley, J.R., et al., *The myonuclear domain in adult skeletal muscle fibres: past, present and future*. *J Physiol*, 2023. **601**(4): p. 723-741.
48. Prasad, V. and D.P. Millay, *Skeletal muscle fibers count on nuclear numbers for growth*. *Semin Cell Dev Biol*, 2021. **119**: p. 3-10.
49. Cramer, A.A.W., et al., *Nuclear numbers in syncytial muscle fibers promote size but limit the development of larger myonuclear domains*. *Nat Commun*, 2020. **11**(1): p. 6287.
50. Hansson, K.A., et al., *Myonuclear content regulates cell size with similar scaling properties in mice and humans*. *Nat Commun*, 2020. **11**(1): p. 6288.
51. Brightwell, C.R., et al., *A glitch in the matrix: the pivotal role for extracellular matrix remodeling during muscle hypertrophy*. *Am J Physiol Cell Physiol*, 2022. **323**(3): p. C763-C771.
52. Widmann, M., A.M. Niess, and B. Munz, *Physical Exercise and Epigenetic Modifications in Skeletal Muscle*. *Sports Med*, 2019. **49**(4): p. 509-523.
53. Jones, P.A., *Functions of DNA methylation: islands, start sites, gene bodies and beyond*. *Nat Rev Genet*, 2012. **13**(7): p. 484-92.
54. Eden, S. and H. Cedar, *Role of DNA methylation in the regulation of transcription*. *Curr Opin Genet Dev*, 1994. **4**(2): p. 255-9.
55. Wu, X. and Y. Zhang, *TET-mediated active DNA demethylation: mechanism, function and beyond*. *Nat Rev Genet*, 2017. **18**(9): p. 517-534.
56. Sexton, C.L., et al., *Skeletal Muscle DNA Methylation and mRNA Responses to a Bout of Higher versus Lower Load Resistance Exercise in Previously Trained Men*. *Cells*, 2023. **12**(2).
57. Moore, L.D., T. Le, and G. Fan, *DNA methylation and its basic function*. *Neuropsychopharmacology*, 2013. **38**(1): p. 23-38.
58. Buitrago, D., et al., *Impact of DNA methylation on 3D genome structure*. *Nat Commun*, 2021. **12**(1): p. 3243.
59. Ruple, B.A., et al., *Resistance training rejuvenates the mitochondrial methylome in aged human skeletal muscle*. *FASEB J*, 2021. **35**(9): p. e21864.

60. Sharples, A.P., C.E. Stewart, and R.A. Seaborne, *Does skeletal muscle have an 'epi'-memory? The role of epigenetics in nutritional programming, metabolic disease, aging and exercise*. *Aging Cell*, 2016. **15**(4): p. 603-16.
61. Figueiredo, V.C., et al., *Genetic and epigenetic regulation of skeletal muscle ribosome biogenesis with exercise*. *J Physiol*, 2021. **599**(13): p. 3363-3384.
62. Von Walden, F., et al., *The myonuclear DNA methylome in response to an acute hypertrophic stimulus*. *Epigenetics*, 2020. **15**(11): p. 1151-1162.
63. Wen, Y., et al., *Nucleus Type-Specific DNA Methylation Reveals Epigenetic "Memory" of Prior Adaptation in Skeletal Muscle*. *Function (Oxf)*, 2021. **2**(5): p. zqab038.
64. Murach, K.A., et al., *Epigenetic evidence for distinct contributions of resident and acquired myonuclei during long-term exercise adaptation using timed in vivo myonuclear labeling*. *Am J Physiol Cell Physiol*, 2022. **322**(1): p. C86-C93.
65. Jones, R.G., 3rd, et al., *A molecular signature defining exercise adaptation with ageing and in vivo partial reprogramming in skeletal muscle*. *J Physiol*, 2023. **601**(4): p. 763-782.
66. McGee, S.L. and M. Hargreaves, *Histone modifications and exercise adaptations*. *J Appl Physiol* (1985), 2011. **110**(1): p. 258-63.
67. McGee, S.L., et al., *Exercise-induced histone modifications in human skeletal muscle*. *J Physiol*, 2009. **587**(Pt 24): p. 5951-8.
68. Gates, L.A., C.E. Foulds, and B.W. O'Malley, *Histone Marks in the 'Driver's Seat': Functional Roles in Steering the Transcription Cycle*. *Trends Biochem Sci*, 2017. **42**(12): p. 977-989.
69. Thalacker-Mercer, A., et al., *Cluster analysis reveals differential transcript profiles associated with resistance training-induced human skeletal muscle hypertrophy*. *Physiol Genomics*, 2013. **45**(12): p. 499-507.
70. Kirby, T.J., et al., *Myonuclear transcription is responsive to mechanical load and DNA content but uncoupled from cell size during hypertrophy*. *Mol Biol Cell*, 2016. **27**(5): p. 788-98.
71. Seaborne, R.A., et al., *Human Skeletal Muscle Possesses an Epigenetic Memory of Hypertrophy*. *Sci Rep*, 2018. **8**(1): p. 1898.
72. McCarthy, J.J., *The MyomiR network in skeletal muscle plasticity*. *Exerc Sport Sci Rev*, 2011. **39**(3): p. 150-4.
73. Luo, W., Q. Nie, and X. Zhang, *MicroRNAs involved in skeletal muscle differentiation*. *J Genet Genomics*, 2013. **40**(3): p. 107-16.
74. Horak, M., J. Novak, and J. Bienertova-Vasku, *Muscle-specific microRNAs in skeletal muscle development*. *Dev Biol*, 2016. **410**(1): p. 1-13.
75. McCarthy, J.J. and K.A. Esser, *MicroRNA-1 and microRNA-133a expression are decreased during skeletal muscle hypertrophy*. *J Appl Physiol* (1985), 2007. **102**(1): p. 306-13.
76. Mueller, M., et al., *Different molecular and structural adaptations with eccentric and conventional strength training in elderly men and women*. *Gerontology*, 2011. **57**(6): p. 528-38.
77. Drummond, M.J., et al., *Aging differentially affects human skeletal muscle microRNA expression at rest and after an anabolic stimulus of resistance exercise and essential amino acids*. *Am J Physiol Endocrinol Metab*, 2008. **295**(6): p. E1333-40.

78. Fyfe, J.J., et al., *Concurrent exercise incorporating high-intensity interval or continuous training modulates mTORC1 signaling and microRNA expression in human skeletal muscle*. *Am J Physiol Regul Integr Comp Physiol*, 2016. **310**(11): p. R1297-311.
79. Davidsen, P.K., et al., *High responders to resistance exercise training demonstrate differential regulation of skeletal muscle microRNA expression*. *J Appl Physiol* (1985), 2011. **110**(2): p. 309-17.
80. Vechetti, I.J., Jr., et al., *Life-long reduction in myomiR expression does not adversely affect skeletal muscle morphology*. *Sci Rep*, 2019. **9**(1): p. 5483.
81. Root-Bernstein, M. and R. Root-Bernstein, *The ribosome as a missing link in the evolution of life*. *J Theor Biol*, 2015. **367**: p. 130-158.
82. von Walden, F., *Ribosome biogenesis in skeletal muscle: coordination of transcription and translation*. *J Appl Physiol* (1985), 2019. **127**(2): p. 591-598.
83. Fromont-Racine, M., et al., *Ribosome assembly in eukaryotes*. *Gene*, 2003. **313**: p. 17-42.
84. Thomson, E., S. Ferreira-Cerca, and E. Hurt, *Eukaryotic ribosome biogenesis at a glance*. *J Cell Sci*, 2013. **126**(Pt 21): p. 4815-21.
85. Wen, Y., A.P. Alimov, and J.J. McCarthy, *Ribosome Biogenesis is Necessary for Skeletal Muscle Hypertrophy*. *Exerc Sport Sci Rev*, 2016. **44**(3): p. 110-5.
86. Moore, P.B. and T.A. Steitz, *The involvement of RNA in ribosome function*. *Nature*, 2002. **418**(6894): p. 229-35.
87. Wilson, D.N. and J.H. Doudna Cate, *The structure and function of the eukaryotic ribosome*. *Cold Spring Harb Perspect Biol*, 2012. **4**(5).
88. Valasek, L.S., *'Ribozomin'--translation initiation from the perspective of the ribosome-bound eukaryotic initiation factors (eIFs)*. *Curr Protein Pept Sci*, 2012. **13**(4): p. 305-30.
89. Hellen, C.U. and P. Sarnow, *Internal ribosome entry sites in eukaryotic mRNA molecules*. *Genes Dev*, 2001. **15**(13): p. 1593-612.
90. Xu, B., L. Liu, and G. Song, *Functions and Regulation of Translation Elongation Factors*. *Front Mol Biosci*, 2021. **8**: p. 816398.
91. Basharov, M.A., *Protein folding*. *J Cell Mol Med*, 2003. **7**(3): p. 223-37.
92. Waudby, C.A., C.M. Dobson, and J. Christodoulou, *Nature and Regulation of Protein Folding on the Ribosome*. *Trends Biochem Sci*, 2019. **44**(11): p. 914-926.
93. Kim, H.G., B. Guo, and G.A. Nader, *Regulation of Ribosome Biogenesis During Skeletal Muscle Hypertrophy*. *Exerc Sport Sci Rev*, 2019. **47**(2): p. 91-97.
94. Chaillou, T., T.J. Kirby, and J.J. McCarthy, *Ribosome biogenesis: emerging evidence for a central role in the regulation of skeletal muscle mass*. *J Cell Physiol*, 2014. **229**(11): p. 1584-94.
95. Grummt, I., *Regulation of mammalian ribosomal gene transcription by RNA polymerase I*. *Prog Nucleic Acid Res Mol Biol*, 1999. **62**: p. 109-54.
96. Leary, D.J. and S. Huang, *Regulation of ribosome biogenesis within the nucleolus*. *FEBS Lett*, 2001. **509**(2): p. 145-50.
97. Grandori, C., et al., *c-Myc binds to human ribosomal DNA and stimulates transcription of rRNA genes by RNA polymerase I*. *Nat Cell Biol*, 2005. **7**(3): p. 311-8.
98. Arabi, A., et al., *c-Myc associates with ribosomal DNA and activates RNA polymerase I transcription*. *Nat Cell Biol*, 2005. **7**(3): p. 303-10.
99. Figueiredo, V.C. and J.J. McCarthy, *Regulation of Ribosome Biogenesis in Skeletal Muscle Hypertrophy*. *Physiology* (Bethesda), 2019. **34**(1): p. 30-42.

100. Brook, M.S., et al., *It's not just about protein turnover: the role of ribosomal biogenesis and satellite cells in the regulation of skeletal muscle hypertrophy*. Eur J Sport Sci, 2019. **19**(7): p. 952-963.
101. Miller, G., et al., *hRRN3 is essential in the SL1-mediated recruitment of RNA Polymerase I to rRNA gene promoters*. EMBO J, 2001. **20**(6): p. 1373-82.
102. Nader, G.A., T.J. McLoughlin, and K.A. Esser, *mTOR function in skeletal muscle hypertrophy: increased ribosomal RNA via cell cycle regulators*. Am J Physiol Cell Physiol, 2005. **289**(6): p. C1457-65.
103. Poortinga, G., et al., *c-MYC coordinately regulates ribosomal gene chromatin remodeling and Pol I availability during granulocyte differentiation*. Nucleic Acids Res, 2011. **39**(8): p. 3267-81.
104. Hirsch, C.A., *Quantitative determination of the ribosomal ribonucleic acid content of liver and Novikoff hepatoma from fed and from fasted rats*. J Biol Chem, 1967. **242**(12): p. 2822-7.
105. Millward, D.J., et al., *Relationship between protein synthesis and RNA content in skeletal muscle*. Nature, 1973. **241**(5386): p. 204-5.
106. Roberts, M.D., et al., *Synergist ablation-induced hypertrophy occurs more rapidly in the plantaris than soleus muscle in rats due to different molecular mechanisms*. Am J Physiol Regul Integr Comp Physiol, 2020. **318**(2): p. R360-R368.
107. Goldberg, A.L., et al., *Mechanism of work-induced hypertrophy of skeletal muscle*. Med Sci Sports, 1975. **7**(3): p. 185-98.
108. Adams, G.R., F. Haddad, and K.M. Baldwin, *Time course of changes in markers of myogenesis in overloaded rat skeletal muscles*. J Appl Physiol (1985), 1999. **87**(5): p. 1705-12.
109. Haddad, F. and G.R. Adams, *Aging-sensitive cellular and molecular mechanisms associated with skeletal muscle hypertrophy*. J Appl Physiol (1985), 2006. **100**(4): p. 1188-203.
110. Wong, T.S. and F.W. Booth, *Skeletal muscle enlargement with weight-lifting exercise by rats*. J Appl Physiol (1985), 1988. **65**(2): p. 950-4.
111. Kotani, T., et al., *Consecutive bouts of electrical stimulation-induced contractions alter ribosome biogenesis in rat skeletal muscle*. J Appl Physiol (1985), 2019. **126**(6): p. 1673-1680.
112. Nakada, S., et al., *Correlation between Ribosome Biogenesis and the Magnitude of Hypertrophy in Overloaded Skeletal Muscle*. PLoS One, 2016. **11**(1): p. e0147284.
113. Kirby, T.J., et al., *Blunted hypertrophic response in aged skeletal muscle is associated with decreased ribosome biogenesis*. J Appl Physiol (1985), 2015. **119**(4): p. 321-7.
114. von Walden, F., et al., *Mechanical loading induces the expression of a Pol I regulon at the onset of skeletal muscle hypertrophy*. Am J Physiol Cell Physiol, 2012. **302**(10): p. C1523-30.
115. Nader, G.A., et al., *Resistance exercise training modulates acute gene expression during human skeletal muscle hypertrophy*. J Appl Physiol (1985), 2014. **116**(6): p. 693-702.
116. Fyfe, J.J., et al., *Enhanced skeletal muscle ribosome biogenesis, yet attenuated mTORC1 and ribosome biogenesis-related signalling, following short-term concurrent versus single-mode resistance training*. Sci Rep, 2018. **8**(1): p. 560.
117. Bickel, C.S., et al., *Time course of molecular responses of human skeletal muscle to acute bouts of resistance exercise*. J Appl Physiol (1985), 2005. **98**(2): p. 482-8.

118. Kadi, F., et al., *The effects of heavy resistance training and detraining on satellite cells in human skeletal muscles*. J Physiol, 2004. **558**(Pt 3): p. 1005-12.
119. Damas, F., et al., *Resistance training-induced changes in integrated myofibrillar protein synthesis are related to hypertrophy only after attenuation of muscle damage*. J Physiol, 2016. **594**(18): p. 5209-22.
120. Goreham, C., et al., *High-resistance training and muscle metabolism during prolonged exercise*. Am J Physiol, 1999. **276**(3): p. E489-96.
121. Hammarstrom, D., et al., *Benefits of higher resistance-training volume are related to ribosome biogenesis*. J Physiol, 2020. **598**(3): p. 543-565.
122. Hammarstrom, D., et al., *Ribosome accumulation during early phase resistance training in humans*. Acta Physiol (Oxf), 2022. **235**(1): p. e13806.
123. von Walden, F., et al., *mTOR signaling regulates myotube hypertrophy by modulating protein synthesis, rDNA transcription, and chromatin remodeling*. Am J Physiol Cell Physiol, 2016. **311**(4): p. C663-C672.
124. Keith, C.T. and S.L. Schreiber, *PIK-related kinases: DNA repair, recombination, and cell cycle checkpoints*. Science, 1995. **270**(5233): p. 50-1.
125. Laplante, M. and D.M. Sabatini, *mTOR signaling in growth control and disease*. Cell, 2012. **149**(2): p. 274-93.
126. Vainshtein, A. and M. Sandri, *Signaling Pathways That Control Muscle Mass*. Int J Mol Sci, 2020. **21**(13).
127. Menon, S., et al., *Spatial control of the TSC complex integrates insulin and nutrient regulation of mTORC1 at the lysosome*. Cell, 2014. **156**(4): p. 771-85.
128. Sancak, Y., et al., *Ragulator-Rag complex targets mTORC1 to the lysosomal surface and is necessary for its activation by amino acids*. Cell, 2010. **141**(2): p. 290-303.
129. Yoon, M.S., *mTOR as a Key Regulator in Maintaining Skeletal Muscle Mass*. Front Physiol, 2017. **8**: p. 788.
130. Saxton, R.A. and D.M. Sabatini, *mTOR Signaling in Growth, Metabolism, and Disease*. Cell, 2017. **168**(6): p. 960-976.
131. Lee, Y.L., et al., *Strain-Dependent Nanowrinkle Confinement of Block Copolymers*. Nano Lett, 2020. **20**(2): p. 1433-1439.
132. Yoon, M.S., et al., *Class III PI-3-kinase activates phospholipase D in an amino acid-sensing mTORC1 pathway*. J Cell Biol, 2011. **195**(3): p. 435-47.
133. Hornberger, T.A., et al., *The role of phospholipase D and phosphatidic acid in the mechanical activation of mTOR signaling in skeletal muscle*. Proc Natl Acad Sci U S A, 2006. **103**(12): p. 4741-6.
134. Marabita, M., et al., *S6K1 Is Required for Increasing Skeletal Muscle Force during Hypertrophy*. Cell Rep, 2016. **17**(2): p. 501-513.
135. Proud, C.G., *Role of mTOR signalling in the control of translation initiation and elongation by nutrients*. Curr Top Microbiol Immunol, 2004. **279**: p. 215-44.
136. Meyuhas, O., *Ribosomal Protein S6 Phosphorylation: Four Decades of Research*. Int Rev Cell Mol Biol, 2015. **320**: p. 41-73.
137. Bodine, S.C., *The role of mTORC1 in the regulation of skeletal muscle mass*. Fac Rev, 2022. **11**: p. 32.
138. Bond, P., *Regulation of mTORC1 by growth factors, energy status, amino acids and mechanical stimuli at a glance*. J Int Soc Sports Nutr, 2016. **13**: p. 8.

139. Rodgers, J.T., et al., *mTORC1 controls the adaptive transition of quiescent stem cells from G0 to G(Alert)*. *Nature*, 2014. **510**(7505): p. 393-6.
140. Santos, A.R., et al., *Different Resistance-Training Regimens Evoked a Similar Increase in Myostatin Inhibitors Expression*. *Int J Sports Med*, 2015. **36**(9): p. 761-8.
141. Liu, G.Y. and D.M. Sabatini, *mTOR at the nexus of nutrition, growth, ageing and disease*. *Nat Rev Mol Cell Biol*, 2020. **21**(4): p. 183-203.
142. Baar, K. and K. Esser, *Phosphorylation of p70(S6k) correlates with increased skeletal muscle mass following resistance exercise*. *Am J Physiol*, 1999. **276**(1): p. C120-7.
143. Nader, G.A. and K.A. Esser, *Intracellular signaling specificity in skeletal muscle in response to different modes of exercise*. *J Appl Physiol* (1985), 2001. **90**(5): p. 1936-42.
144. Bodine, S.C., et al., *Akt/mTOR pathway is a crucial regulator of skeletal muscle hypertrophy and can prevent muscle atrophy in vivo*. *Nat Cell Biol*, 2001. **3**(11): p. 1014-9.
145. Hornberger, T.A., et al., *Selenoprotein-deficient transgenic mice exhibit enhanced exercise-induced muscle growth*. *J Nutr*, 2003. **133**(10): p. 3091-7.
146. Bentzinger, C.F., et al., *Differential response of skeletal muscles to mTORC1 signaling during atrophy and hypertrophy*. *Skelet Muscle*, 2013. **3**(1): p. 6.
147. Martin, T.D., et al., *mTORC1 and JNK coordinate phosphorylation of the p70S6K1 autoinhibitory domain in skeletal muscle following functional overloading*. *Am J Physiol Endocrinol Metab*, 2014. **306**(12): p. E1397-405.
148. Chale-Rush, A., et al., *Effects of chronic overload on muscle hypertrophy and mTOR signaling in young adult and aged rats*. *J Gerontol A Biol Sci Med Sci*, 2009. **64**(12): p. 1232-9.
149. Hamilton, D.L., et al., *Molecular brakes regulating mTORC1 activation in skeletal muscle following synergist ablation*. *Am J Physiol Endocrinol Metab*, 2014. **307**(4): p. E365-73.
150. Karlsson, H.K., et al., *Branched-chain amino acids increase p70S6k phosphorylation in human skeletal muscle after resistance exercise*. *Am J Physiol Endocrinol Metab*, 2004. **287**(1): p. E1-7.
151. Dreyer, H.C., et al., *Resistance exercise increases AMPK activity and reduces 4E-BP1 phosphorylation and protein synthesis in human skeletal muscle*. *J Physiol*, 2006. **576**(Pt 2): p. 613-24.
152. Burd, N.A., et al., *Resistance exercise volume affects myofibrillar protein synthesis and anabolic signalling molecule phosphorylation in young men*. *J Physiol*, 2010. **588**(Pt 16): p. 3119-30.
153. Hodson, N., et al., *Differential localization and anabolic responsiveness of mTOR complexes in human skeletal muscle in response to feeding and exercise*. *Am J Physiol Cell Physiol*, 2017. **313**(6): p. C604-C611.
154. Mazzulla, M., et al., *LAT1 and SNAT2 Protein Expression and Membrane Localization of LAT1 Are Not Acutely Altered by Dietary Amino Acids or Resistance Exercise Nor Positively Associated with Leucine or Phenylalanine Incorporation in Human Skeletal Muscle*. *Nutrients*, 2021. **13**(11).
155. Teigland, M.B., *Medical examination of horses at auction sales*. *Vet Clin North Am Equine Pract*, 1992. **8**(2): p. 413-20.
156. Haun, C.T., et al., *Molecular, neuromuscular, and recovery responses to light versus heavy resistance exercise in young men*. *Physiol Rep*, 2017. **5**(18).

157. Mitchell, C.J., et al., *Resistance exercise load does not determine training-mediated hypertrophic gains in young men*. J Appl Physiol (1985), 2012. **113**(1): p. 71-7.
158. Reidy, P.T., et al., *Protein blend ingestion following resistance exercise promotes human muscle protein synthesis*. J Nutr, 2013. **143**(4): p. 410-6.
159. Gundermann, D.M., et al., *Activation of mTORC1 signaling and protein synthesis in human muscle following blood flow restriction exercise is inhibited by rapamycin*. Am J Physiol Endocrinol Metab, 2014. **306**(10): p. E1198-204.
160. Brook, M.S., et al., *Skeletal muscle hypertrophy adaptations predominate in the early stages of resistance exercise training, matching deuterium oxide-derived measures of muscle protein synthesis and mechanistic target of rapamycin complex 1 signaling*. FASEB J, 2015. **29**(11): p. 4485-96.
161. Eliasson, J., et al., *Maximal lengthening contractions increase p70 S6 kinase phosphorylation in human skeletal muscle in the absence of nutritional supply*. Am J Physiol Endocrinol Metab, 2006. **291**(6): p. E1197-205.
162. Kapoor, J.R., R. Kapoor, and T.L. Assimes, *Digital ischemia*. J Cardiovasc Med (Hagerstown), 2008. **9**(12): p. 1285-6.
163. Langer, H.T., et al., *Myofibrillar protein synthesis rates are increased in chronically exercised skeletal muscle despite decreased anabolic signaling*. Sci Rep, 2022. **12**(1): p. 7553.
164. Hahn-Windgassen, A., et al., *Akt activates the mammalian target of rapamycin by regulating cellular ATP level and AMPK activity*. J Biol Chem, 2005. **280**(37): p. 32081-9.
165. Psilander, N., R. Damsgaard, and H. Pilegaard, *Resistance exercise alters MRF and IGF-I mRNA content in human skeletal muscle*. J Appl Physiol (1985), 2003. **95**(3): p. 1038-44.
166. Roberts, M.D., et al., *IGF-I splice variant and IGF-I peptide expression patterns in young and old human skeletal muscle prior to and following sequential exercise bouts*. Eur J Appl Physiol, 2010. **110**(5): p. 961-9.
167. Hameed, M., et al., *Expression of IGF-I splice variants in young and old human skeletal muscle after high resistance exercise*. J Physiol, 2003. **547**(Pt 1): p. 247-54.
168. Adams, G.R. and F. Haddad, *The relationships among IGF-1, DNA content, and protein accumulation during skeletal muscle hypertrophy*. J Appl Physiol (1985), 1996. **81**(6): p. 2509-16.
169. Philippou, A., et al., *The role of the insulin-like growth factor 1 (IGF-1) in skeletal muscle physiology*. In Vivo, 2007. **21**(1): p. 45-54.
170. Schiaffino, S. and C. Mammucari, *Regulation of skeletal muscle growth by the IGF1-Akt/PKB pathway: insights from genetic models*. Skelet Muscle, 2011. **1**(1): p. 4.
171. Adams, G.R., *Role of insulin-like growth factor-I in the regulation of skeletal muscle adaptation to increased loading*. Exerc Sport Sci Rev, 1998. **26**: p. 31-60.
172. Philp, A., D.L. Hamilton, and K. Baar, *Signals mediating skeletal muscle remodeling by resistance exercise: PI3-kinase independent activation of mTORC1*. J Appl Physiol (1985), 2011. **110**(2): p. 561-8.
173. Hornberger, T.A., et al., *Mechanical stimuli regulate rapamycin-sensitive signalling by a phosphoinositide 3-kinase-, protein kinase B- and growth factor-independent mechanism*. Biochem J, 2004. **380**(Pt 3): p. 795-804.

174. Simon, S., et al., *DOG1 regulates growth and IGFBP5 in gastrointestinal stromal tumors*. *Cancer Res*, 2013. **73**(12): p. 3661-70.
175. Maruyama, Y., et al., *High-intensity muscle contraction-mediated increases in Akt1 and Akt2 phosphorylation do not contribute to mTORC1 activation and muscle protein synthesis*. *J Appl Physiol* (1985), 2020. **128**(4): p. 830-837.
176. Miyazaki, M., et al., *Early activation of mTORC1 signalling in response to mechanical overload is independent of phosphoinositide 3-kinase/Akt signalling*. *J Physiol*, 2011. **589**(Pt 7): p. 1831-46.
177. MacKenzie, M.G., et al., *mVps34 is activated following high-resistance contractions*. *J Physiol*, 2009. **587**(1): p. 253-60.
178. Roberson, P.A., et al., *LAT1 Protein Content Increases Following 12 Weeks of Resistance Exercise Training in Human Skeletal Muscle*. *Front Nutr*, 2020. **7**: p. 628405.
179. Hodson, N., et al., *Characterisation of L-Type Amino Acid Transporter 1 (LAT1) Expression in Human Skeletal Muscle by Immunofluorescent Microscopy*. *Nutrients*, 2017. **10**(1).
180. Huang, J. and B.D. Manning, *The TSC1-TSC2 complex: a molecular switchboard controlling cell growth*. *Biochem J*, 2008. **412**(2): p. 179-90.
181. Jacobs, B.L., et al., *Eccentric contractions increase the phosphorylation of tuberous sclerosis complex-2 (TSC2) and alter the targeting of TSC2 and the mechanistic target of rapamycin to the lysosome*. *J Physiol*, 2013. **591**(18): p. 4611-20.
182. Jacobs, B.L., et al., *Identification of mechanically regulated phosphorylation sites on tuberin (TSC2) that control mechanistic target of rapamycin (mTOR) signaling*. *J Biol Chem*, 2017. **292**(17): p. 6987-6997.
183. Vandenburg, H.H., *Motion into mass: how does tension stimulate muscle growth?* *Med Sci Sports Exerc*, 1987. **19**(5 Suppl): p. S142-9.
184. Klossner, S., et al., *Mechano-transduction to muscle protein synthesis is modulated by FAK*. *Eur J Appl Physiol*, 2009. **106**(3): p. 389-98.
185. Fluck, M. and H. Hoppeler, *Molecular basis of skeletal muscle plasticity--from gene to form and function*. *Rev Physiol Biochem Pharmacol*, 2003. **146**: p. 159-216.
186. Durieux, A.C., et al., *Mechanotransduction in striated muscle via focal adhesion kinase*. *Biochem Soc Trans*, 2007. **35**(Pt 5): p. 1312-3.
187. You, J.S., et al., *The role of diacylglycerol kinase zeta and phosphatidic acid in the mechanical activation of mammalian target of rapamycin (mTOR) signaling and skeletal muscle hypertrophy*. *J Biol Chem*, 2014. **289**(3): p. 1551-63.
188. O'Neil, T.K., et al., *The role of phosphoinositide 3-kinase and phosphatidic acid in the regulation of mammalian target of rapamycin following eccentric contractions*. *J Physiol*, 2009. **587**(Pt 14): p. 3691-701.
189. You, J.S., J.W. Frey, and T.A. Hornberger, *Mechanical stimulation induces mTOR signaling via an ERK-independent mechanism: implications for a direct activation of mTOR by phosphatidic acid*. *PLoS One*, 2012. **7**(10): p. e47258.
190. You, J.S., et al., *A DGKzeta-FoxO-ubiquitin proteolytic axis controls fiber size during skeletal muscle remodeling*. *Sci Signal*, 2018. **11**(530).
191. Fluck, M., et al., *Focal adhesion proteins FAK and paxillin increase in hypertrophied skeletal muscle*. *Am J Physiol*, 1999. **277**(1): p. C152-62.

192. Crossland, H., et al., *Focal adhesion kinase is required for IGF-I-mediated growth of skeletal muscle cells via a TSC2/mTOR/S6K1-associated pathway*. *Am J Physiol Endocrinol Metab*, 2013. **305**(2): p. E183-93.
193. Parsons, J.T., *Focal adhesion kinase: the first ten years*. *J Cell Sci*, 2003. **116**(Pt 8): p. 1409-16.
194. Paul, R., et al., *FAK activates AKT-mTOR signaling to promote the growth and progression of MMTV-Wnt1-driven basal-like mammary tumors*. *Breast Cancer Res*, 2020. **22**(1): p. 59.
195. Lee, F.Y., et al., *The mTOR-FAK mechanotransduction signaling axis for focal adhesion maturation and cell proliferation*. *Am J Transl Res*, 2017. **9**(4): p. 1603-1617.
196. Gan, B., Y. Yoo, and J.L. Guan, *Association of focal adhesion kinase with tuberous sclerosis complex 2 in the regulation of s6 kinase activation and cell growth*. *J Biol Chem*, 2006. **281**(49): p. 37321-9.
197. Boppart, M.D., D.J. Burkin, and S.J. Kaufman, *Alpha7beta1-integrin regulates mechanotransduction and prevents skeletal muscle injury*. *Am J Physiol Cell Physiol*, 2006. **290**(6): p. C1660-5.
198. Glover, E.I., et al., *Resistance exercise decreases eIF2Bepsilon phosphorylation and potentiates the feeding-induced stimulation of p70S6K1 and rpS6 in young men*. *Am J Physiol Regul Integr Comp Physiol*, 2008. **295**(2): p. R604-10.
199. Eftestol, E., et al., *JNK activation in TA and EDL muscle is load-dependent in rats receiving identical excitation patterns*. *Sci Rep*, 2021. **11**(1): p. 16405.
200. Takala, T.E. and P. Virtanen, *Biochemical composition of muscle extracellular matrix: the effect of loading*. *Scand J Med Sci Sports*, 2000. **10**(6): p. 321-5.
201. Halper, J. and M. Kjaer, *Basic components of connective tissues and extracellular matrix: elastin, fibrillin, fibulins, fibrinogen, fibronectin, laminin, tenascins and thrombospondins*. *Adv Exp Med Biol*, 2014. **802**: p. 31-47.
202. Kjaer, M., et al., *Extracellular matrix adaptation of tendon and skeletal muscle to exercise*. *J Anat*, 2006. **208**(4): p. 445-50.
203. Humphrey, J.D., E.R. Dufresne, and M.A. Schwartz, *Mechanotransduction and extracellular matrix homeostasis*. *Nat Rev Mol Cell Biol*, 2014. **15**(12): p. 802-12.
204. Kjaer, M., *Role of extracellular matrix in adaptation of tendon and skeletal muscle to mechanical loading*. *Physiol Rev*, 2004. **84**(2): p. 649-98.
205. Mendias, C.L., et al., *Changes in muscle fiber contractility and extracellular matrix production during skeletal muscle hypertrophy*. *J Appl Physiol (1985)*, 2017. **122**(3): p. 571-579.
206. White, J.P., et al., *Overload-induced skeletal muscle extracellular matrix remodelling and myofibre growth in mice lacking IL-6*. *Acta Physiol (Oxf)*, 2009. **197**(4): p. 321-32.
207. Calve, S., et al., *Hyaluronic acid, HAS1, and HAS2 are significantly upregulated during muscle hypertrophy*. *Am J Physiol Cell Physiol*, 2012. **303**(5): p. C577-88.
208. Guzzoni, V., et al., *Effect of Resistance Training on Extracellular Matrix Adaptations in Skeletal Muscle of Older Rats*. *Front Physiol*, 2018. **9**: p. 374.
209. Murach, K.A., et al., *Multi-transcriptome analysis following an acute skeletal muscle growth stimulus yields tools for discerning global and MYC regulatory networks*. *J Biol Chem*, 2022. **298**(11): p. 102515.

210. Khan, Y., et al., *Increased biological relevance of transcriptome analyses in human skeletal muscle using a model-specific pipeline*. BMC Bioinformatics, 2020. **21**(1): p. 548.
211. Angleri, V., et al., *Resistance training variable manipulations are less relevant than intrinsic biology in affecting muscle fiber hypertrophy*. Scand J Med Sci Sports, 2022. **32**(5): p. 821-832.
212. Moore, D.R., et al., *Myofibrillar and collagen protein synthesis in human skeletal muscle in young men after maximal shortening and lengthening contractions*. Am J Physiol Endocrinol Metab, 2005. **288**(6): p. E1153-9.
213. Mackey, A.L., et al., *Skeletal muscle collagen content in humans after high-force eccentric contractions*. J Appl Physiol (1985), 2004. **97**(1): p. 197-203.
214. MacDougall, J.D., et al., *Muscle fiber number in biceps brachii in bodybuilders and control subjects*. J Appl Physiol Respir Environ Exerc Physiol, 1984. **57**(5): p. 1399-403.
215. Godwin, J.S., et al., *Extracellular matrix content and remodeling markers do not differ in college-aged men classified as higher and lower responders to resistance training*. J Appl Physiol (1985), 2023. **134**(3): p. 731-741.
216. Allen, R.E. and L.K. Boxhorn, *Regulation of skeletal muscle satellite cell proliferation and differentiation by transforming growth factor-beta, insulin-like growth factor I, and fibroblast growth factor*. J Cell Physiol, 1989. **138**(2): p. 311-5.
217. Rotwein, P., *Insulin-like growth factor action and skeletal muscle growth, an in vivo perspective*. Growth Horm IGF Res, 2003. **13**(6): p. 303-5.
218. Iozzo, R.V., et al., *Decorin antagonizes IGF receptor I (IGF-IR) function by interfering with IGF-IR activity and attenuating downstream signaling*. J Biol Chem, 2011. **286**(40): p. 34712-21.
219. Suzuki, K., et al., *Decorin activates Akt downstream of IGF-IR and promotes myoblast differentiation*. Anim Sci J, 2013. **84**(9): p. 669-74.
220. Imai, K., et al., *Degradation of decorin by matrix metalloproteinases: identification of the cleavage sites, kinetic analyses and transforming growth factor-beta1 release*. Biochem J, 1997. **322** (Pt 3)(Pt 3): p. 809-14.
221. Gumucio, J.P., K.B. Sugg, and C.L. Mendias, *TGF-beta superfamily signaling in muscle and tendon adaptation to resistance exercise*. Exerc Sport Sci Rev, 2015. **43**(2): p. 93-9.
222. Massague, J., et al., *Type beta transforming growth factor is an inhibitor of myogenic differentiation*. Proc Natl Acad Sci U S A, 1986. **83**(21): p. 8206-10.
223. Droguett, R., et al., *Extracellular proteoglycans modify TGF-beta bio-availability attenuating its signaling during skeletal muscle differentiation*. Matrix Biol, 2006. **25**(6): p. 332-41.
224. Demonbreun, A.R., et al., *Anti-latent TGFbeta binding protein 4 antibody improves muscle function and reduces muscle fibrosis in muscular dystrophy*. Sci Transl Med, 2021. **13**(610): p. eabf0376.
225. Pawlikowski, B., et al., *Regulation of skeletal muscle stem cells by fibroblast growth factors*. Dev Dyn, 2017. **246**(5): p. 359-367.
226. Velleman, S.G., et al., *Effects of glypican-1 on turkey skeletal muscle cell proliferation, differentiation and fibroblast growth factor 2 responsiveness*. Dev Growth Differ, 2006. **48**(4): p. 271-6.
227. Pisconti, A., J.D. Bernet, and B.B. Olwin, *Syndecans in skeletal muscle development, regeneration and homeostasis*. Muscles Ligaments Tendons J, 2012. **2**(1): p. 1-9.

228. Velleman, S.G., C.S. Coy, and D.C. McFarland, *Effect of syndecan-1, syndecan-4, and glypican-1 on turkey muscle satellite cell proliferation, differentiation, and responsiveness to fibroblast growth factor 2*. *Poult Sci*, 2007. **86**(7): p. 1406-13.
229. McKellar, D.W., et al., *Large-scale integration of single-cell transcriptomic data captures transitional progenitor states in mouse skeletal muscle regeneration*. *Commun Biol*, 2021. **4**(1): p. 1280.
230. Fry, C.S., et al., *Myogenic Progenitor Cells Control Extracellular Matrix Production by Fibroblasts during Skeletal Muscle Hypertrophy*. *Cell Stem Cell*, 2017. **20**(1): p. 56-69.
231. Kaneshige, A., et al., *Relayed signaling between mesenchymal progenitors and muscle stem cells ensures adaptive stem cell response to increased mechanical load*. *Cell Stem Cell*, 2022. **29**(2): p. 265-280 e6.
232. Schuler, S.C., et al., *Extensive remodeling of the extracellular matrix during aging contributes to age-dependent impairments of muscle stem cell functionality*. *Cell Rep*, 2021. **35**(10): p. 109223.
233. Fry, C.S., et al., *Regulation of the muscle fiber microenvironment by activated satellite cells during hypertrophy*. *FASEB J*, 2014. **28**(4): p. 1654-65.
234. Lemos, D.R., et al., *Nilotinib reduces muscle fibrosis in chronic muscle injury by promoting TNF-mediated apoptosis of fibro/adipogenic progenitors*. *Nat Med*, 2015. **21**(7): p. 786-94.
235. Murach, K.A., et al., *Fusion-Independent Satellite Cell Communication to Muscle Fibers During Load-Induced Hypertrophy*. *Function (Oxf)*, 2020. **1**(1): p. zqaa009.
236. Fry, C.S., et al., *Inducible depletion of satellite cells in adult, sedentary mice impairs muscle regenerative capacity without affecting sarcopenia*. *Nat Med*, 2015. **21**(1): p. 76-80.
237. Goh, Q. and D.P. Millay, *Requirement of myomaker-mediated stem cell fusion for skeletal muscle hypertrophy*. *Elife*, 2017. **6**.
238. Goh, Q., et al., *Myonuclear accretion is a determinant of exercise-induced remodeling in skeletal muscle*. *Elife*, 2019. **8**.
239. Englund, D.A., et al., *Skeletal muscle aging, cellular senescence, and senotherapeutics: Current knowledge and future directions*. *Mech Ageing Dev*, 2021. **200**: p. 111595.
240. Snijders, T., et al., *Myonuclear content and domain size in small versus larger muscle fibres in response to 12 weeks of resistance exercise training in older adults*. *Acta Physiol (Oxf)*, 2021. **231**(4): p. e13599.
241. Petrella, J.K., et al., *Potent myofiber hypertrophy during resistance training in humans is associated with satellite cell-mediated myonuclear addition: a cluster analysis*. *J Appl Physiol (1985)*, 2008. **104**(6): p. 1736-42.
242. Wang, S., et al., *Mechanotransduction via the LINC complex regulates DNA replication in myonuclei*. *J Cell Biol*, 2018. **217**(6): p. 2005-2018.
243. Malm, C., et al., *Leukocytes, cytokines, growth factors and hormones in human skeletal muscle and blood after uphill or downhill running*. *J Physiol*, 2004. **556**(Pt 3): p. 983-1000.
244. Fielding, R.A., et al., *Acute phase response in exercise. III. Neutrophil and IL-1 beta accumulation in skeletal muscle*. *Am J Physiol*, 1993. **265**(1 Pt 2): p. R166-72.
245. Dos Santos, M., et al., *Single-nucleus RNA-seq and FISH identify coordinated transcriptional activity in mammalian myofibers*. *Nat Commun*, 2020. **11**(1): p. 5102.

246. Mauro, A., *Satellite cell of skeletal muscle fibers*. J Biophys Biochem Cytol, 1961. **9**(2): p. 493-5.
247. Mackey, A.L., et al., *Enhanced satellite cell proliferation with resistance training in elderly men and women*. Scand J Med Sci Sports, 2007. **17**(1): p. 34-42.
248. Seale, P., et al., *Pax7 is required for the specification of myogenic satellite cells*. Cell, 2000. **102**(6): p. 777-86.
249. Bachman, J.F., et al., *Prepubertal skeletal muscle growth requires Pax7-expressing satellite cell-derived myonuclear contribution*. Development, 2018. **145**(20).
250. Bachman, J.F., et al., *Radiation-Induced Damage to Prepubertal Pax7+ Skeletal Muscle Stem Cells Drives Lifelong Deficits in Myofiber Size and Nuclear Number*. iScience, 2020. **23**(11): p. 101760.
251. Dayanidhi, S. and R.L. Lieber, *Skeletal muscle satellite cells: mediators of muscle growth during development and implications for developmental disorders*. Muscle Nerve, 2014. **50**(5): p. 723-32.
252. Moss, F.P. and C.P. Leblond, *Nature of dividing nuclei in skeletal muscle of growing rats*. J Cell Biol, 1970. **44**(2): p. 459-62.
253. Moss, F.P. and C.P. Leblond, *Satellite cells as the source of nuclei in muscles of growing rats*. Anat Rec, 1971. **170**(4): p. 421-35.
254. Schiaffino, S., S.P. Bormioli, and M. Aloisi, *The fate of newly formed satellite cells during compensatory muscle hypertrophy*. Virchows Arch B Cell Pathol, 1976. **21**(2): p. 113-8.
255. Schiaffino, S., S.P. Bormioli, and M. Aloisi, *Cell proliferation in rat skeletal muscle during early stages of compensatory hypertrophy*. Virchows Arch B Cell Pathol, 1972. **11**(3): p. 268-73.
256. Murphy, M.M., et al., *Satellite cells, connective tissue fibroblasts and their interactions are crucial for muscle regeneration*. Development, 2011. **138**(17): p. 3625-37.
257. Liu, W., et al., *Inducible depletion of adult skeletal muscle stem cells impairs the regeneration of neuromuscular junctions*. Elife, 2015. **4**.
258. Shuler, K.T., et al., *Muscle Stem Cell-Derived Extracellular Vesicles Reverse Hydrogen Peroxide-Induced Mitochondrial Dysfunction in Mouse Myotubes*. Cells, 2020. **9**(12).
259. Yablonka-Reuveni, Z. and C. Lepper, *New Insight into a Classic Stem Cell: the Satellite Cell may Communicate with the Muscle Fiber via Extracellular Vesicles-A Perspective on "Fusion-Independent Satellite Cell Communication to Muscle Fibers During Load-Induced Hypertrophy"*. Function (Oxf), 2020. **1**(2): p. zqaa015.
260. Murach, K.A., et al., *Early satellite cell communication creates a permissive environment for long-term muscle growth*. iScience, 2021. **24**(4): p. 102372.
261. Abou Sawan, S., et al., *Satellite cell and myonuclear accretion is related to training-induced skeletal muscle fiber hypertrophy in young males and females*. J Appl Physiol (1985), 2021. **131**(3): p. 871-880.
262. Lundberg, T.R., et al., *Early accentuated muscle hypertrophy is strongly associated with myonuclear accretion*. Am J Physiol Regul Integr Comp Physiol, 2020. **319**(1): p. R50-R58.
263. Olsen, S., et al., *Creatine supplementation augments the increase in satellite cell and myonuclei number in human skeletal muscle induced by strength training*. J Physiol, 2006. **573**(Pt 2): p. 525-34.

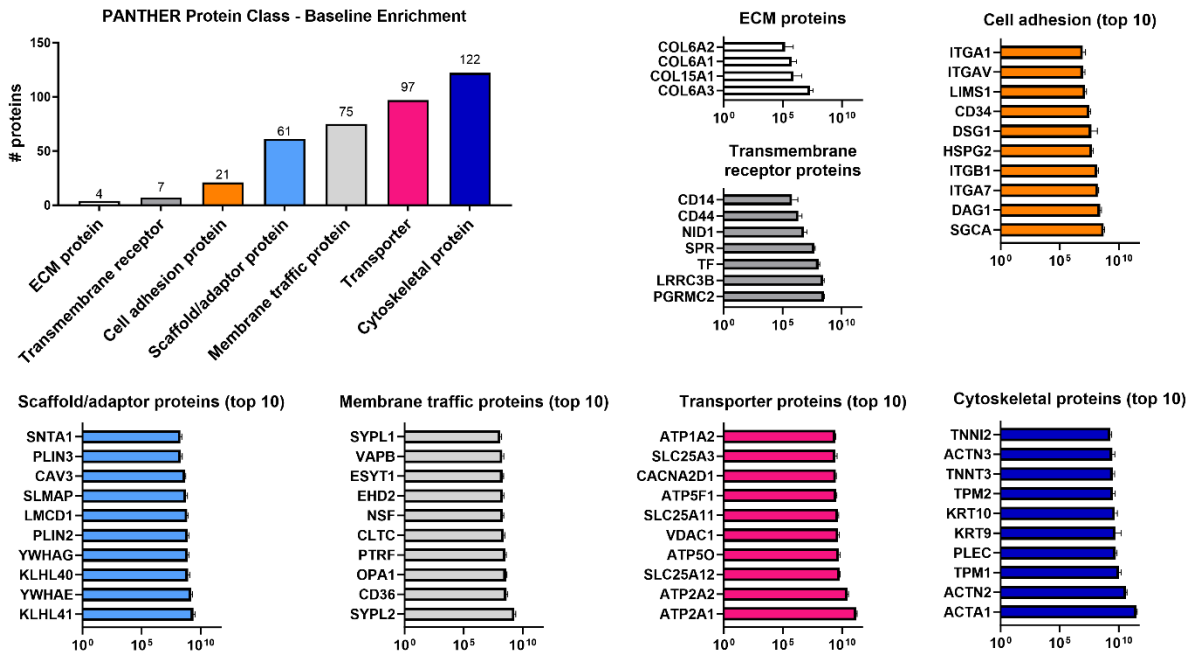
264. Kadi, F. and L.E. Thornell, *Concomitant increases in myonuclear and satellite cell content in female trapezius muscle following strength training*. *Histochem Cell Biol*, 2000. **113**(2): p. 99-103.
265. Snijders, T., et al., *Changes in myonuclear domain size do not precede muscle hypertrophy during prolonged resistance-type exercise training*. *Acta Physiol (Oxf)*, 2016. **216**(2): p. 231-9.
266. Reidy, P.T., et al., *Protein Supplementation Does Not Affect Myogenic Adaptations to Resistance Training*. *Med Sci Sports Exerc*, 2017. **49**(6): p. 1197-1208.
267. Kadi, F., et al., *Cellular adaptation of the trapezius muscle in strength-trained athletes*. *Histochem Cell Biol*, 1999. **111**(3): p. 189-95.
268. Murach, K.A., et al., *Myonuclear Domain Flexibility Challenges Rigid Assumptions on Satellite Cell Contribution to Skeletal Muscle Fiber Hypertrophy*. *Front Physiol*, 2018. **9**: p. 635.
269. Damas, F., et al., *Early- and later-phases satellite cell responses and myonuclear content with resistance training in young men*. *PLoS One*, 2018. **13**(1): p. e0191039.
270. Herman-Montemayor, J.R., R.S. Hikida, and R.S. Staron, *Early-Phase Satellite Cell and Myonuclear Domain Adaptations to Slow-Speed vs. Traditional Resistance Training Programs*. *J Strength Cond Res*, 2015. **29**(11): p. 3105-14.
271. Conceicao, M.S., et al., *Muscle Fiber Hypertrophy and Myonuclei Addition: A Systematic Review and Meta-analysis*. *Med Sci Sports Exerc*, 2018. **50**(7): p. 1385-1393.
272. Mobley, C.B., et al., *CORP: Using transgenic mice to study skeletal muscle physiology*. *J Appl Physiol (1985)*, 2020. **128**(5): p. 1227-1239.
273. McCarthy, J.J., et al., *Effective fiber hypertrophy in satellite cell-depleted skeletal muscle*. *Development*, 2011. **138**(17): p. 3657-66.
274. Egner, I.M., J.C. Bruusgaard, and K. Gundersen, *Satellite cell depletion prevents fiber hypertrophy in skeletal muscle*. *Development*, 2016. **143**(16): p. 2898-906.
275. Murach, K.A., et al., *Differential requirement for satellite cells during overload-induced muscle hypertrophy in growing versus mature mice*. *Skelet Muscle*, 2017. **7**(1): p. 14.
276. Millay, D.P., et al., *Myomaker is a membrane activator of myoblast fusion and muscle formation*. *Nature*, 2013. **499**(7458): p. 301-5.
277. Englund, D.A., et al., *Satellite Cell Depletion Disrupts Transcriptional Coordination and Muscle Adaptation to Exercise*. *Function (Oxf)*, 2021. **2**(1): p. zqaa033.
278. Murach, K.A., et al., *Starring or Supporting Role? Satellite Cells and Skeletal Muscle Fiber Size Regulation*. *Physiology (Bethesda)*, 2018. **33**(1): p. 26-38.
279. Mackey, A.L., et al., *Human skeletal muscle fibroblasts stimulate in vitro myogenesis and in vivo muscle regeneration*. *J Physiol*, 2017. **595**(15): p. 5115-5127.
280. Hyldahl, R.D., et al., *Extracellular matrix remodeling and its contribution to protective adaptation following lengthening contractions in human muscle*. *FASEB J*, 2015. **29**(7): p. 2894-904.
281. Abou-Khalil, R., R. Mounier, and B. Chazaud, *Regulation of myogenic stem cell behavior by vessel cells: the "menage a trois" of satellite cells, periendothelial cells and endothelial cells*. *Cell Cycle*, 2010. **9**(5): p. 892-6.
282. Mathew, S.J., et al., *Connective tissue fibroblasts and Tcf4 regulate myogenesis*. *Development*, 2011. **138**(2): p. 371-84.

283. Zou, Y., et al., *Muscle interstitial fibroblasts are the main source of collagen VI synthesis in skeletal muscle: implications for congenital muscular dystrophy types Ullrich and Bethlem*. J Neuropathol Exp Neurol, 2008. **67**(2): p. 144-54.
284. Fry, C.S., et al., *ACL injury reduces satellite cell abundance and promotes fibrogenic cell expansion within skeletal muscle*. J Orthop Res, 2017. **35**(9): p. 1876-1885.
285. Malecova, B., et al., *Dynamics of cellular states of fibro-adipogenic progenitors during myogenesis and muscular dystrophy*. Nat Commun, 2018. **9**(1): p. 3670.
286. Warwick, R., et al., *A scenario-based volcanic hazard assessment for the Mount Meager Volcanic Complex, British Columbia*. J Appl Volcanol, 2022. **11**(1): p. 5.
287. Sugg, K.B., et al., *Inhibition of platelet-derived growth factor signaling prevents muscle fiber growth during skeletal muscle hypertrophy*. FEBS Lett, 2017. **591**(5): p. 801-809.
288. Heredia, J.E., et al., *Type 2 innate signals stimulate fibro/adipogenic progenitors to facilitate muscle regeneration*. Cell, 2013. **153**(2): p. 376-88.
289. Joe, A.W., et al., *Muscle injury activates resident fibro/adipogenic progenitors that facilitate myogenesis*. Nat Cell Biol, 2010. **12**(2): p. 153-63.
290. Wosczyzna, M.N., et al., *Mesenchymal Stromal Cells Are Required for Regeneration and Homeostatic Maintenance of Skeletal Muscle*. Cell Rep, 2019. **27**(7): p. 2029-2035 e5.
291. Stearns-Reider, K.M., et al., *Aging of the skeletal muscle extracellular matrix drives a stem cell fibrogenic conversion*. Aging Cell, 2017. **16**(3): p. 518-528.
292. Loomis, T., et al., *Matrix stiffness and architecture drive fibro-adipogenic progenitors' activation into myofibroblasts*. Sci Rep, 2022. **12**(1): p. 13582.
293. Farup, J., et al., *Pericyte response to contraction mode-specific resistance exercise training in human skeletal muscle*. J Appl Physiol (1985), 2015. **119**(10): p. 1053-63.
294. Gaulton, N., et al., *Twist2-expressing cells reside in human skeletal muscle and are responsive to aging and resistance exercise training*. FASEB J, 2022. **36**(12): p. e22642.
295. Bernard, C., et al., *Role of macrophages during skeletal muscle regeneration and hypertrophy-Implications for immunomodulatory strategies*. Physiol Rep, 2022. **10**(19): p. e15480.
296. Minari, A.L.A. and R.V. Thomatieli-Santos, *From skeletal muscle damage and regeneration to the hypertrophy induced by exercise: what is the role of different macrophage subsets?* Am J Physiol Regul Integr Comp Physiol, 2022. **322**(1): p. R41-R54.
297. Walton, R.G., et al., *Human skeletal muscle macrophages increase following cycle training and are associated with adaptations that may facilitate growth*. Sci Rep, 2019. **9**(1): p. 969.
298. Walton, R.G., et al., *Metformin blunts muscle hypertrophy in response to progressive resistance exercise training in older adults: A randomized, double-blind, placebo-controlled, multicenter trial: The MASTERS trial*. Aging Cell, 2019. **18**(6): p. e13039.
299. Jensen, S.M., et al., *Macrophage Subpopulations and the Acute Inflammatory Response of Elderly Human Skeletal Muscle to Physiological Resistance Exercise*. Front Physiol, 2020. **11**: p. 811.
300. DiPasquale, D.M., et al., *Urokinase-type plasminogen activator and macrophages are required for skeletal muscle hypertrophy in mice*. Am J Physiol Cell Physiol, 2007. **293**(4): p. C1278-85.

301. Tonkin, J., et al., *Monocyte/Macrophage-derived IGF-1 Orchestrates Murine Skeletal Muscle Regeneration and Modulates Autocrine Polarization*. Mol Ther, 2015. **23**(7): p. 1189-1200.
302. Juban, G., et al., *AMPK Activation Regulates LTBP4-Dependent TGF-beta1 Secretion by Pro-inflammatory Macrophages and Controls Fibrosis in Duchenne Muscular Dystrophy*. Cell Rep, 2018. **25**(8): p. 2163-2176 e6.
303. Peck, B.D., et al., *A muscle cell-macrophage axis involving matrix metalloproteinase 14 facilitates extracellular matrix remodeling with mechanical loading*. FASEB J, 2022. **36**(2): p. e22155.
304. Long, D.E., et al., *Skeletal muscle properties show collagen organization and immune cell content are associated with resistance exercise response heterogeneity in older persons*. J Appl Physiol (1985), 2022. **132**(6): p. 1432-1447.
305. Sexton, C.L., et al., *Effects of Peanut Protein Supplementation on Resistance Training Adaptations in Younger Adults*. Nutrients, 2021. **13**(11).
306. Levin, Y., *The role of statistical power analysis in quantitative proteomics*. Proteomics, 2011. **11**(12): p. 2565-7.
307. Wen, Y., et al., *MyoVision: software for automated high-content analysis of skeletal muscle immunohistochemistry*. J Appl Physiol (1985), 2018. **124**(1): p. 40-51.
308. Libardi, C.A., et al., *Effects of low-load resistance training with blood flow restriction on muscle fiber myofibrillar and extracellular area*. Front Physiol, 2024. **15**: p. 1368646.
309. Rupert, J.E., D.H.A. Jengelle, and T.A. Zimmers, *In Vitro, In Vivo, and In Silico Methods for Assessment of Muscle Size and Muscle Growth Regulation*. Shock, 2020. **53**(5): p. 605-615.
310. Wen, Y., et al., *High-yield skeletal muscle protein recovery from TRIzol after RNA and DNA extraction*. Biotechniques, 2020. **69**(4): p. 264-269.
311. Tabula Muris, C., et al., *Single-cell transcriptomics of 20 mouse organs creates a Tabula Muris*. Nature, 2018. **562**(7727): p. 367-372.
312. Cheng, F., et al., *Vimentin coordinates fibroblast proliferation and keratinocyte differentiation in wound healing via TGF-beta-Slug signaling*. Proc Natl Acad Sci U S A, 2016. **113**(30): p. E4320-7.
313. Wang, R.C., et al., *Akt-mediated regulation of autophagy and tumorigenesis through Beclin 1 phosphorylation*. Science, 2012. **338**(6109): p. 956-9.
314. Wilhelmsson, U., et al., *Vimentin is required for normal accumulation of body fat*. Biol Chem, 2019. **400**(9): p. 1157-1162.
315. Charge, S.B. and M.A. Rudnicki, *Cellular and molecular regulation of muscle regeneration*. Physiol Rev, 2004. **84**(1): p. 209-38.
316. Guttsches, A.K., et al., *ATOH8: a novel marker in human muscle fiber regeneration*. Histochem Cell Biol, 2015. **143**(5): p. 443-52.
317. Rittling, S.R. and R. Baserga, *Functional analysis and growth factor regulation of the human vimentin promoter*. Mol Cell Biol, 1987. **7**(11): p. 3908-15.
318. Izmailova, E.S., et al., *A GC-box is required for expression of the human vimentin gene*. Gene, 1999. **235**(1-2): p. 69-75.

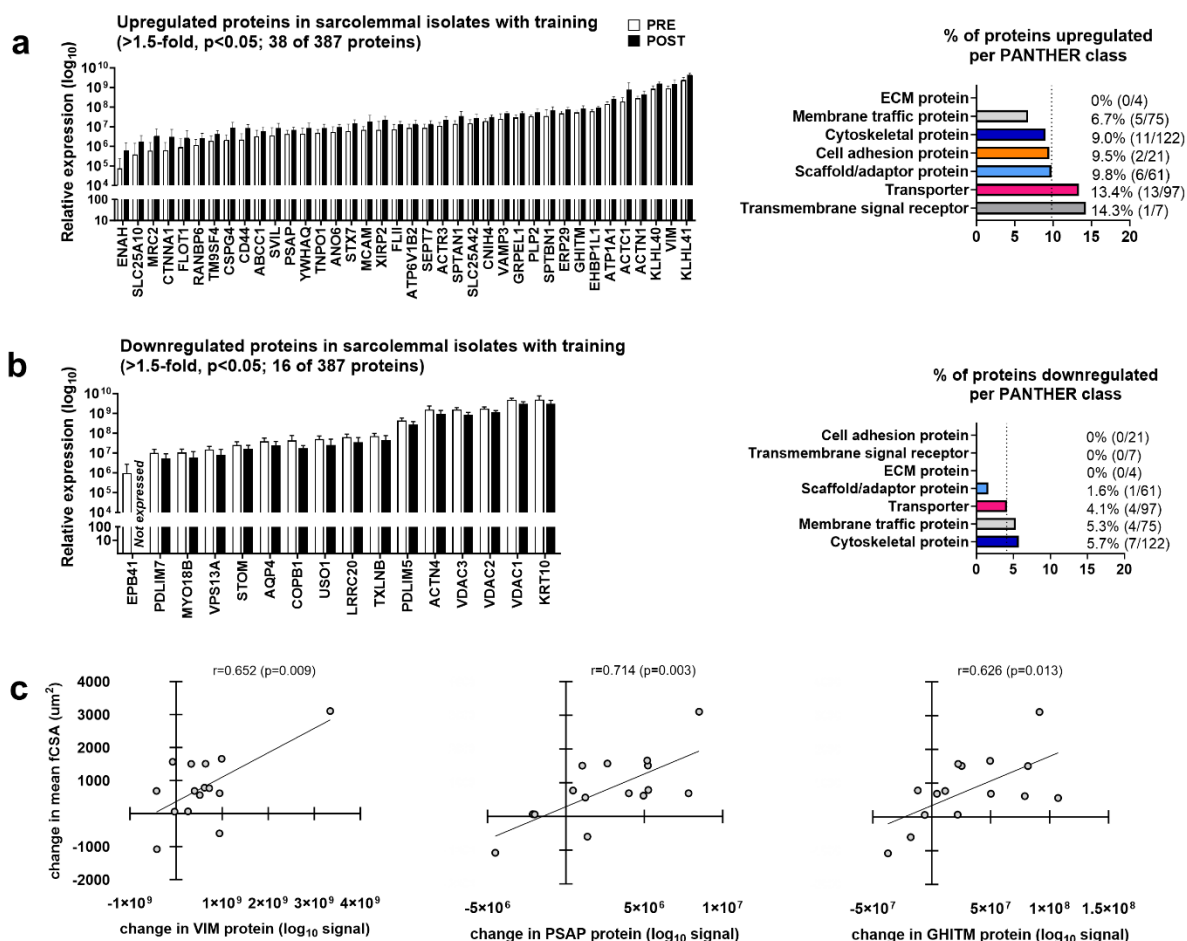
FIGURES & LEGENDS

Figure 1. Basal state (pre-intervention) human sarcolemmal proteome data.



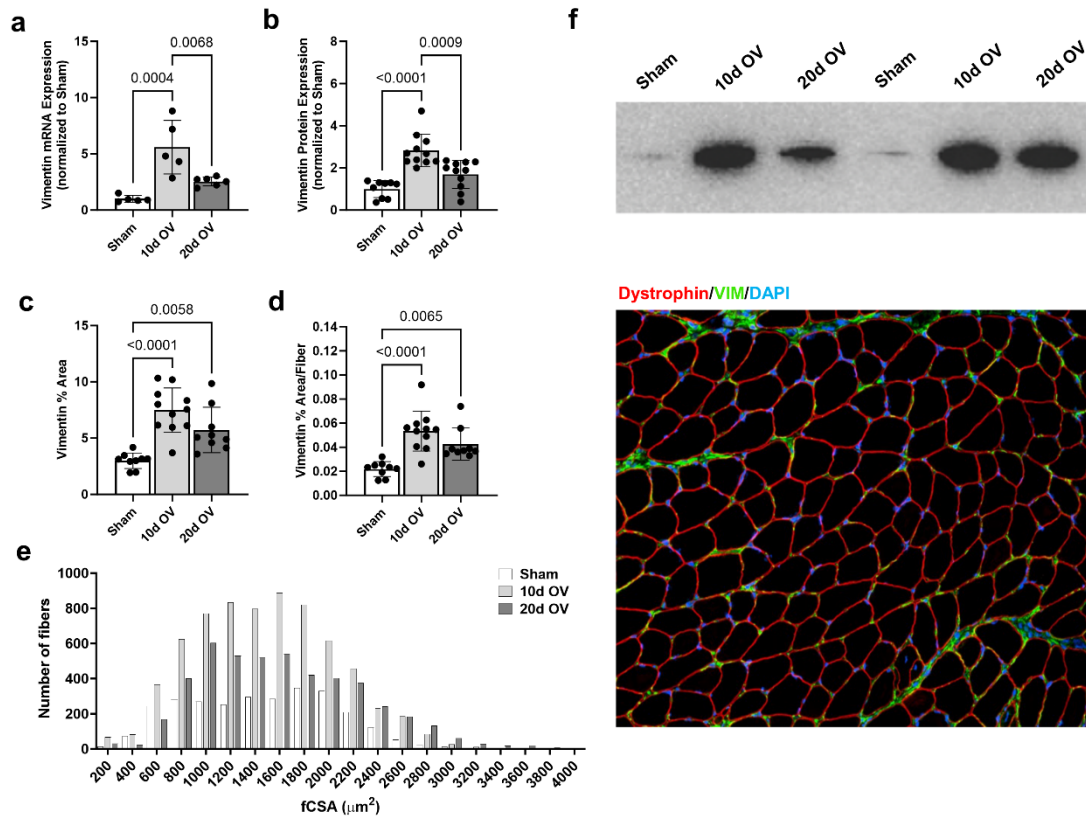
Legend: a) represents the number of targets per PANTHER protein class identified in the sarcolemmal protein isolates via shotgun proteomics from pre-training human skeletal muscle biopsies (grand sum = 387 total targets identified). b-h) are the top enriched proteins (listed by gene name) for each protein class; note, d-h are limited to the top 10 targets due to space limitations. Additional note: bar graph data for b-h) are presented as mean and standard deviation values for all 15 participants.

Figure 2. Human sarcolemmal proteome response to resistance training.



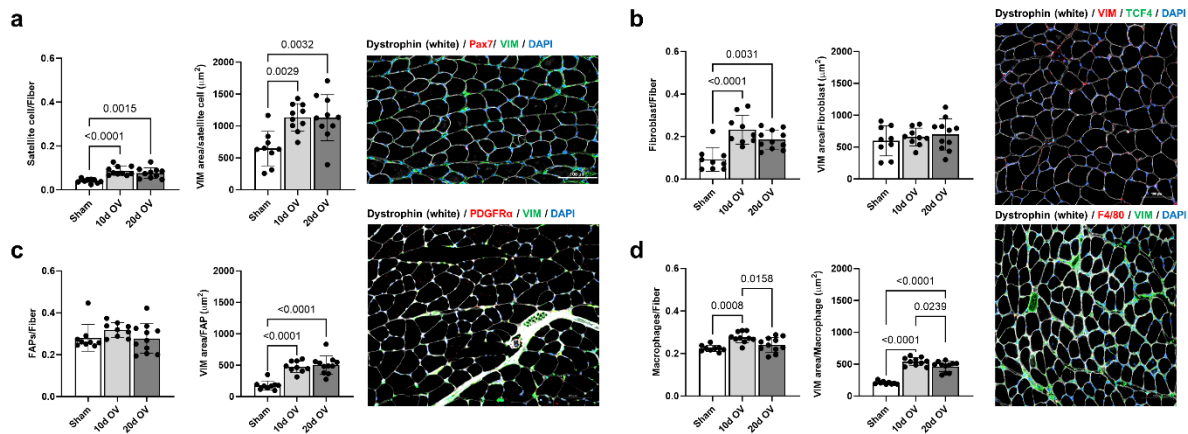
Legend: a) upregulated proteins identified in the sarcolemmal fraction following training including percentage of proteins up-regulated upregulated in each PANTHER protein class. b) downregulated proteins identified in the sarcolemmal fraction following training including percentage of proteins down-regulated upregulated in each PANTHER protein class. c) significant correlations between pre-to-post changes in sarcolemmal proteins that were significantly up-regulated following resistance training and mean fiber cross-sectional area. Additional note: bar graph data for a/b) are presented as mean and standard deviation values for all 15 participants.

Figure 3. Plantaris muscle vimentin expression response to 10- and 20-days of mechanical overload via synergist ablation.



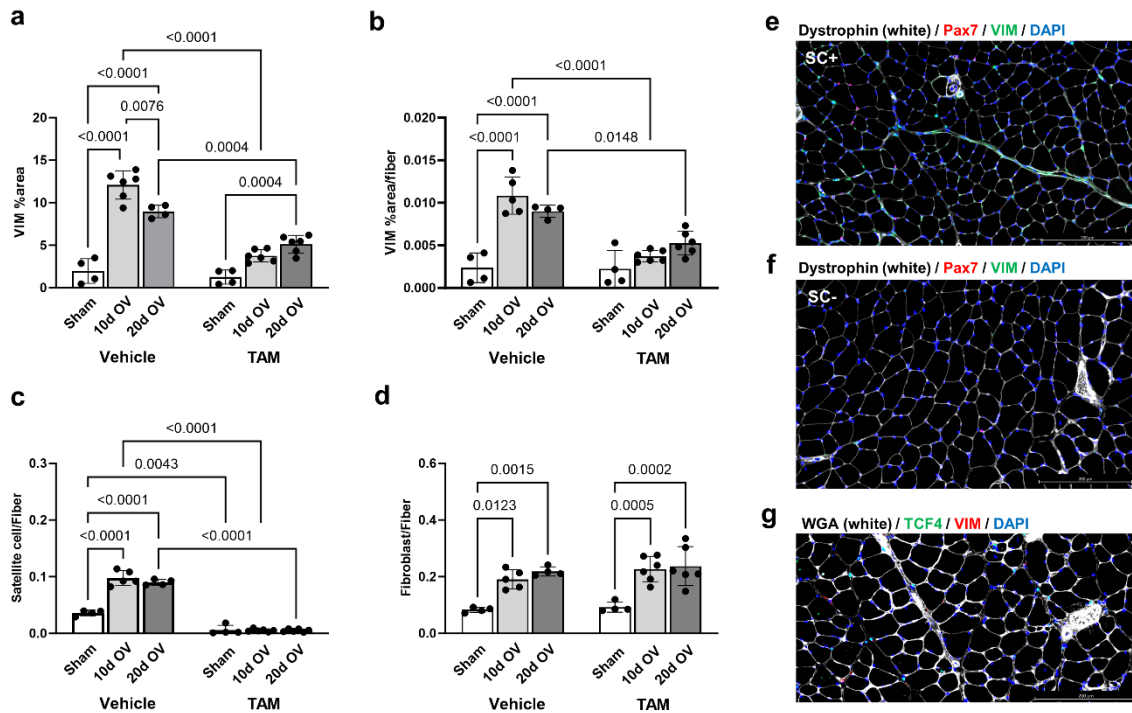
Legend: All bar graph data (aside from histogram data) are presented as mean and standard deviation values with qPCR data containing 4-6 mice per condition and other data containing 9-11 mice per condition. a) mRNA expression of VIM via qPCR following 10- and 20-days MOV. b) Protein expression of VIM via western blotting following 10- and 20-days of MOV. c) Percent area of plantaris cross-section occupied by VIM following 10- and 20-days of MOV (determined via IHC). d) Percent area of plantaris cross-section occupied by VIM (normalized to fiber number) following 10- and 20-days of MOV. e) Fiber size distribution following 10- and 20-day MOV. f) Representative western blot IHC images.

Figure 4. Vimentin co-localization with stromal cells following mechanical overload.



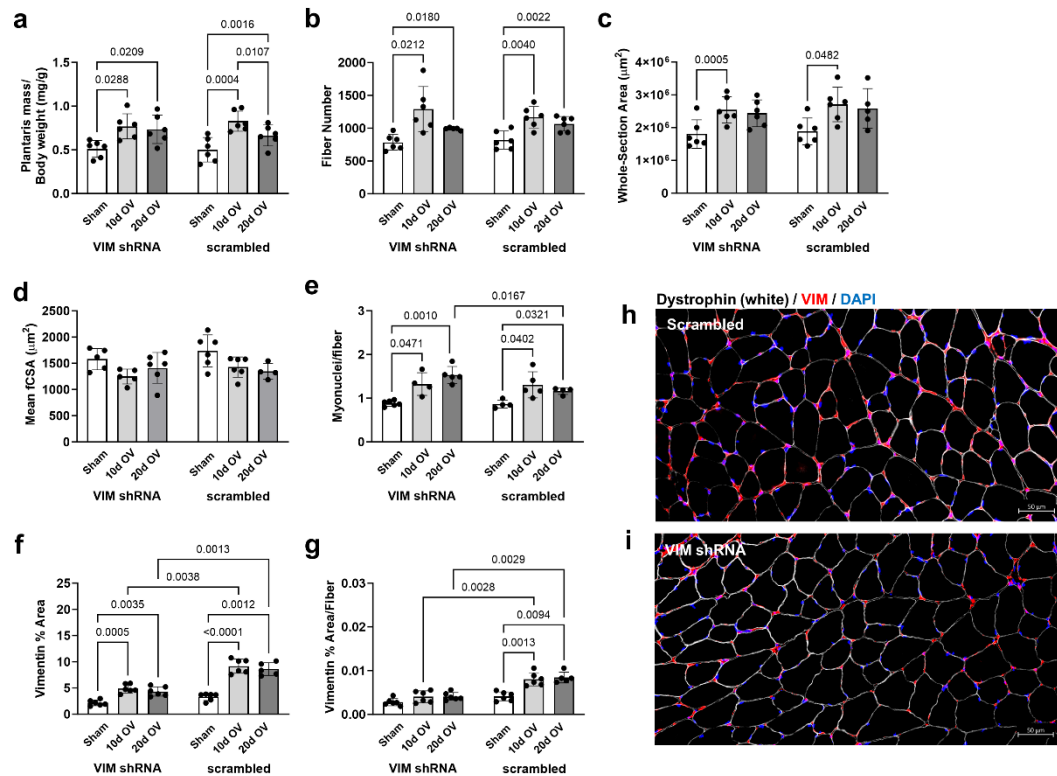
Legend: All bar graph data are presented as mean and standard deviation values with 4-6 mice per condition. a) Percent area of plantaris cross-section occupied by VIM following 10- and 20-days of MOV. b) Percent area of plantaris cross-section occupied by VIM (normalized to fiber number) following 10- and 20-days of MOV. c) Satellite cell number per fiber following 10- and 20-days of MOV. d) Fibroblast number per fiber following 10- and 20-days of MOV. e) Representative image of a satellite cell intact (SC+) mouse with VIM expression. f) Representative image of a satellite cell depleted (SC-) mouse with VIM expression. g) Representative image of fibroblast staining.

Figure 5. Vimentin expression in satellite cell depleted muscle following mechanical overload.



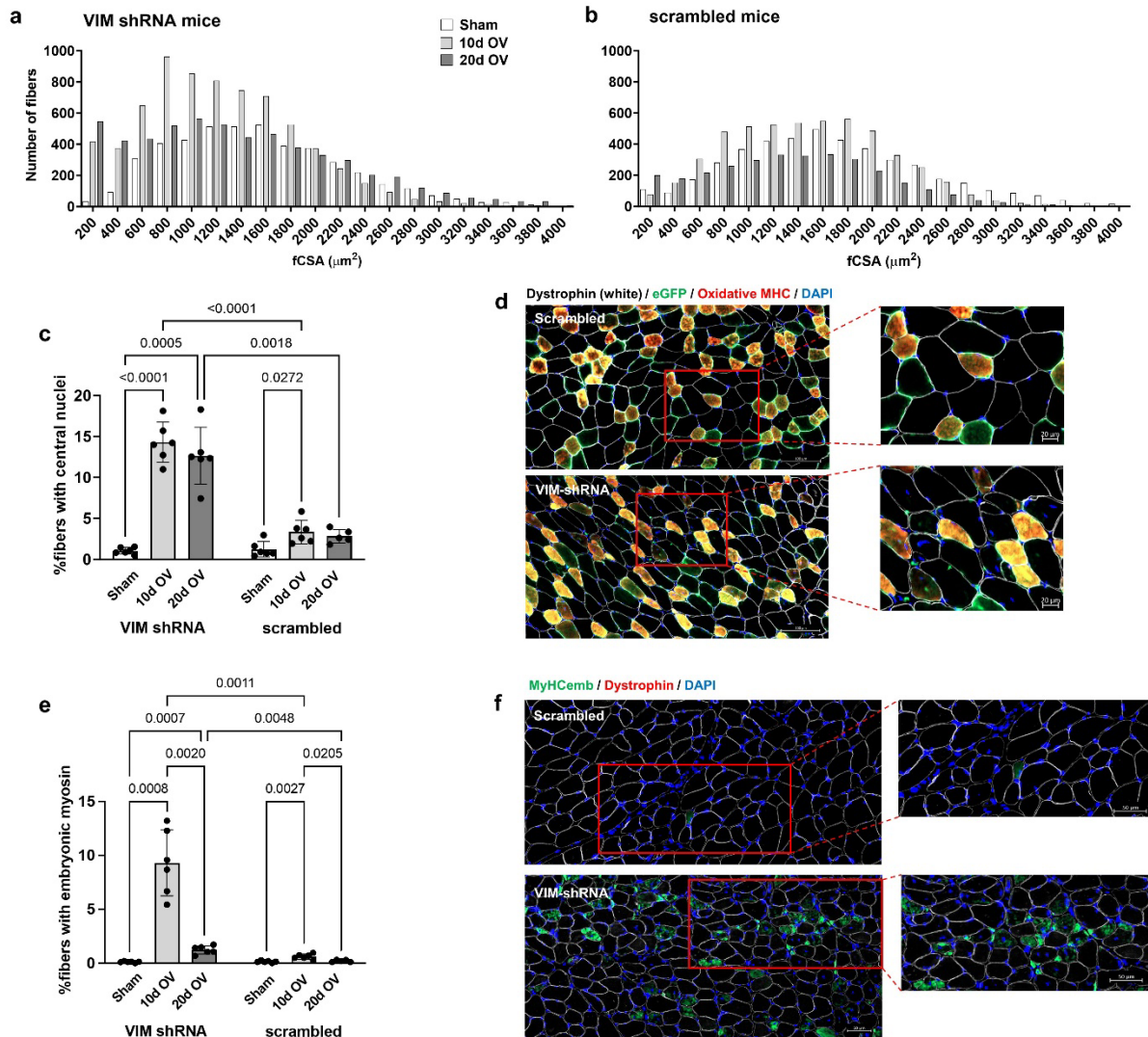
Legend: All bar graph data are presented as mean and standard deviation values with 4-6 mice per condition. a) Percent area of plantaris cross-section occupied by VIM following 10- and 20-days of MOV. b) Percent area of plantaris cross-section occupied by VIM (normalized to fiber number) following 10- and 20-days of MOV. c) Satellite cell number per fiber following 10- and 20-days of MOV. d) Fibroblast number per fiber following 10- and 20-days of MOV. e) Representative image of a satellite cell intact (SC+) mouse with VIM expression. f) Representative image of a satellite cell depleted (SC-) mouse with VIM expression. g) Representative image of fibroblast staining.

Figure 6. General muscle characteristics and vimentin expression in mice treated with AAV9-VIM-shRNA.



Legend: All bar graph data are presented as mean and standard deviation values with 4-6 mice per condition. a) Plantaris masses (normalized wet to body weight) following 10- and 20-days of MOV. b) Number of fibers present in whole cross-section following 10- and 20-days of MOV. c) Cross-sectional area of whole section following 10- and 20-days of MOV. d) mean fiber cross-sectional area following 10- and 20-days of MOV. e) Myonuclei per fiber following 10- and 20-days of MOV. f) Percent area of cross-section occupied by VIM following 10- and 20-days of MOV. g) Percent area of cross-section occupied by VIM (normalized to fiber number) following 10- and 20-days of MOV. h) Representative image for dystrophin (fCSA) and VIM abundance in AAV-scrambled mice. i) Representative image for dystrophin (fCSA) and VIM abundance in AAV-VIM-shRNA mice.

Figure 7. AAV-VIM-shRNA mice present a shift toward smaller fibers and more centrally located nuclei.



Legend: All bar graph data are presented as mean and standard deviation values with 4-6 mice per condition. a) Histogram for fiber size distribution in AAV9 VIM-shRNA following 10- and 20-day MOV. b) Histogram for fiber size distribution in AAV9 scrambled mice following 10- and 20-day MOV. c) Percentage of fibers that display centrally located nuclei following 10- and 20-day MOV between AAV9 injection groups with representative IHC images in panel d. e) Percentage of fibers positive for embryonic myosin heavy chain (MyHC_{emb}) following 10- and 20-day MOV between AAV9 injection groups with representative IHC images in panel f.